



Characterisation and modelling of lightning strikes as point events in time and space

Uldis Zandovskis¹, Davide Pigoli², Bruce D. Malamud³,

¹King's College London, Department of Geography, London, United Kingdom

²King's College London, Department of Mathematics, London, United Kingdom

³Durham University, Institute of Hazard, Risk and Resilience (IHRR), Durham, United Kingdom

Correspondence to: Uldis Zandovskis (uldis.zandovskis@gmail.com)

Abstract. Lightning is a spatio-temporal phenomenon comprised of individual strikes with specific occurrence times and spatial coordinates. This study models and characterises lightning strikes from single thunderstorms, treating each strike as a point event. Utilising real-world datasets, we characterise and model lightning strikes' physical properties. Our analysis involves two severe UK thunderstorm systems selected based on published synoptic analyses. These systems enable subdivision of the lightning dataset into subsets, each representing a distinct thunderstorm. Our two major storm systems feature three thunderstorms each: Storm system A with 7955, 11988, and 5655 strikes over the English Midlands on 28 June 2012; Storm system B with 4218, 455, and 1926 strikes characterised over northern England on 1–2 July 2015. These six datasets exemplify individual thunderstorms with three physical attributes: movement speed, lightning inter-event time distribution, and spatial spread about the storm track. Applying least-squares plane and linear fits in the spatio-temporal and lag spaces, we estimate movement speeds of 47–59 km/h and 67–111 km/h for Storm systems A and B, respectively. The inter-event time distribution ranges from 0.01 to 100 seconds, with density peaks around 0.1 seconds and at 1–10 seconds. Autocorrelation analysis in natural time reveals significant autocorrelation in all storms, varying from short-range to long-range. For spatial spread, calculated as the distance from the storm track to the strikes, we employ a linear filter to establish the storm track. This analysis yields typical spatial spreads up to 80 km in either northing or easting dimensions, with an outlier of 226 km in the northing dimension for one storm. The paper concludes with a synthetic lightning strike model. This model allows the selection of each storm's starting points, directions, and movement speeds, generating point events based on our characterisation findings. This comprehensive study of lightning strikes in time and space accurately reflects severe thunderstorms' behaviour and informs statistical models for simulating lightning events.



1 Introduction

30 This study focuses on the characterisation and modelling of lightning strike spatial location and times of occurrence data. A lightning strike dataset recorded by the ATDnet system (Nash et al., 2006) over an area between (13°W and 5°E) and (49°N and 61°N) over the time period 2008 to 2016 is used to separate two case studies of individual days of significant lightning activity. The data used in this study can be categorised for characterisation and modelling methodologies as spatio-temporal point events produced by a moving point source (Kisilevich et al., 2009) (i.e. a thunderstorm producing a cluster of lightning strike point events).

35 For spatio-temporal natural hazard data, both spatial and temporal domains, if considered separately, can give insight about different variables of the hazardous process producing the events. The extent and density of lightning flashes or strikes can be gridded over global (Mezuman et al., 2014) or continental (e.g. [Anderson and Klugmann, 2014; Enno et al., 2020]) spatial scales and varying time periods. The combined spatio-temporal domain allows us to observe dependencies among measurements in the spatial and temporal dimensions (i.e. autocorrelation and heterogeneity) (Atluri et al., 2018). Natural hazard point events are therefore, structurally related to each other in space and time and show varying properties in different spatial regions, time periods and their combined spatio-temporal windows.

40 As natural hazards are inherently spatio-temporal processes, characterising the natural hazard over the combined spatio-temporal domain allows us to gain more sophisticated insight into the extent and evolution of the hazardous process. For wildfires, spatio-temporal interaction can be modelled directly as one of the parameters for a given point process intensity function (e.g. [Møller and Díaz-Avalos, 2010; Serra et al., 2014]). For earthquakes, the spatio-temporal domain can be used with earthquake magnitude to inform the separation of foreshock, mainshock and aftershock clusters (Zaliapin et al., 2008; Zaliapin and Ben-Zion, 2013). The spatio-temporal domain can not only directly inform the modelling of a given natural hazard process but also provide additional insight into the natural hazard and its properties.

45 For lightning strikes, a spatio-temporal point event model was developed in (Finke, 1999), while physics-based models are more common (e.g. [Rakov and Uman, 2003; Yair et al., 2009]). The main objective of this study is to extend the work (Finke, 1999) by characterising various physical lightning variables based on real-world case study data and incorporating them into a general spatio-temporal framework to statistically model spatio-temporal point events produced by a moving point source. This framework can be used to generate multiple synthetic point event datasets that would be representative of lightning strike data. The publication is organised as follows:

- 55 • **Section 2** (background) expands on the existing literature on characterising and modelling lightning, identifying individual approaches to represent and analyse spatio-temporal point event data.
- **Section 3** (data collection) details two case studies from the ATDnet dataset that will be considered in this work. Each case study refers to a separate day of increased lightning activity with available synoptic analysis. These analyses identify individual thunderstorms that were producing lightning strikes, and from location, time of occurrence, Doppler radar and additional data, lightning strikes can be assigned to particular identified thunderstorms.



- 60
- **Section 4** (methods) details the methodologies used to characterise physical variables for all the identified thunderstorms and model these physical variables as input parameters for a spatio-temporal point event model.
 - **Section 5** (results) then discusses the results of these methodologies and the resulting characterisation of lightning strikes events.
 - **Section 6** (modelling) details the approach taken for modelling the lightning strikes as point events produced by a moving point source by including the characterised physical variables as parameters of a statistical model. It further gives examples of using the modelling approach to create point event datasets representative of lightning strikes and demonstrates the ability of flexible input parameters to create various point events datasets for other applications (e.g., validation of spatio-temporal clustering methodologies).
 - **Section 7** (discussion) critically assesses the approach taken in this study, its limitations, potential improvements, and future directions.
- 65
- 70

2 Background on lightning and characterisation of spatio-temporal modelling for natural hazard point events

2.1. Lightning

Lightning from a physics perspective can be defined as an electric spark (typically 5–10 km in length), caused when the resistance of the intervening air between areas of positive and negative charge is overcome (Dwyer and Uman, 2014).

75 Thunderstorms that produce lightning have a basic dipolar charge structure consisting of a negative charge at mid-levels of the storm and a positive charge in the upper level (Shao and Krehbiel, 1996). This creates intracloud (IC) lightning strikes within the storm, intercloud lightning between different storms, and cloud-to-air and cloud-to-ground (CG) lightning.

Characterisation of lightning as a physical phenomenon has been done on data recorded directly from a current transducer (Chowdhuri et al., 2005), from digital high-speed cameras (Ballarotti et al., 2012), from the electromagnetic radiation in the very high frequency (VHF) and ultra-high frequency (UHF) bands (Richard et al., 1986; Shao and Krehbiel, 1996) or as point events by on-ground detection networks (Steiger et al., 2002; Anderson and Klugmann, 2014; Galanaki et al., 2015) or satellite detectors (Beirle et al., 2014). This study does not focus on characterising the physics of lightning initiation but rather on characterising physical variables of lightning events as point events. The physical variables describing the point event set are characterised based on the available data. They are used to statistically model lightning strikes as spatio-temporal point events produced by a moving point source.

85

The recording methodology establishes the lightning variables that are characterised. For example, by measuring current directly, variables such as peak current, waveshape and return stroke velocity can be characterised (Chowdhuri et al., 2005). This study focuses on characterising lightning strikes as spatio-temporal point events produced by a moving point source and as recorded by an on-ground detection network over a short temporal scale. Previous studies have used lightning data of various spatial (i.e. global, continental, regional or national), but consistently long temporal scales (from 5 (Anderson and Klugmann,

90



2014) to 11 (Steiger et al., 2002) years). Characterised variables include flash density (strikes per km² per year), strike distribution by month, strikes per hour over land or sea and percent of positive flashes (availability dependent on the capabilities of the detection network).

2.2 Modelling spatial-temporal characteristics of natural hazard point events

95 Multiple approaches are possible to model spatio-temporal point events, depending on the desired purpose. In this study, we require two properties to be satisfied by our model: (i) the inclusion of characterised physical variables and (ii) the ability to produce synthetic data representing the hazard process. A brief literature review was conducted to overview the various approaches to model spatio-temporal point event data of any natural hazard. For each of the 20 publications, this review (**Table A1 in Appendix A**) identified:

- 100
- Data attributes: the size and spatial and temporal scales of the data.
 - Variables that inform the model: physical variables incorporated into the model framework.
 - Main mathematical model: the statistical model that has been implemented.

As the main mathematical model, various statistical point process models (González et al., 2016) were used to model 6 different natural hazards:

- 105
- avalanches (Eckert et al., 2010),
 - volcano eruptions (Jaquet et al., 2012),
 - tornadoes (González et al., 2020),
 - earthquakes (van Lieshout et al., 2012),
 - hurricanes (Economou et al., 2014),
- 110
- wildfires (Serra et al., 2014; Møller and Díaz-Avalos, 2010; Xu and Schoenberg, 2011).

Different point process models were extensively used for wildfire modelling in particular. Existing studies used the Cox point process to incorporate different variables and covariates (e.g., cause of fire, spatial covariates and meteorological variables).

A purely statistical model approach was not found to be common for lightning strikes. There is extensive research for modelling the possible modes of charge transfer to the ground during lightning discharges (i.e. dart-leader–return-stroke sequence, continuing current and M-component [Rakov and Uman, 2003]). Lightning physics has also been modelled as a coupled network of thunderstorm cells (Yair et al., 2009). These thunderstorm clouds consist of electrically active cells that can be interacting or non-interacting. The electric field in a specific thundercloud region is modelled and generates a lightning flash when passing its maximum.

115

While able to describe and model lightning physics, these above models do not apply to model lightning as point events. For the spatial and temporal domains, point processes have been used to count the number of total lightning strikes (Artigas, 2012) and to model lightning only in the temporal domain (Telesca et al., 2008). In the combined spatio-temporal domain, a Gaussian cloud approach has been proposed to model the propagation of thunderstorms and generate lightning point events (Finke,

120



1999). The distribution function of lightning point locations is approximated by a cloud of constant circular shape, moving with constant velocity. It is assumed that the lightning point event occurrence times are distributed uniformly.

125 In this publication, we follow a similar approach to the one in (Finke, 1999), but with a data-driven strategy for choosing the parameters in the model. For example, we do not assume a uniform distribution of lightning strike occurrence times but aim to estimate that from the data empirically. The occurrence times are incorporated by empirically sampling inter-event time distributions (**Sections 4.2** and **6.1**). The movement speed (**Section 4.3**) and spatial spread (**Section 4.4**) are lightning variables that are also incorporated into the model, but by different methodologies (**Sections 5.2, 5.3**) than (Finke, 1999). All three
130 model variables are informed by or sampled from real-world lightning strike data from two case studies of increased lightning activity (**Section 3**). The model implementation details and examples of synthetic data are given in **Section 6**.

3. Data collection of lightning and storms

This section first presents the ADT lightning data collection system and its parameters (**Section 3.1**). To identify and assign lightning strikes to individual thunderstorms, two case studies of increased lightning activity over two individual days are
135 detailed (**Sections 3.2** and **3.3**). Each case study includes additional synoptic analysis information from available literature (Clark and Webb, 2013; Lewis and Silkstone, 2017) and presents the lightning strikes assigned to three individual thunderstorms in each case study.

3.1 ATDnet lightning detection system and available data

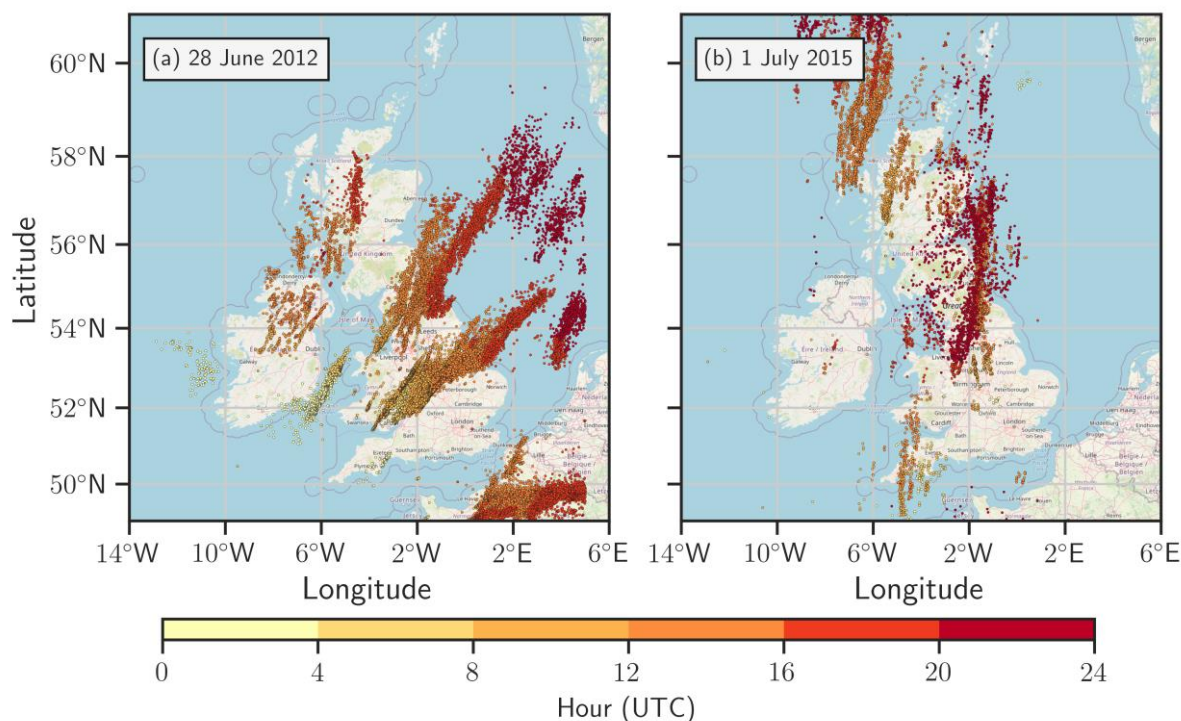
The lightning data used in this study is recorded by a very low frequency (VLF) long-range lightning location system (LLS).
140 Over the United Kingdom, the Met Office operates the ATDnet LLS (Nash et al., 2006), which locates lightning discharges using the arrival time difference (ATD) method (Lee, 1986). ATDnet predominantly detects sferics (electromagnetic waves in the VLF range propagating in the earth–ionosphere waveguide [Rakov and Uman 2003]) created by CG lightning strikes. As the energy and polarisation of sferics created by CG return strikes mean that they can travel more efficiently in the Earth–ionosphere waveguide, they are more likely to be detected at longer ranges (Enno et al., 2016).

145 The system takes advantage of the long propagation paths of sferics to cover large areas with only a limited number of sensors. The effective range of ATDnet encompasses Europe, northern Africa, and northern parts of the Atlantic, but in our study, the range is focused on an area between (13°W and 5°E) and (49°N and 61°N) and over the time period 2008 to 2016 as provided by the Met Office (2017).

Two days from this large dataset are selected, one for each case study. The first day of increased lightning activity was the 28
150 June 2012, and the corresponding synoptical analysis is provided by (Clark and Webb, 2013). The second day occurred on 1 July 2015 and was analysed by (Lewis and Silkstone, 2017). Both synoptic analyses give initiation and propagation details of three individual thunderstorms with auxiliary data from Doppler radars in the region and observations of other natural hazards.



For both days, the spatial extent and propagation (in 4-hour intervals) of the available lightning strike data subsets are shown in **Fig. 1**. This figure will be discussed in more detail in **Section 3.2** and **Section 3.3**.



155

Figure 1: The spatial extent of lightning strike occurrences as recorded by the ATDnet system (Gaffard et al., 2008) from 00:00 to 23:59 UTC on (a) 28 June 2012 and (b) 1 July 2015. Timestamps of all lightning strikes are categorised into 4-hour intervals with times indicated by the colour scale. Lightning strike data from Met Office from 2008–2016 (2017) and covering an area between (13.0°W and 5.0°E) and (49.0°N and 61.0°N). Background map information from OSM (© OpenStreetMap contributors 2022. Distributed under the Open Data Commons Open Database License (ODbL) v1.0.).

160

3.2 Case study 1: Three supercell thunderstorms across English Midlands on 28 June 2012

The first case study in **Figure 1a** is based on a synoptic analysis of three supercell thunderstorms that crossed the English Midlands on 28 June 2012 during the 24-hour time period 00:00 to 23:59 UTC (Clark and Webb, 2013). The three thunderstorms are identified by their approximate time and location of initiation, propagation path in descriptive terms and snapshots of the location around Doppler radar stations. From the synoptic analysis, we denote the three thunderstorms as Storm 1A, 1B and 1C, respectively, corresponding to supercells ‘A’, ‘B’ and ‘C’. In this case study, for Storm 1B, the location and temporal information of the observed hail and tornado are used to assign lightning strikes to individual thunderstorms.

165

To use the available identifying information from the synoptic analysis, the lightning strike location data, a total of $N_L = 77,252$ strikes, is projected onto the OSGB 1936 (EPSG:27700) northing/easting coordinates. In this three-dimensional spatio-temporal space, planes are drawn to separate the lightning strike dataset, as described in more detail in **Fig. 3** and **Fig. 4** below.

170

Points (i.e., position and time of observation) on these planes are selected based on the synoptic analysis, auxiliary data from Doppler radars in Clee Hill and Ingham, and observations of a tornado in Sleaford (Clark and Webb, 2013).

Using Storm 1B as an example for this assignment procedure, the initial limitation on the available lightning strike point events is placed spatially and temporally. From the synoptic analysis (Clark and Webb, 2013), Storm 1B formed shortly after 10:00 UTC, started merging with smaller cells around 13:00 UTC and was tracked until 14:37 UTC. Spatially, the study area is focused on 350–600 km in easting and 200–450 km in northing coordinates. This spatial area includes the Clee Hill station, from which Storm 1B was always observed eastwards and places Sleaford close to the centroid of the study area. The lightning strike data subset available for assigning lightning strikes to Storm 1B is shown in **Fig. 2**.

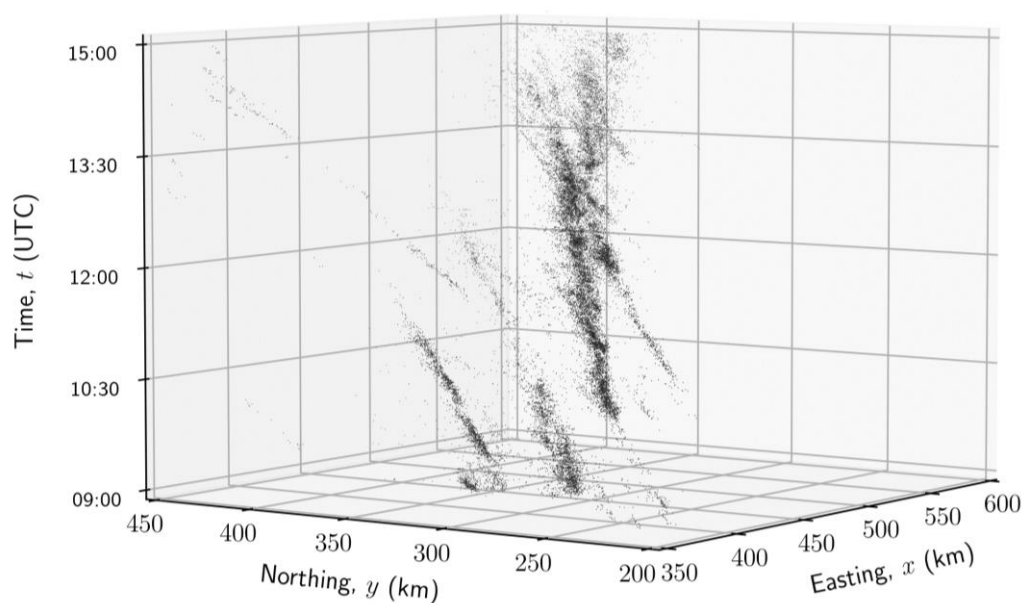


Figure 2: The lightning strike data subset available for assignment to Storm 1B of the first case study. The case study is based on a synoptic analysis of three supercell thunderstorms that crossed the English Midlands on 28 June 2012. The spatial extent was restricted to $x = (350,600)$ km and $y = (200,450)$ in the OSGB 1936 (EPSG:27700) easting/northing coordinates, respectively. Temporal extent was considered from 09:00–15:00 UTC. All available lightning strikes are indicated as black scatter points.

Spatial and temporal scales can be further restricted from the auxiliary Doppler radar data available from the Clee Hill and Ingham stations. Snapshots of the Storm 1B location relative to these stations are available at 10:00, 12:00 and 14:00 UTC. Unprocessed reflectivity data is also available in 10-minute intervals from 11:02–11:52 UTC in Clee Hill and in 10- or 15-minute intervals from 12:42–13:37 UTC in Ingham. The snapshot frames move with the storm, so they are not useful in determining the exact location of Storm 1B relative to the stations, but they aid in understanding the storm’s evolution. The relative positions of the Clee Hill and Ingham radar stations to the lightning strike subset from **Fig. 2** are shown in **Fig. 3** at 12:00 and 14:00 UTC.

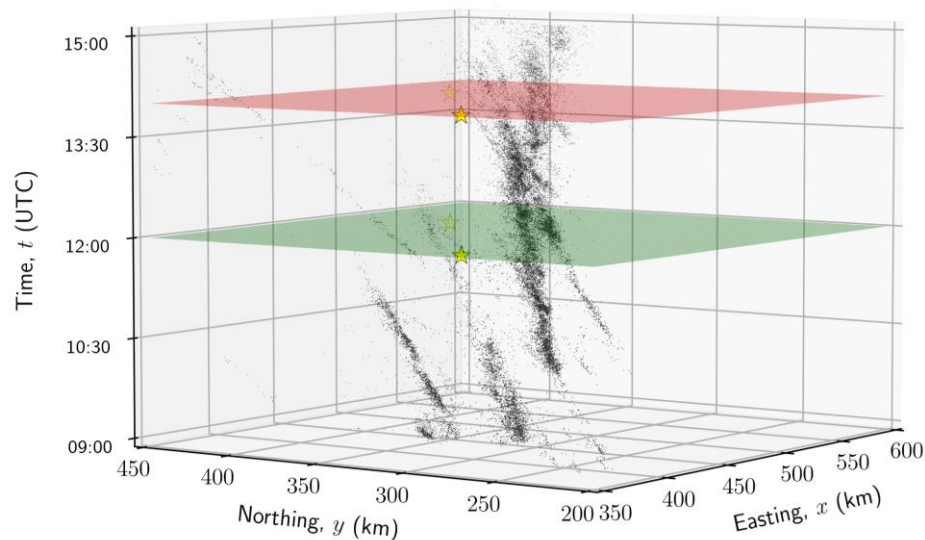
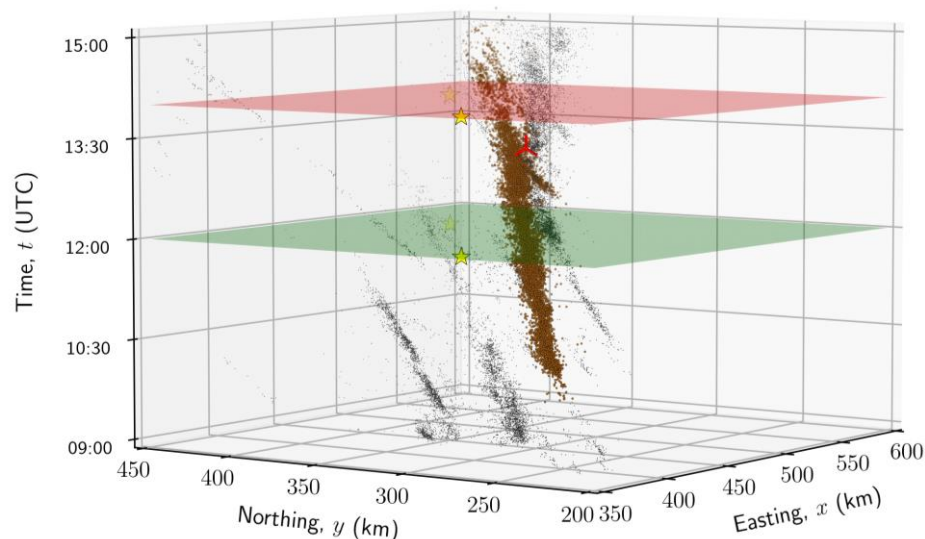


Figure 3: The availability of Doppler radar station location information for the first case study's assignment of lightning strikes to Storm 1B. All available lightning strikes are indicated as black scatter points. The locations of the Clee Hill and Ingham radar stations are marked as yellow star scatter points at two time points: 12:00 (green plane) and 14:00 (red plane) UTC.

195 Observation and tracking information available on the Sleaford tornado and hail further confirm the development and propagation of Storm 1B. The storm is tracked from 11:22–13:52 UTC through hail observation and radar data. The Sleaford tornado developed between 13:12–13:37 UTC. Both time intervals include the merge with smaller storm cells to the south of Storm 1B, complicating the exact assignment of lightning strikes.



200 **Figure 4:** The first case study's assignment of lightning strikes to Storm 1B (dark brown scatter points). The locations of the Clee Hill and Ingham radar stations are marked as yellow star scatter points at two time points: 12:00 (green plane) and 14:00 (red plane) UTC. The location and first approximated time of occurrence (13:12 UTC) for the Sleaford tornado is marked as a red triangular line marker. The remaining unassigned lightning strikes are indicated as black scatter points.



205

Figure 4 shows that for the majority of the lightning strikes, assignment to Storm 1B was not complicated due to the clear separation of supercell thunderstorms, as noted in the synoptic analysis (Clark and Webb, 2013). The exact formation time was not indicated in the synoptic analysis but was chosen to be any time after 10:00 UTC due to Storm 1B not being identified at the 10:00 UTC Doppler radar snapshot. The noted merging of Storm 1B and local cells to the south at approximately 13:00 UTC is the main source of assignment uncertainty for individual lightning strikes. The exact termination time was also not noted in the synoptic analysis and was extended until 15:00 UTC to include any lightning strikes that still followed the general propagation direction of Storm 1B.

210

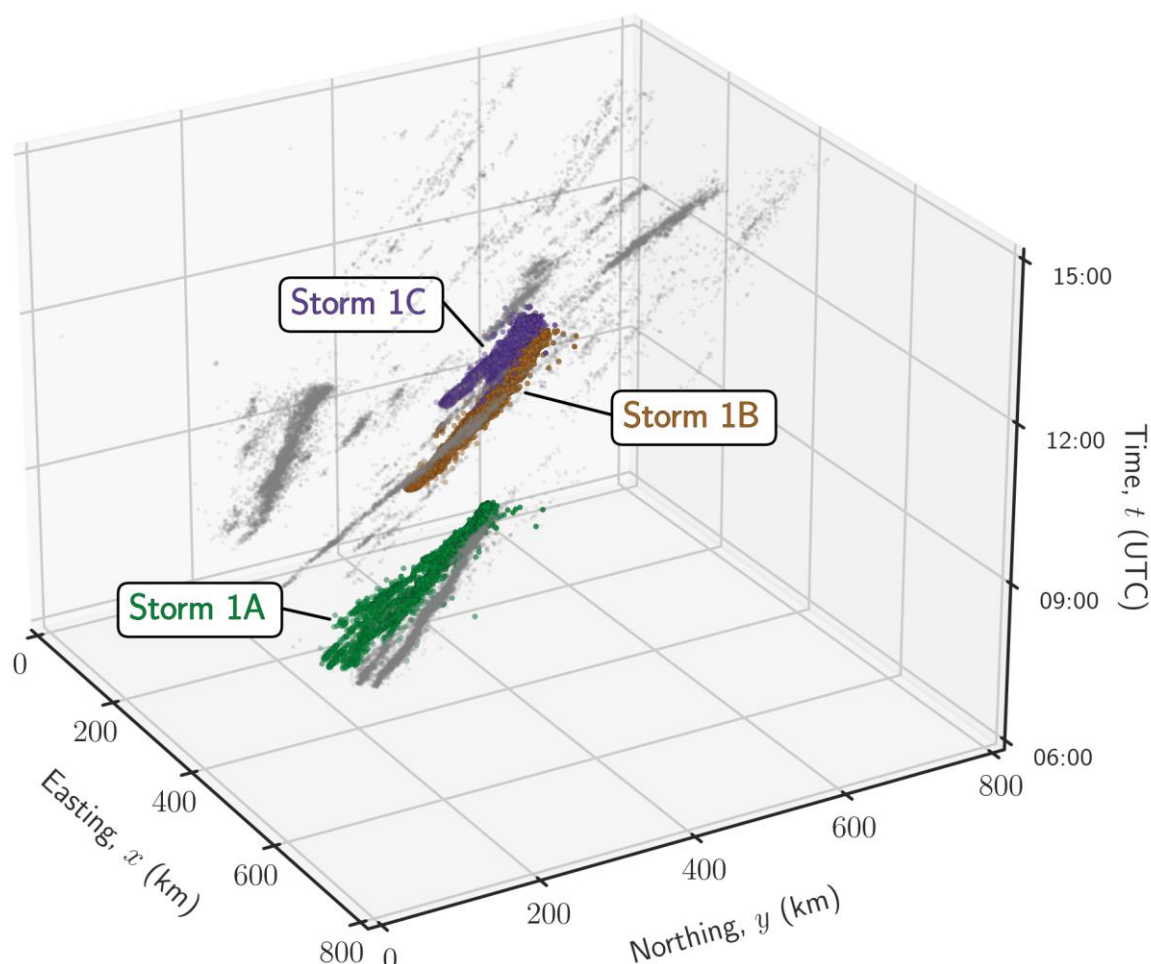
The summary of the initial spatial and temporal limitations on the lightning strike dataset, the time instances used from Doppler radar data and any additional use of auxiliary data is shown in **Table 1**.

Table 1: Variables and their values used for the assignment procedure of individual lightning strikes to the six thunderstorms on 28 June 2012 (Storms 1A, 1B, 1C) and 1 July 2015 (Storms 2A, 2B, 2C).

Date	Storm	Spatial extent	Temporal extent	Time instances of available Doppler radar data UTC	Doppler radar stations	Auxiliary data
		x_{min}, x_{max} y_{min}, y_{max} (km)	t_{min}, t_{max} UTC			
28 June 2012	1A	200, 600 150, 500	06:00, 12:00	10:00, 12:00		-
	1B	350, 600 200, 450	09:00, 15:00	12:00, 14:00	Clee Hill, Ingham	Hail, Tornado
	1C	400, 600 150, 400	12:00, 15:00	12:00, 14:00		-
1 July 2015	2A	400, 475 420, 1000	12:00, 17:00	14:08	Hameldon	-
	2B	350, 435 400, 700	14:00, 24:00	19:02, 19:52	Hill, High Moorsley,	-
	2C	200, 1000 200, 1000	19:00, 24:00	21:51	Ingham	-

215

A three-dimensional plot of the assigned lightning strikes and all unassigned strikes recorded between 06:00 and 15:00 UTC is displayed in **Fig. 5**. Additional perspectives of the same plot in the three-dimensional space can be found in **Appendix Fig. B1**.



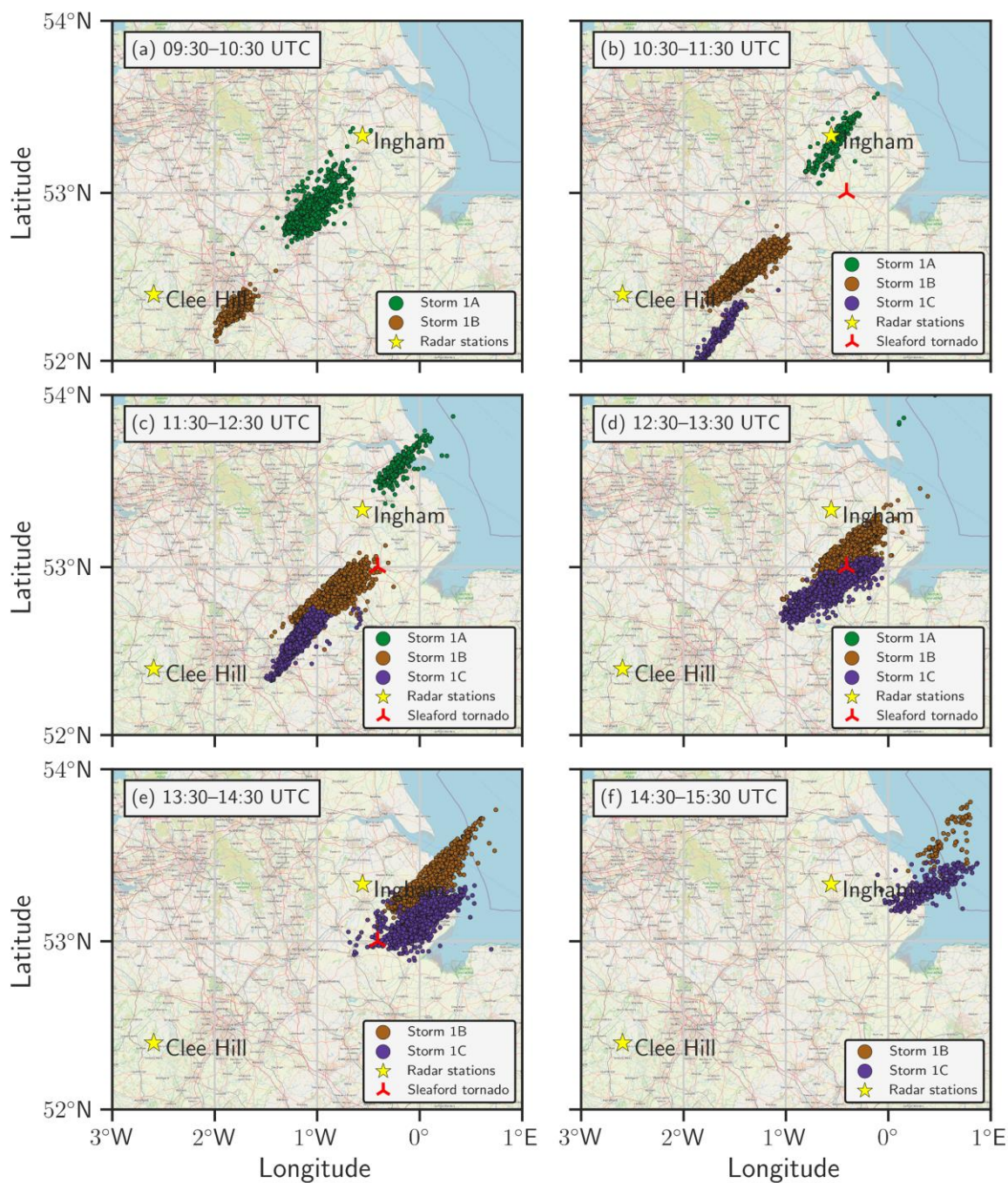
220 **Figure 5:** Spatial extent and propagation of the lightning strike occurrences as recorded on 28 June 2012 by the ATDnet system (Gaffard et al., 2008) and projected onto the OSGB 1936 / British National Grid northing/easting coordinates. Lightning strikes are assigned to the three identified thunderstorms (Storms 1A, 1B, 1C) corresponding to the relevant synoptical analysis (Clark and Webb, 2013). All the remaining unassigned strikes are coloured as per the legend.

225 **Figure 5** shows the separation of the individual thunderstorms from the unassigned lightning strikes. Storm 1B had the most detailed synoptic analysis with additional information and figures of the observed Sleaford tornado and associated hail. It is noted that there is a discrepancy between the level of detail of synoptic analysis and additional information between the storms. Storms 1B and 1C are close to each other in time, and there are subsets of unassigned lightning strikes close to the identified



thunderstorms in the spatio-temporal domain. This introduces a level of ambiguity in assigning the lightning strikes to individual thunderstorms.

230 To indicate the relative position of the assigned lightning strikes to the region's geography and their propagation, six one-hour intervals of the assigned lightning strikes are shown in **Fig. 6**. The lightning strikes are separated by their assignment to a particular individual thunderstorm and are shown relative to the locations of the two Doppler radar stations and the observed tornado in Sleaford. These six intervals were chosen to cover the full temporal range of the lightning strikes as produced by the three thunderstorms.



235

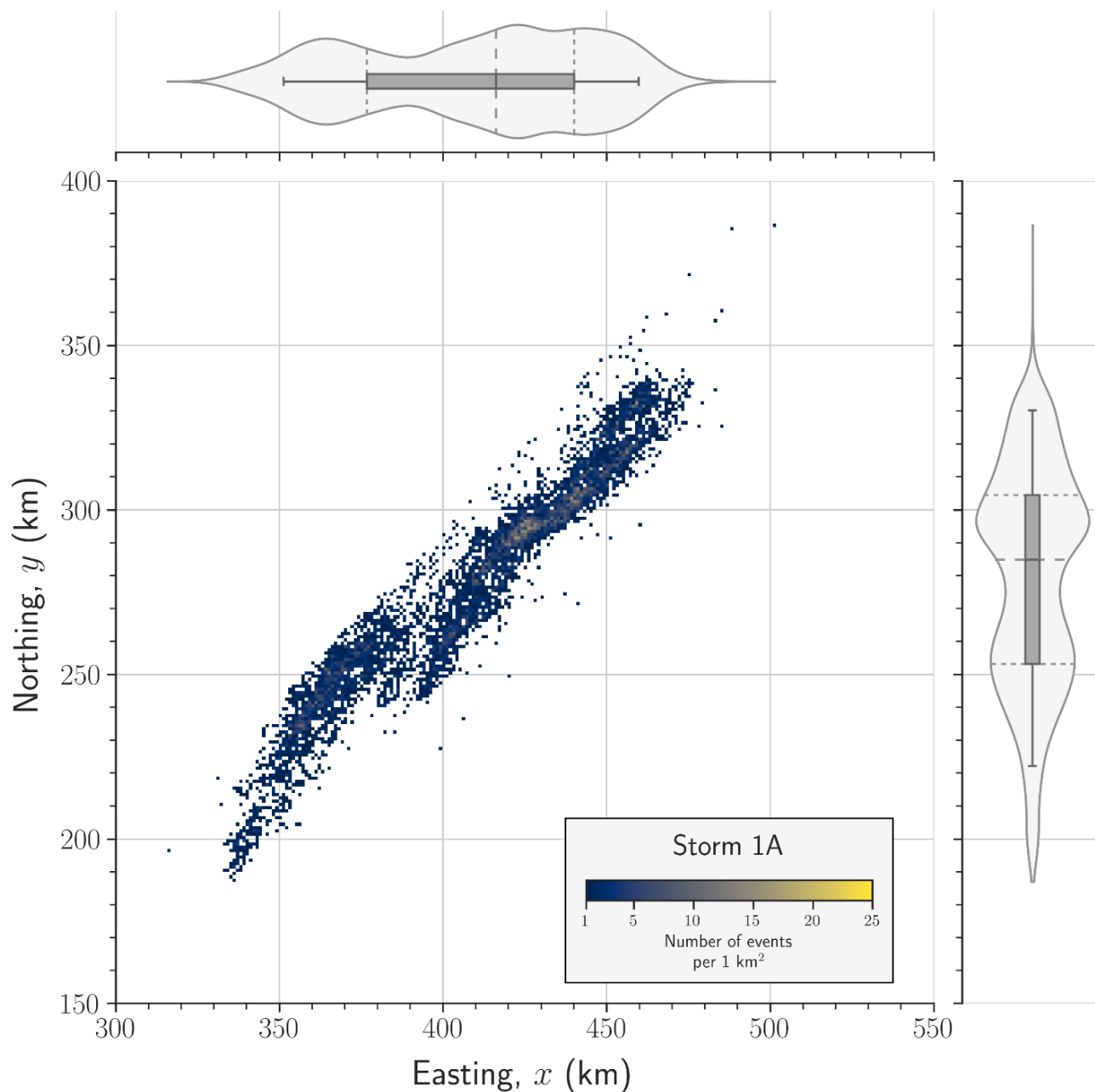
Figure 6: Spatial extent for 28 June 2012 of the lightning strike occurrences as recorded by the ATDnet system (Gaffard et al., 2008) over times intervals corresponding to the relevant synoptical analysis (Clark and Webb, 2013): (a) 09:30–10:30, (b) 10:30–11:30, (c) 11:30–12:30, (d) 12:30–13:30, (e) 13:30–14:30 and (f) 14:30–15:30 UTC. Only lightning strikes assigned to any of the three selected thunderstorms (Storms 1A, 1B, 1C) are shown. Locations of relevant Doppler radar stations and the observed location of the Sleaford tornado are added as per the legend for direct comparison with synoptic analysis. Background map information from OSM (© OpenStreetMap contributors 2022. Distributed under the Open Data Commons Open Database License (ODbL) v1.0).

240



As seen from **Fig. 6**, all three thunderstorms (Storms 1A, 1B, 1C) cross the Midlands in a SW–NE direction when viewed in the projected two-dimensional spatial domain. The locations of the Clee Hill and Ingham radar stations and the Sleaford tornado allow for direct comparison with relevant figures in the synoptic analysis.

245 To characterise the lightning strikes in the spatio-temporal domain for an individual thunderstorm, we can investigate a two-dimensional spatial count of lightning strikes per 1 km². This is displayed in **Fig. 7** for Storm 1A. Violin and box plots of the marginal distributions of northing and easting positions of the lightning strikes are added to the y-axis and x-axis, respectively. These plots provide information on the shape of the empirical distribution, quartiles, and the 5th and 95th percentiles. For other storms, similar figures can be seen in **Appendix C**.



250

Figure 7: 2D spatial count of lightning strikes per 1 km² of the OSGB 1936 / British National Grid northing/easting coordinates for Storm 1A (28 June 2012). Only bins with more than one lightning strike are coloured. Note that the northing and easting extents are the same, but the axes limits differ. The marginal distribution is indicated by overlapping boxplots and violin plots for both the easting and northing values. Boxplots indicate the quartiles and have whiskers for the 5th and 95th percentiles, while the violin plots include all values.

255



In **Fig. 7**, the lightning strikes assigned to Storm 1A cover the same spatial scale of close to 200 km in both northing and easting directions. The strike spatial count does not exceed 20–25 strikes/km², and areas of such lightning intensity are located further along the propagation track of the storm. The marginal distributions show a decrease in lightning intensity as there is a separation between two areas of increased count values at $x = 390$ km and $y = 275$ km.

260 **3.3 Case study 2: Three structurally distinct severe thunderstorms across northern England on 1 July 2015**

The second case study in **Fig. 1b** is based on a synoptic analysis of three supercell thunderstorms that crossed the United Kingdom on 1 July 2015 (Lewis and Silkstone, 2017). The three thunderstorms are again identified by their approximate time and location of initiation, propagation path in descriptive terms and snapshots of the location around Doppler radar stations. We denote these three thunderstorms as Storm 2A, 2B and 2C, corresponding to the three storms identified in their synoptic analysis. In this case study, there is no additional information from occurrences of other natural hazards.

265 For this second case study, $N_L = 12,521$ strikes are recorded and projected onto the OSGB 1936 (EPSG:27700) northing/easting coordinates. Identical to the first case study, planes are drawn to separate the lightning strike dataset in the three-dimensional spatio-temporal space. Points on these planes are selected based on the synoptic analysis and the information from only the Doppler radar stations as no other natural hazard were noted in this case study. A three-dimensional plot of the assigned lightning strikes and all unassigned strikes recorded between 12:00 and 24:00 UTC is displayed in **Fig. 8**. Additional perspectives of the same plot in the three-dimensional space can be found in **Appendix Fig. B2**.

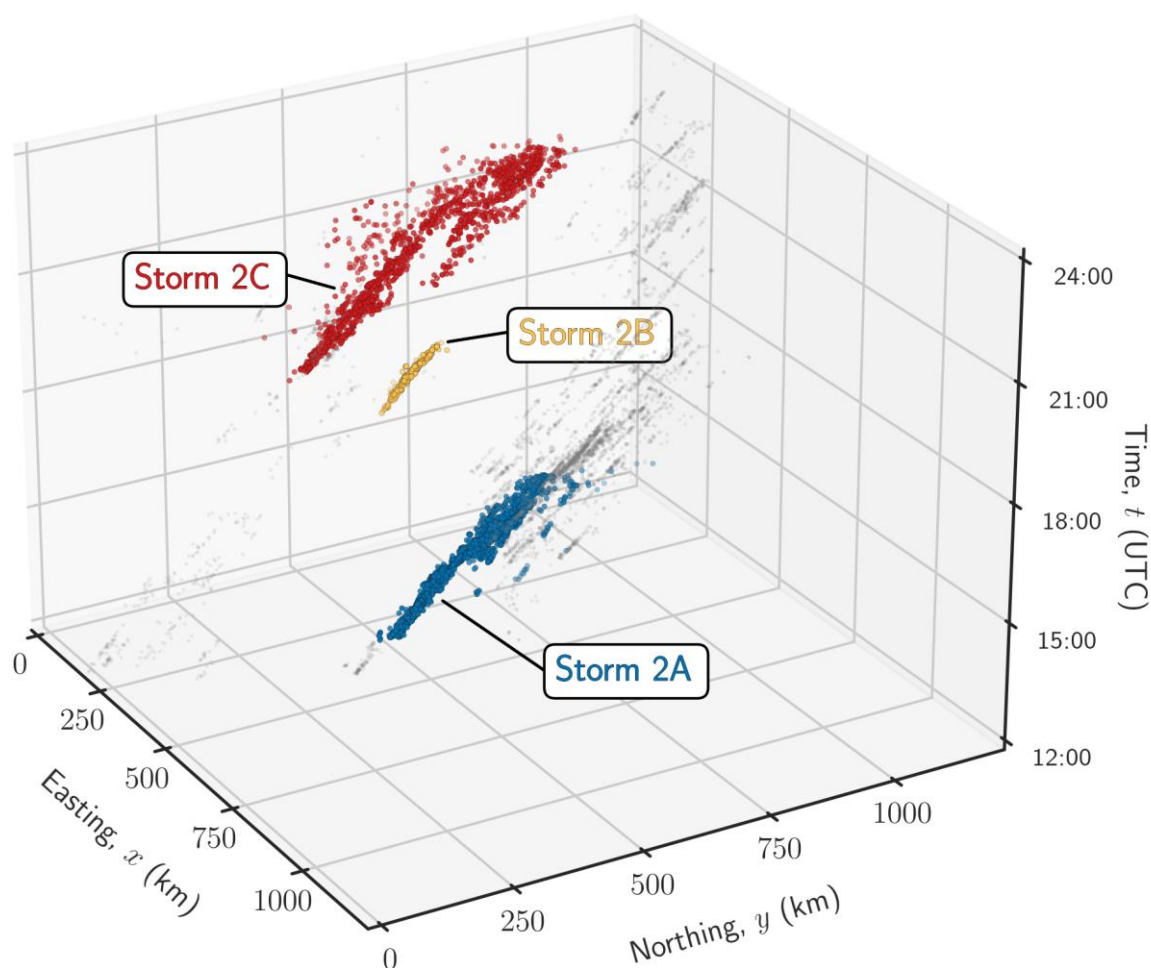


Figure 8: Spatial extent and propagation of the lightning strike occurrences as recorded on 1 July 2015 by the ATDnet system (Gaffard et al., 2008) and projected onto the OSGB 1936 / British National Grid northing/easting coordinates. Lightning strikes assigned to the identified thunderstorms (Storms 2A, 2B, 2C) correspond to the relevant synoptical analysis (Lewis and Silkstone, 2017) and all the remaining unassigned strikes are coloured as per the legend.

In **Fig. 8**, the separation of the three individual thunderstorms on 1 July 2015 from the unassigned lightning strikes is clearer than the lightning strike clusters on 28 June 2012, as shown in **Fig. 2**. There are fewer unassigned lightning strikes for 1 July 2015, and the temporal separation is greater than in the first case study, for 28 June 2012. For this second case study, all three storms had the same level of descriptive and radar information available and does not add ambiguity to the assignment of individual lightning strikes to thunderstorms.



285

For this second case study, the six one-hour intervals of the lightning strikes as assigned to the individual thunderstorms relative to the locations of the three Doppler radar stations are shown in **Fig. 9**. These six intervals were chosen to cover the full temporal range of the lightning strikes as produced by the three thunderstorms but are not continuous due to the significant temporal gap between Storms 2A and 2B.

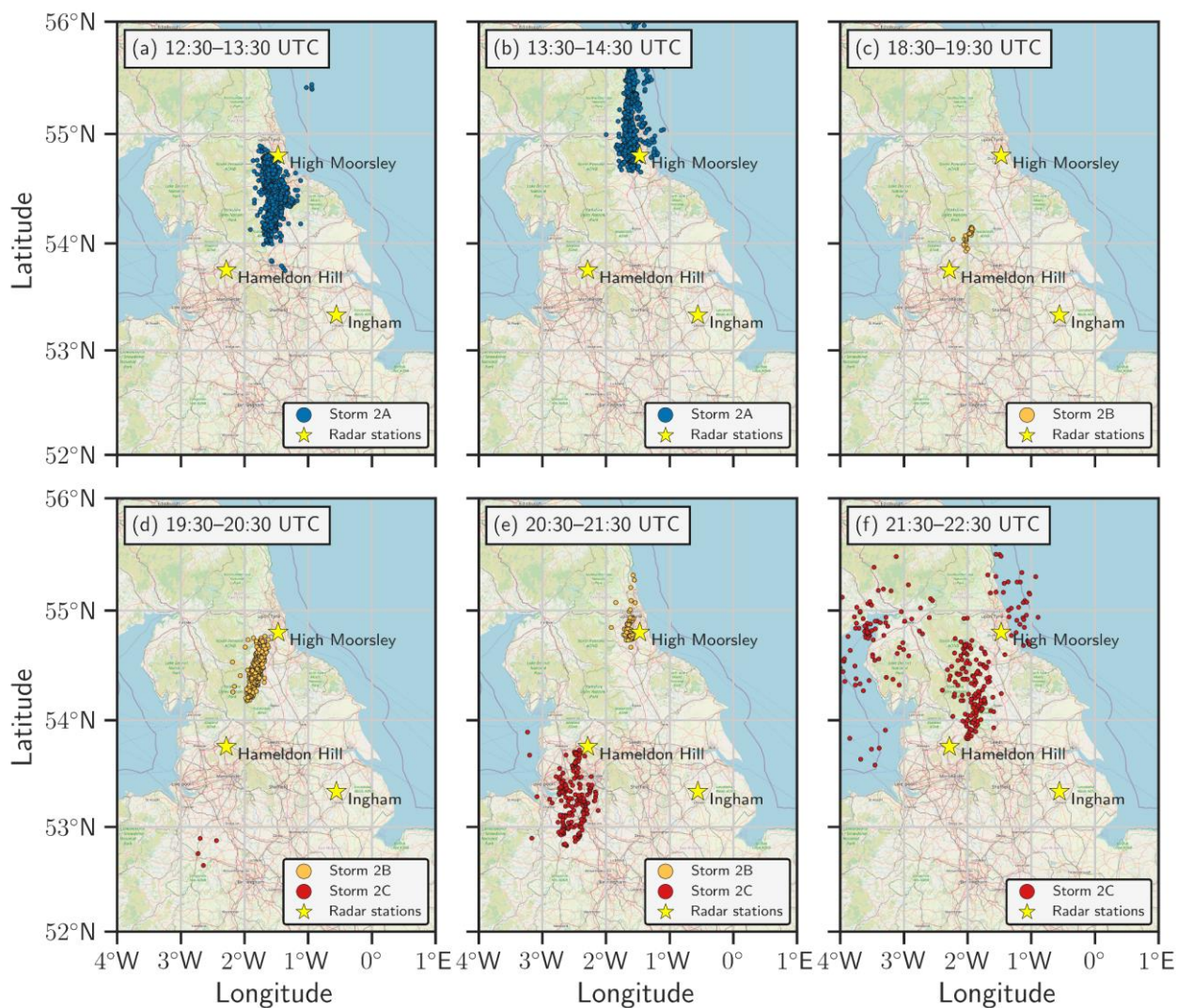


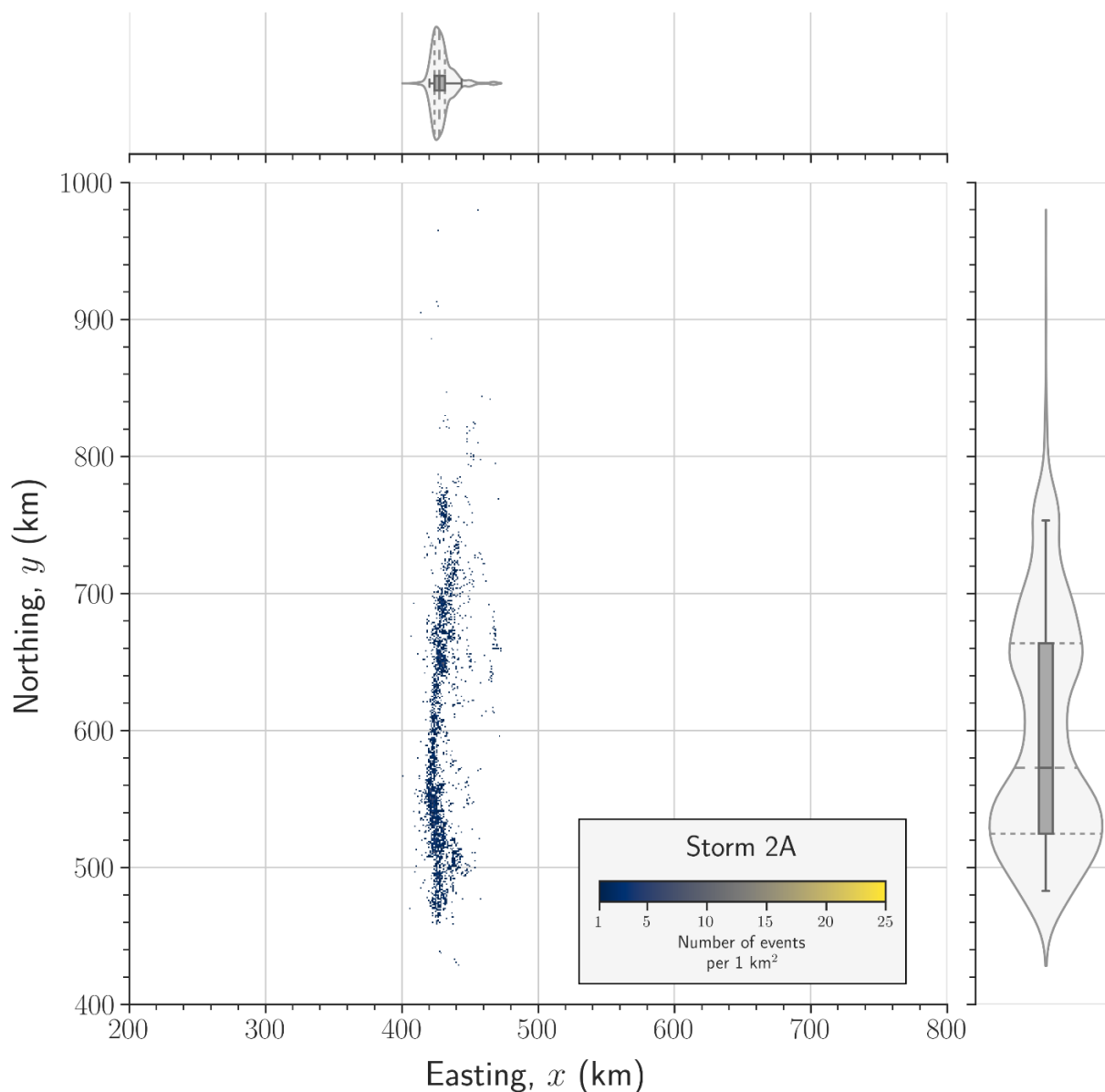
Figure 9: Spatial extent for 1 July 2015 of the lightning strike occurrences as recorded by the ATDnet system (Gaffard et al., 2008) over times intervals corresponding to the relevant synoptical analysis (Lewis and Silkstone, 2017) (a) 12:30–13:30, (b) 13:30–14:30, (c) 18:30–19:30, (d) 19:30–20:30, (e) 20:30–21:30 and (f) 21:30–22:30 UTC. Note that not every one-hour interval is plotted. Only lightning strikes assigned to any of the three selected thunderstorms (Storms 2A, 2B, 2C) are shown. Locations of relevant Doppler radar stations are added as per the legend for direct comparison with synoptical analysis. Background map information from OSM (© OpenStreetMap contributors 2022. Distributed under the Open Data Commons Open Database License (ODbL) v1.0.).

290



295

All three thunderstorms from 1 July 2015, when viewed in the projected two-dimensional spatial domain, cross northern England in a south-to-north direction. The locations of the Hameldon Hill, High Moorsley and Ingham radar stations allow for direct comparison with relevant figures in the synoptic analysis. The two-dimensional spatial count of lightning strikes per 1 km² for Storm 2A is displayed in **Fig. 10**. The same plots for Storm 2B and Storm 2C can be found in **Appendix C**.



300

Figure 10: 2D spatial count of lightning strikes per 1 km² of the OSGB 1936 / British National Grid northing/easting coordinates for thunderstorm 2A (1 July 2015). Only bins with more than one lightning strike are coloured. Note that the northing and easting extents are the same, but the axes limits differ. The marginal distribution is indicated by overlapping boxplots and violin plots for both the easting and northing values. Boxplots indicate the quartiles and have whiskers for the 5th and 95th percentiles, while the violin plots include all values.



As Storm 2A travels in the S-N direction, the lightning strikes assigned to Storm 2A cover a significantly larger scale in the northing direction (from 420 km to 980 km), while in the easting direction – from 400 km to 480 km. Areas of relatively higher lightning intensity are located at the beginning of the propagation track of the storm. The marginal distribution of the northing coordinates shows a separation between two areas of increased count values at $y = 600$ km.

To gain an overview of the spatial and temporal extents for the six identified thunderstorms, a summary table from the marginal distributions of the northing and easting coordinates and the times of occurrence is presented in **Table 2**. The occurrence time values are presented as hours starting at 00:00 UTC on 28 June 2012 for the first case study and 00:00 UTC on 1 July 2015 for the second.

Table 2: Ranges for spatial and temporal coordinates for the six thunderstorms on 28 June 2012 (Storms 1A, 1B, 1C) and 1 July 2015 (Storms 2A, 2B, 2C).

Date	Storm	Extent of easting values	Easting 5 th and 95 th percentiles	Extent of northing values	Northing 5 th and 95 th percentiles	Extent of time of occurrence values	Time of occurrence 5 th and 95 th percentiles
		$X_{\max} - X_{\min}$ (km)	X_5, X_{95} (km)	$Y_{\max} - Y_{\min}$ (km)	Y_5, Y_{95} (km)	$t_{\max} - t_{\min}$ (h)	t_5, t_{95} (h)
28 June 2012	1A	186	351, 460	199	222, 330	4.4	7.0, 9.74
	1B	153	419, 517	139	273, 363	3.2	10.5, 13.3
	1C	136	451, 528	90	293, 356	1.8	12.1, 13.7
1 July 2015	2A	73	420, 444	562	483, 753	3.2	12.8, 15.5
	2B	41	403, 424	115	477, 547	1.6	18.5, 19.6
	2C	322	296, 455	543	359, 768	4.7	19.9, 23.8

4. Methods to characterise and model lightning strike variables in time and space

This section first introduces the physical variables used as characteristics of lightning strikes (**Section 4.1**). Three physical variables are then selected for characterisation and inclusion in a spatio-temporal model framework: lightning strike inter-event occurrence time (**Section 4.2**), lightning strike cluster movement speed (**Section 4.3**) and spatial spread (**Section 4.4**). Each of these variable subsections first presents the methodologies used to characterise the variable and then details the approach taken to include the variable into a spatio-temporal point event model framework. Then in **Section 5**, characterisation results for all three variables are presented and analysed, while in **Section 6**, the modelling approach is detailed, analysed and examples of synthetic point event datasets representative of lightning strikes are shown.



4.1 Lightning variables

Lightning as a natural hazard has been characterised by various methodologies, depending on the data type and purpose of the particular study. Characteristic variables depend on whether lightning data is analysed as a physical phenomenon (i.e. lightning flash) or as a point event in time and space. Each approach has distinct variables that can be characterised and used for various modelling approaches.

Lightning as a physical phenomenon has extensive research on the underlying physics that determine the initiation, propagation and phenomena related to lightning (Rakov, 2013; Dwyer and Uman, 2014). From direct current measurement, the most common variables related to this approach to lightning characterisation include peak current, waveshape, the velocity of the return stroke and the total flash charge (Chowdhuri et al., 2005). Using high-speed cameras, characterisation focuses on continuing current duration, time intervals between strokes, number of strokes per flash, total flash duration, flash multiplicity and inter-stroke intervals (Saba et al., 2006; Ballarotti et al., 2012). When analysing lightning strikes as point events recorded by the lightning location systems (described in **Section 3.1**), the relevant variables are not directly physical. This publication focuses on the statistical properties of the events process (identified at the individual storm) more than on physical characteristics.

Variables such as lightning event (either as lightning flash or strike) count, density per month and/or per area unit, distribution per time unit, mean inter-stroke intervals, and multiplicity have been used to characterise lightning point events. Spatial extent for these variables varies from global (Mezuman et al., 2014), continental (e.g. Europe [Anderson and Klugmann, 2014; Enno et al., 2020]), regional (e.g. eastern Mediterranean [Yair et al., 2014], Mediterranean [Kotroni and Lagouvardos, 2016], Iberian Peninsula grid [Soriano et al., 2005]) to national (e.g. Austria [Schulz et al., 2005], Poland [Taszarek et al., 2015]) scales. In these studies, the spatial domain is gridded by either latitude/longitude (e.g. $0.1^\circ \times 0.1^\circ$ grid (Kotroni and Lagouvardos, 2016), $0.2^\circ \times 0.2^\circ$ grid [Soriano et al., 2005; Anderson and Klugmann, 2014; Enno et al., 2020]) or directly on Cartesian grid cells (e.g. $10 \text{ km} \times 10 \text{ km}$ cells [Taszarek et al., 2015]). Temporal scales for these variables range from hourly, diurnal, monthly, seasonal to yearly characterisation.

These variables are also characterised not only per spatial and/or temporal unit but also by introducing additional lightning-specific nomenclature, stratification of lightning events, or consideration of their relationship with other meteorological variables. For example, the variables can be characterised per thunderstorm day (i.e. at least two flashes occurring within 20 km from the centre of a grid cell from 00:00 to 23:59 UTC [Enno et al., 2020]). The lightning events can be stratified by their occurrence over land or sea areas (Mezuman et al., 2014). Variables can also be characterised by their relationship to sea surface temperature (Kotroni and Lagouvardos, 2016).



This publication selects lightning strike variables to characterise the storm behaviour in both spatial and temporal domains. Initial data stratification occurs by grouping the lightning strike data into individual thunderstorms (**Section 3.2** and **Section 3.3**). For each thunderstorm, the behaviour in the temporal domain is first characterised by analysing the lightning strike inter-event time variable $\Delta\tau$ (**Section 4.2**). In the spatial domain, the lightning strike spread is analysed around an estimated thunderstorm movement track. This spread is characterised by easting and northing distances (Δx and Δy) from the movement track (**Section 4.4**). In the combined spatio-temporal domain, the estimated movement speed v of the individual thunderstorms producing the lightning strikes is characterised (**Section 4.3**).

4.2 Variable $\Delta\tau$: Lightning strike inter-event time

The first physical variable that is characterised and modelled is the inter-event occurrence time $\Delta\tau$, with

$$\Delta\tau_i = t_{i+1} - t_i \text{ for } i = 1, \dots, N - 1$$

(1)

where t is time, and i an index on t representing discrete instances where events (lightning strikes) occur, noting that these events are not equally spaced in time. For each thunderstorm, the characterisation process of the inter-event time data consists of descriptive analysis of inter-event occurrence time $\Delta\tau$ distribution. Distributions are analysed for each thunderstorm's complete lightning strike dataset and in one-hour time intervals for their duration (**Section 5.1**).

To include inter-event occurrence time as an input parameter for the spatio-temporal lightning strike model (**Section 6.1**), the inter-event occurrence time $\Delta\tau$ data is processed in two steps:

Step 1. Sampling from an empirical cumulative distribution function eCDF – synthetic inter-event time occurrence time values $\Delta\tau$ are generated to create a synthetic dataset without any temporal structure.

Step 2. Re-indexing sampled inter-event times $\Delta\tau$ – temporal structure is added to the synthetic data by using autocorrelation function $C(\Delta k)$ in inter-event occurrence times $\Delta\tau$ arranged in order of occurrence k from the individual thunderstorm datasets.

Inter-event time step 1 follows a methodology for non-parametric sampling from an empirical cumulative distribution (Ivezić et al., 2014). To generate a set of sampled inter-event occurrence time $\Delta\tau$ values from a real-world dataset, the Step 1 sampling methodology consists of three individual operations:

1.1 Sorting – the set of inter-event occurrence times $\Delta\tau$ is sorted, and the rank of each time value is used to approximate the empirical cumulative distribution.

1.2 Inverting cumulative distribution – the empirical cumulative distribution eCDF has the axes inverted to give the inverse empirical cumulative distribution.

1.3 Spline fitting – a cubic spline fit to the inverse distribution is performed. As a result, a uniformly sampled x -axis value maps to a y -axis value, approximating the observed inter-event occurrence time probability distribution function.

Inter-event time step 2 introduces temporal structure in the synthetic inter-event occurrence time $\Delta\tau$ dataset from the individual thunderstorms. Such information on the temporal structure can be given by applying the autocorrelation function to the $N-1$



inter-event occurrence times $\Delta\tau$. The dataset from each individual thunderstorm is set in the order of occurrence k and the formulation of the autocorrelation function $C(\Delta k)$ (Priestley, 1981) for a given lag Δk is

$$C(\Delta k) = \frac{1}{\sigma_{\Delta\tau}^2} \frac{1}{N-1-\Delta k} \sum_{k=1}^{N-1-\Delta k} (\Delta\tau_{k+\Delta k} - \overline{\Delta\tau})(\Delta\tau_k - \overline{\Delta\tau}) \quad (2)$$

After Step 1, a synthetic inter-event occurrence time dataset T_S is generated with the same length as any of the individual thunderstorm inter-event occurrence time datasets (T_{1A}, \dots, T_{2C}). The methodology used in Step 2 for these two datasets consists of three individual operations:

- 2.1 Sorting – the inter-event occurrence time datasets T_S and corresponding thunderstorm dataset are sorted by their value and ranked.
- 2.2 Re-indexing – the synthetic dataset T_S has its inter-event occurrence times re-indexed to replicate the same ranking of inter-event occurrence times as the thunderstorm dataset.
- 2.3 Autocorrelation comparison – autocorrelation function $C(\Delta k)$ is applied to both datasets to ensure that the temporal structure of the thunderstorm data remains in the synthetic dataset T_S .

4.3 Variable v : Lightning strike cluster movement speed

The second physical variable that can be characterised and modelled is the assumed constant movement speed v of the lightning strikes as a point-event cluster (i.e. representative of an individual thunderstorm). The approach to estimating the movement speed of the cluster is to perform a least-squares plane and linear fits to the lightning strike data. The lightning strike occurrence times t are assumed to depend on the easting x and northing y values as the thunderstorms producing these strikes move through the area and time of the study. Such a relationship between the dimensions can be expressed as

$$\begin{pmatrix} x_1 & y_1 & 1 \\ \vdots & \vdots & \vdots \\ x_N & y_N & 1 \end{pmatrix} \begin{pmatrix} a \\ b \\ c \end{pmatrix} = \begin{pmatrix} t_1 \\ \vdots \\ t_N \end{pmatrix}$$

or

$$\mathbf{A}\boldsymbol{\beta} = \mathbf{t} \quad (3)$$

where \mathbf{A} is the matrix of the available spatial data (easting x and northing y values) as the first two columns. Vector $\boldsymbol{\beta}$ contains the three plane parameters that will be estimated by the best plane-fit. Vector \mathbf{t} contains all the occurrence time t values. Finding the plane parameters in vector $\boldsymbol{\beta}$ is an over-determined problem (the number of equations outnumbers the unknowns), so the left pseudo-inverse of the matrix \mathbf{A} is calculated. The least-squares approach then minimises the vertical (i.e. temporal) distance between the lightning strikes and the plane, returning the best plane-fit that can be thought of as the cross-**Section** of the thunderstorm producing these strikes (**Section 5.2**).



As the best-fit plane coefficients are estimated from the least-squares fit, the movement speed v can be estimated as the inverse of the dip angle as given by these coefficients a and b

$$415 \quad v = \frac{1}{\sqrt{a^2 + b^2}} \quad (4)$$

To further characterise the movement speed v after using the least-squares fit, the movement speed is returned with a goodness-of-fit calculation for each thunderstorm. This calculation consists of finding the root square mean error (RMSE) of the residuals between vector \mathbf{t} and $\mathbf{A}\boldsymbol{\beta}^*$ where $\boldsymbol{\beta}^*$ is the resulting parameter vector as found by the least-squares plane-fit.

420 A least-squares linear fit can also be used to estimate the movement speed v . Such approach (applied for aftershock identification in seismology [Zaliapin and Ben-Zion, 2013], tornado touchdown location clustering and movement speed calculation [Malamud et al., 2016] and storm movement speed [Finke, 1999]) works in the spatio-temporal lag space $\{\Delta s, \Delta t\}$, where the spatial lag Δs and the temporal lag Δt between any two lightning strikes $i = 1, \dots, N$ and $j = 1, \dots, N-1$ is the Euclidean distance and the time difference between them respectively

$$425 \quad \Delta s_{ij} = \sqrt{(x_i - x_j)^2 + (y_i - y_j)^2} \quad (5)$$

$$\Delta t_{ij} = |t_i - t_j| \quad (6)$$

430 As $\Delta s_{ij} = \Delta s_{ji}$ and $\Delta t_{ij} = \Delta t_{ji}$, the duplicate data points are removed. It is assumed that in the spatio-temporal lag space $\{\Delta s, \Delta t\}$, the least-squares linear fit with an intercept set to pass through the origin returns the movement speed v from

$$\begin{pmatrix} \Delta t_1 \\ \vdots \\ \Delta t_{\frac{N(N-1)}{2}} \end{pmatrix} v = \begin{pmatrix} \Delta s_1 \\ \vdots \\ \Delta s_{\frac{N(N-1)}{2}} \end{pmatrix}$$

or

$$435 \quad \mathbf{T}v = \mathbf{S} \quad (7)$$

where \mathbf{T} is the vector of all temporal and \mathbf{S} is the vector of all spatial lags for N data points. The procedure that follows is the same as for **Eq. 3**. As input for the spatio-temporal lightning strike model (**Section 6.3**), the movement speed v is used as a direct input parameter and assumed constant.

4.4 Variables Δx and Δy : the spatial spread of the lightning strikes as a cluster

440 The third physical variable that is characterised and modelled is the spatial spread of the lightning strike as a cluster belonging to a particular thunderstorm. To characterise this variable, it is necessary to return an estimate of the track of the thunderstorm



to have a reference against which to calculate the spatial spread. The spatial spread in the data can be characterised and modelled by two variables - easting and northing distances to the track (Δx and Δy). The calculation of these variables can be summarised in two steps:

1. Application of uniform filter – uniform filters are applied to easting x and northing y values in order of occurrence k to return a movement track.
2. Calculation of easting and northing distances – for each order of occurrence k , the easting and northing distances to the track (Δx and Δy) are calculated.

For spatial spread step 1, the movement track is assumed to be non-linear. It is estimated by applying a uniform linear filter on the easting/northing (x, y) coordinates (in the OSGB 1936 / British National Grid) of the lightning strike dataset in the order of occurrence k instead of real-time. The filter is used with a window size of Δw . When window size causes the average calculation at a given k to exceed the length of the northing and easting data vectors, the approach uses duplicates of the first or the last values accordingly. For spatial spread step 2, at each order of occurrence k , the calculation of ($\Delta x, \Delta y$) can be directly done with the easting/northing (x, y) and the estimated movement track coordinates (**Section 5.3**).

A methodology for fitting and sampling a bivariate normal distribution is implemented to include the easting and northing distances to the track (Δx and Δy) variables in the spatio-temporal lightning strike model (Ivezić et al., 2014). This methodology is robust with respect to outliers in the data. This is important due to the approach's simplicity in estimating the movement track. To return the parameters of the bivariate normal distribution, it (i) uses the median instead of the mean and (ii) uses the interquartile range to estimate variances.

Once the distribution parameters are found, easting and northing distances to the track (Δx and Δy) are sampled directly from this distribution for implementation in the spatio-temporal lightning strike model (**Section 6.2**).

5. Results of variable characterisation

This section presents the results of characterising the three lightning storm variables (inter-event times, movement speed, and distance to movement track) discussed in **Section 4**. These variable characterisations are for the six lightning strike storms (28 June 2012: Storms 1A, 1B, 1C; 1 July 2015: Storms 2A, 2B, 2C) as detailed in **Section 3**.

5.1 Lightning strike inter-event times

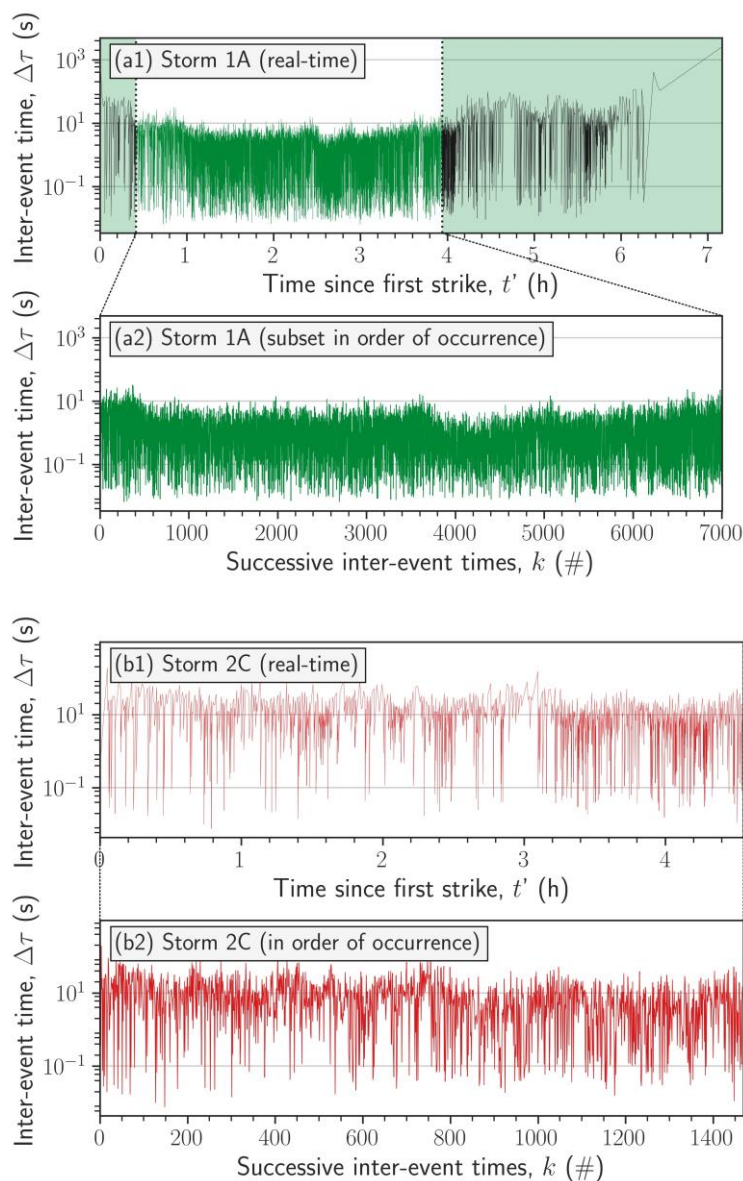
It is observed for most of the storms that the beginning and end are visually different in time, and therefore, we manually remove continuous time intervals from the lightning strike datasets assigned to individual thunderstorms. A subset of each storm's strike dataset was used to characterise the lightning inter-event times. The purpose was to remove those values that either (i) contained relatively large inter-event time values or (ii) had longer time periods between consecutive lightning. The original dataset of inter-event times $\Delta \tau$ without further processing is shown first in real-time. If the time of occurrence of the first lightning strike is t_1 , the time axis is shifted to indicate the time since first strike t'



$$t' = t - t_1$$

(8)

475 After the removal of time periods that were deemed visually different in time, the end inter-event time $\Delta\tau$ dataset for further characterisation is shown in order of occurrence k . This processing step is illustrated for storms 1A and 2C in **Fig. 11** (all storms are shown in **Appendix Fig. D1**).



480 **Figure 11:** Two subplots showing the removal of inter-event time $\Delta\tau$ values in real-time t (removal of the black line in upper subfigure) and the subsequent inter-event time time-series in order of occurrence k (lower subfigure) for thunderstorms (a1) 1A (real-time, 7,000 values), (a2) 1A (subset in order of occurrence, 7,000 values), (b1) 2C (real-time, 1,468 values), (b2) 2C (subset in order of occurrence, 1,468 values).

In **Fig. 11**, we show the selection of a portion of the time series. For Storm 1A in **Fig. 11a1**, there is an increase in inter-event time values for the first 0.2 hours and after the fourth hour of storm duration. There are also several longer time periods between consecutive inter-event times after the fourth hour. These two time periods were removed to leave a lightning strike subset of $n = 7,000$ inter-event times for further characterisation. For storm 2C in **Fig. 11b1**, there were no clear time periods of increased inter-event times or extended time periods between inter-event times. No time periods were removed for storm 2C.

After the data processing to establish light strike subsets with less ambiguity in their assignment to a particular thunderstorm, we can analyse the distribution of the inter-event times. Violin plots for the inter-event time $\Delta\tau$ subsets of all six thunderstorms are shown in **Fig. 12**.

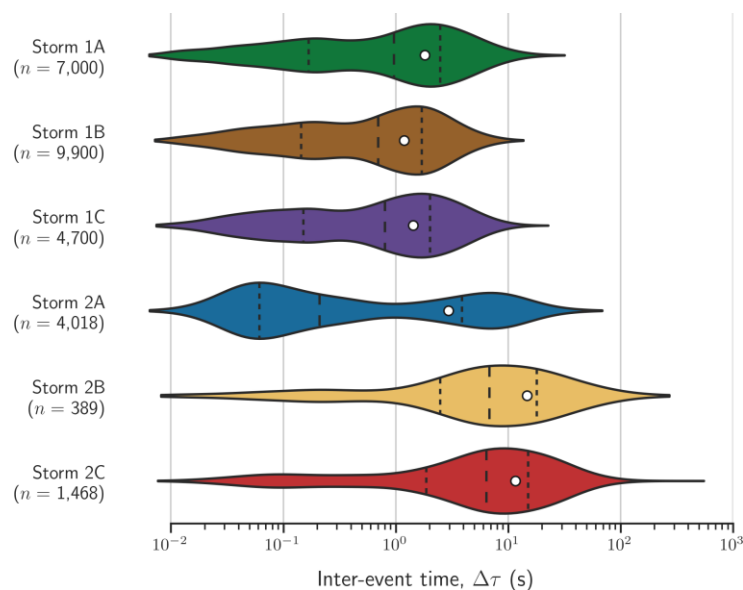


Figure 12: Violin plots of inter-event time $\Delta\tau$ distributions for all six selected thunderstorms. For each thunderstorm, the total number of observations after removing inter-event time values (Fig. 11) of the time-series is indicated by n , dotted lines denote the quartiles, and the white-dot represents the mean.

In **Fig. 12**, the inter-event times for all six thunderstorms cover four orders of magnitude, ranging from below 0.01 s to over 100 s. For storms 1A, 1B and 1C, the empirical distributions cover similar ranges of 0.01 s to 20–30 s. They show two peaks – a smaller one for values around 0.2 s and a larger one around 1–3 s and their quartiles are all within the same order of magnitude over all three storms.

The empirical distributions show more variability for storms 2A, 2B, and 2C. They include larger inter-event time values (more than 100 s) and show varying distribution shapes. Storm 2A has a larger peak around 0.05 s and the smaller one at around 7–8 s, which differs from the other five storms. The empirical distributions for storms 2B and 2C are similar, with a clearer single peak centred at 8–10 s and covering the full range of inter-event times.

For each storm, the empirical distributions of inter-event times are also represented hourly for the full duration of each individual storm in **Fig. 13**.

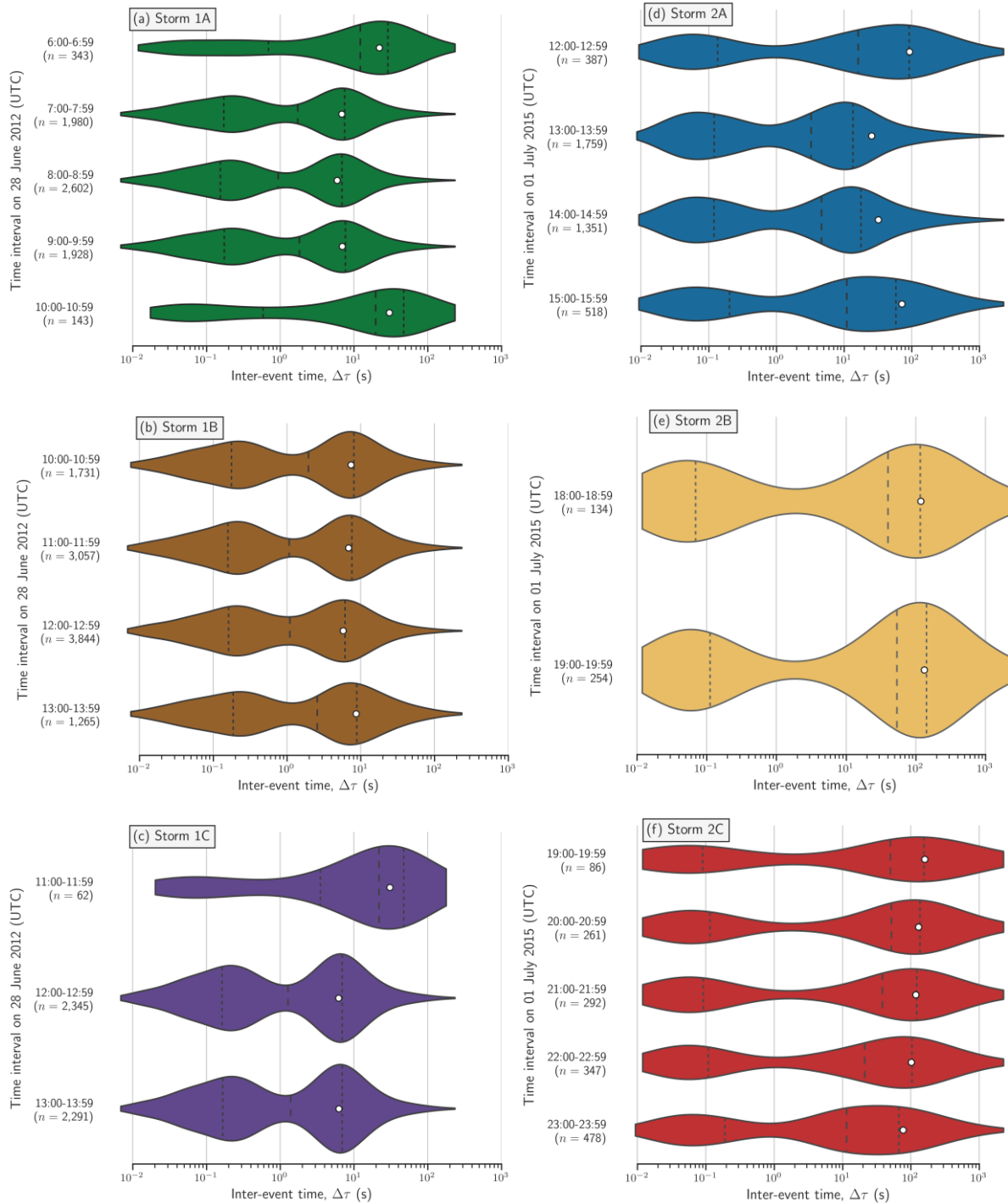


Figure 13: Violin plots of inter-event time $\Delta\tau$ distributions for each one-hour interval when lightning strikes were observed after cutting (Fig. 11) of the time-series for Storm (a) 1A, (b) 1B, (c) 1C, (d) 2A, (e) 2B and (f) 2C. The total number of lightning strikes in each interval is indicated by n , dotted lines denote the quartiles, and the white-dot represents the arithmetic mean.



515

In **Fig. 13**, the empirical distributions, shown in one-hour intervals, allow for assessing each storm's duration and the changes to inter-event time distributions over this duration. Storms (b) 1B, (e) 2B and (f) 2C, while having varied durations, do not exhibit significant changes to the inter-event time distribution over one-hour intervals. Storms (a) 1A, (c) 1C and (d) 2A exhibit a more significant change for the first or last one-hour intervals. For these storms and intervals, the larger peak in the distribution is seen at larger inter-event time values (e.g. mean values of 20–40 s for the first and last one-hour intervals compared to 6–8 s for others from storm 1A) with less significant smaller peak compared to other one-hour intervals.

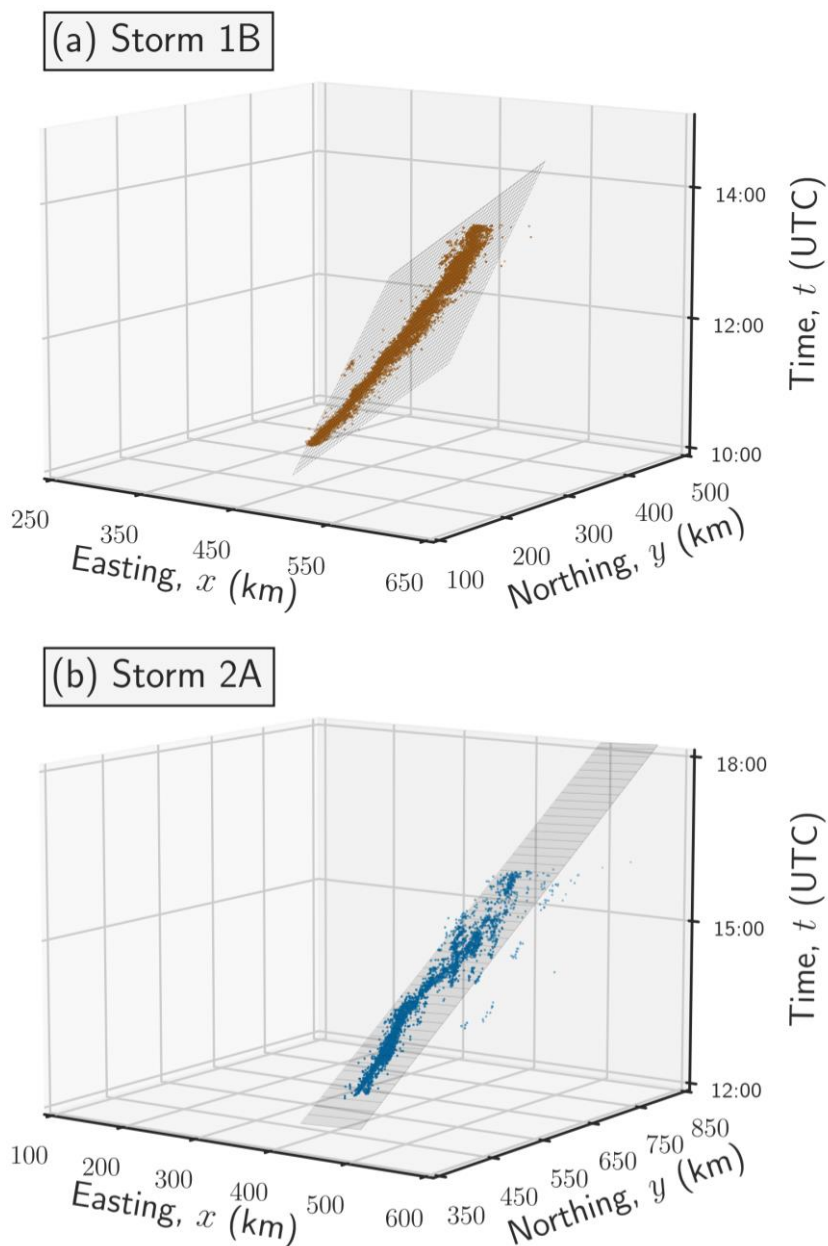
520

Due to the assignment methodology for individual lightning strikes and the cutting of the datasets, it is not easy to analyse these variations in the first and last one-hour intervals as characteristics of the thunderstorms. For storms without a noticeable difference, the cutting could have removed significant time periods from the storm that contained the more detailed beginning and end of the storm. These one-hour intervals are also chosen to cover one-hour intervals from the full hour. Changes to the starting time of the one-hour intervals and to the length of the interval time period could alter the distribution of inter-event times at the beginning and end of the storms.

5.2 Movement speed

525

For the movement speed variable v (**Section 4.3**), the results of the least-squares plane-fit to the lightning strikes assigned to storms 1B and 2A using the thunderstorm datasets as detailed in **Section 5.1** are shown in **Fig. 14** (the best-fit plane solution is overlaid as a wireframe over the individual lightning strikes and all storms shown in **Appendix E**).



530 **Figure 14:** Least-squares plane-fit solution to the lightning strike datasets for (a) Storm 1B (28 June 2012, $n = 9,901$ events, $v = 47$ km h^{-1}), and (b) Storm 2A (1 July 2015, $n = 4,019$ events, $v = 108$ km h^{-1}). The colour scheme for each storm's lightning strikes is consistent with Figs. 2–5 and the best-fit plane is drawn as grey wireframes. Note that all three axes have different extents for each storm, while the ratio between the axes is constant.

535 Converting the lightning strike data into spatial and temporal lag space $\{\Delta s, \Delta t\}$, the resulting movement speed variable v estimates from the linear least-squares fits for storms 1A and 2C are shown in **Fig. 15a** and **Fig. 15b**, respectively (figures for all storms are shown in **Appendix F**).

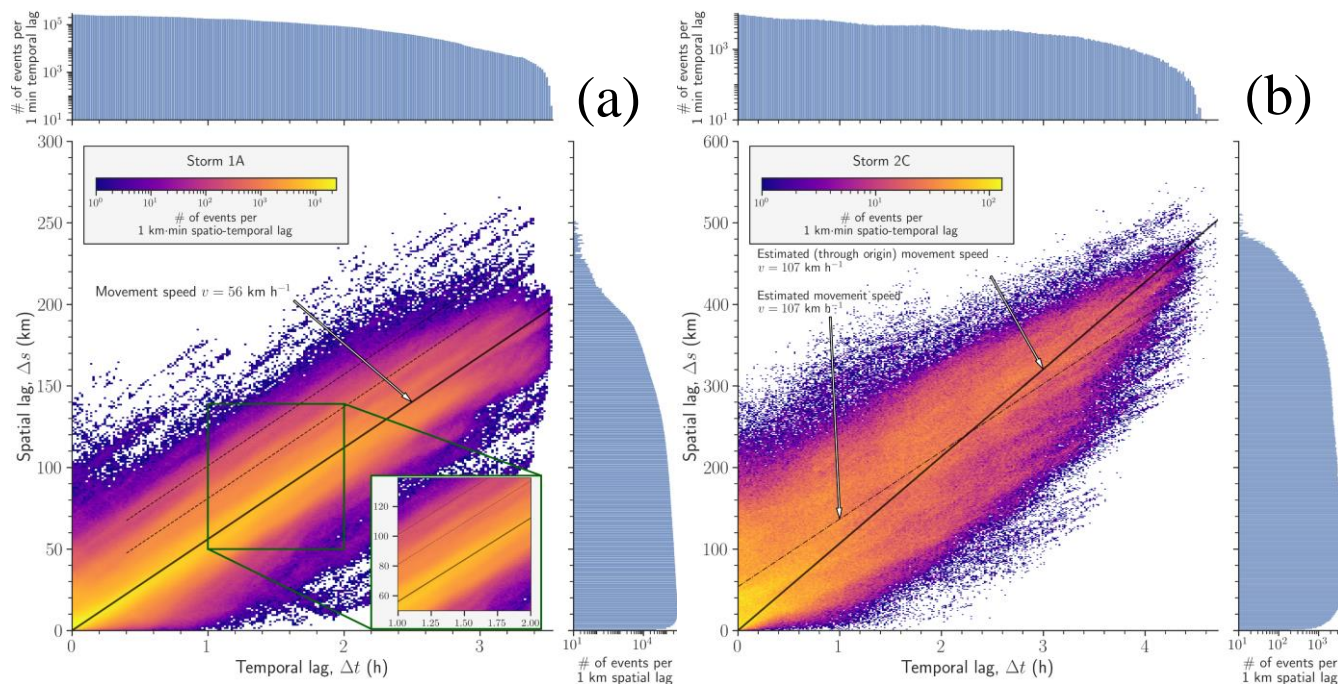


Figure 15: (a) Storm 1A (28 June 2012, $n = 7,001$ events, $v = 56 \text{ km h}^{-1}$) and (b) storm 2C (1 July 2015, $n = 1,469$ events, $v = 107 \text{ km h}^{-1}$) least-squares linear-fit solution and 2D count of lightning strikes per 1 km-min in the spatio-temporal lag space. Bins are coloured according to the given logarithmic colour scale. The marginal bin counts per 1 km spatial lag and 1 min temporal lag are given above and to the right of the main plot. The abrupt vertical end of lightning strike data in (a) at $\Delta t = 3.45 \text{ h}$ occurs due to the removal of inter-event time values (see Fig. 11). The solid black line indicates the best-fit linear line passing through the point of origin, while the dash-dotted line in (b) indicates the best-fit linear line. The two dashed lines in (a) parallel to the dark line, both set with identical $v = 56 \text{ km h}^{-1}$, indicate other areas of increased count density (bandings of orange pixels as seen in the enlarged subfigure in the lower right corner). These lines are set manually to emphasise the visually observable structure in the data.

The results for the movement speed v calculations from the plane-fit (Fig. 14 and Appendix E) and linear-fit (Fig. 14, Fig. 15 and Appendix F) and the RMSE of the residuals between strike data and the best-fit plane-fit are indicated in Table 3.

Table 3: Results of least-squares plane-fit and linear-fit solutions to lightning strike data for six UK thunderstorms.

Date	Storm	Movement speed from best plane-fit, v (km h^{-1})	Movement speed from best linear-fit in lag space, v (km h^{-1})	RMSE of plane-fit residuals (h)
28 June 2012	1A	58	56	0.17
	1B	47	48	0.12
	1C	59	60	0.11
1 July 2015	2A	108	101	0.23
	2B	67	66	0.07
	2C	111	107	0.40

In Table 3, the calculated lag Δt speeds from the two approaches vary between the two storm-systems. Storms 1A, 1B and 1C return similar values in the range of 47–60 km h^{-1} and Storms 2A, 2B and 2C show greater variability and higher



values, ranging from 66–111 km h⁻¹. The goodness-of-fit estimation for the best plane-fit solutions shows low variability between the storms of the first case study (1A, 1B and 1C). For the second case study (2A, 2B and 2C), the variation is higher with storm 2B having the lowest RMSE of 0.07 hours, while storm 2C has the highest at 0.40 hours.

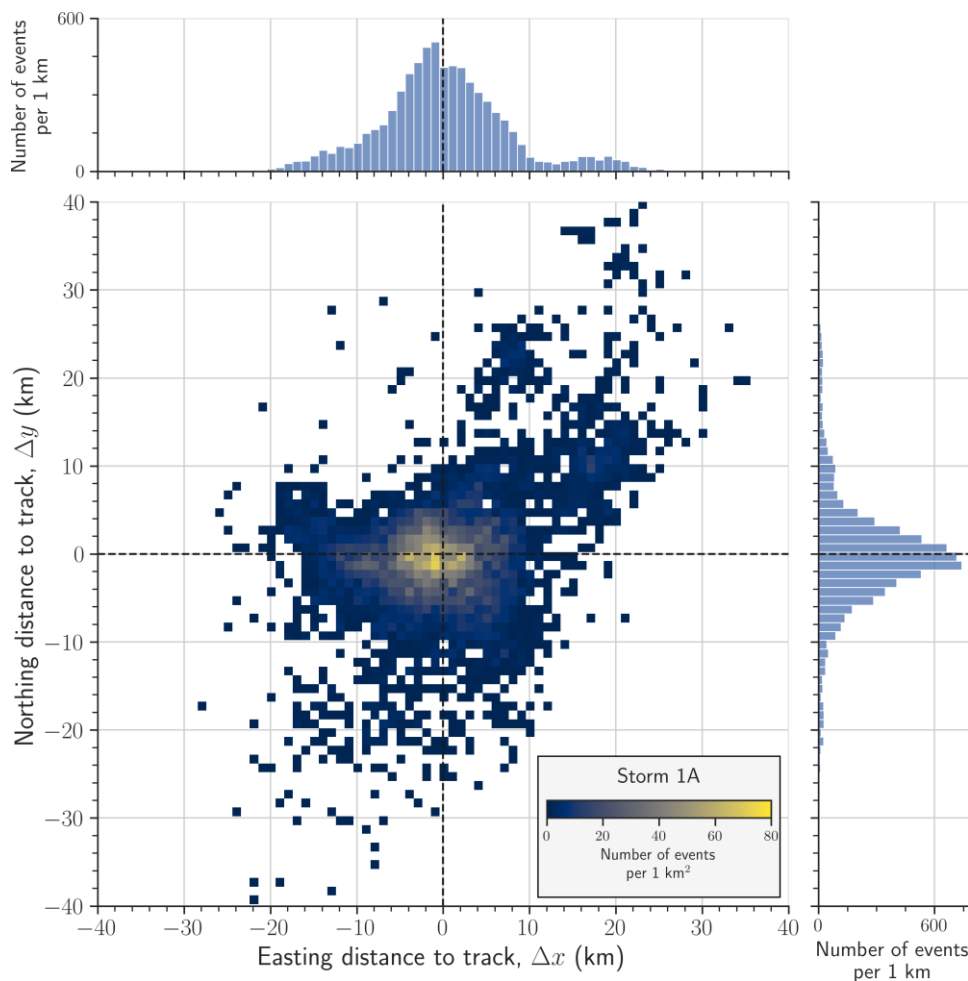
555 In **Fig. 15**, the least-squares linear-fit solution in the spatio-temporal lag space returns more detailed information on the structure of each thunderstorm relative to using just a least-squares plane-fit with a goodness-of-fit estimate (**Fig. 14**). In the spatio-temporal lag space, the storm's movement speed is initially assumed to pass through the point of origin. When looking at the structure of the 2D count plots (**Fig. 15a** for storm 1A, **Fig. 15b** for storm 2C and **Appendix F** for other storms), additional structures can be seen in the data that either do not pass through the point of origin and move at a different movement speed.

560 Initial observation of the 2D count plots shows bandings of pixels that indicate lines in the spatio-temporal lag space that do not pass through the point of origin but have a similar gradient (i.e. movement speed). This would indicate that this larger lightning strike cluster (i.e. thunderstorm) consists of several smaller ones, each moving as part of the cluster with similar movement speeds (as seen by the dashed line examples in the enlarged subfigure for storm 1A in **Fig. 15a**).

565 It is also observed that bandings of pixels with different movement speeds within the same lightning strike dataset exist. The resulting movement speed value also depends on the assumption of the best-fit line passing through the origin (as seen by the dash-dotted and solid line examples for storm 2C in **Fig. 15b**). Other storms (**Appendix F**) also show structures in the data that would either have different movement speeds based on this assumption or have bandings of pixels that indicate the presence of smaller clusters in the data.

570 **5.3 Distance to the movement track**

To investigate the distance to the movement track variable (**Section 4.4**), 2D spatial counts of lightning strikes per 1 km² of easting and northing distances for Storm 1A are shown in **Fig. 16** (all storms shown in **Appendix G**).



575 **Figure 16:** 2D spatial count of lightning strikes per 1 km² of the easting and northing distances to the movement track in natural time k for lightning strikes in thunderstorm 1A (28 June 2012) for window sizes $\Delta w = 500$ events. Only bins with more than 1 lightning strike are coloured and the plot is zoomed onto $[-40, 40]$ km intervals for both easting and northing distance. The marginal bin counts per 1 km are given for both northings and eastings.

In **Fig. 16**, the 2D spatial and marginal bin counts for Storm 1A show that lightning strikes do not exceed 40 km distance to the movement track in either dimension. The 2D spatial count ranges from 0–80 lightning strikes per 1 km², while the marginal bin counts reach values of approximately 450 and 650 lightning strikes per 1 km in the easting and the northing domain, respectively.

The highest 2D spatial and marginal bin count values are observed around the origin ($x = 0, y = 0$) (km) point. The deviation in the 2D spatial and marginal bin counts from the origin is more pronounced in the positive (+,+) and negative (-,-) easting-northing distance quadrants.

585 A summary of the characterisation results for all three lightning strike variables, as presented in **Section 5**, is in **Table 4**.



Table 4: Summary of lightning strike characterisation results.

Storm	Movement speed, v (km h ⁻¹)	Inter-event time distribution		Distance to movement track		
		Quartiles $\Delta\tau_{25}, \Delta\tau_{50}, \Delta\tau_{75}$ (s)	Mean $\overline{\Delta\tau}$ (s)	Highest 2D bin count per 1 km ²	Range of easting distance $\Delta x_{\min}, \Delta x_{\max}$ (km)	Range of northing distance $\Delta y_{\min}, \Delta y_{\max}$ (km)
1A	58	0.17, 0.95, 2.45	1.79	73	-61, 35	-80, 48
1B	47	0.14, 0.69, 1.70	1.18	163	-41, 26	-34, 15
1C	59	0.16, 0.81, 2.04	1.44	58	-60, 36	-20, 20
2A	108	0.06, 0.21, 3.61	2.85	28	-43, 28	-226, 67
2B	67	2.42, 6.62, 17.05	13.02	7	-10, 25	-37, 35
2C	111	1.87, 6.41, 14.99	11.54	4	-124, 176	-136, 170

6. Modelling lightning strikes

590 This section presents an approach to modelling lightning strikes as point events in the line of (Finke, 1999), as mentioned in
Section 2.2. The approach incorporates the three lightning storm variables (inter-event times, movement speed, distance to
 movement track) defined in **Section 4** and characterised in **Section 5** into a spatio-temporal model. The movement speed
 variable is set as a constant (including details from **Section 4.3**), while the approaches for incorporating inter-event time and
 distance to movement track are detailed in **Section 6.1** and **Section 6.2**, respectively. The model details and procedure for
 595 creating a synthetic point event dataset are described in **Section 6.3**, with a discussion on the limitations and uncertainties of
 this approach detailed in **Section 6.4**.

6.1 Sampling inter-event times

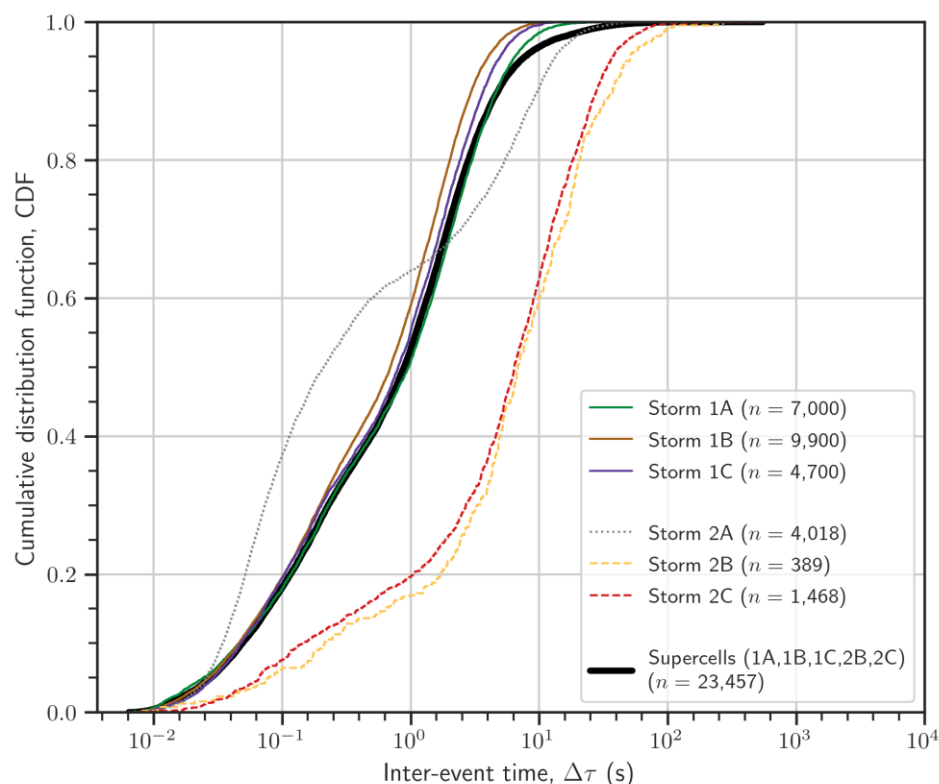
The approach to creating a dataset of inter-event time to use in modelling lightning strikes (**Section 4.2**) involves specifying
 the real-world lightning strike dataset that will control two phases of the approach:

- 600 1. Generation of an empirical distribution – selecting real-world lightning strike data from which to generate an
 empirical distribution function eCDF of inter-event time values $\Delta\tau$.
2. Introduction of autocorrelation – using individual thunderstorms to establish the temporal structure in the data
 representative of lightning data.

The first phase of the inter-event time generation is done to sample inter-event times without any temporal structure. They are
 605 sampled from a larger multi-storm dataset to have values that are not representative of just a single thunderstorm producing
 these events, but of a particular category of thunderstorms. From the synoptic analyses (Clark and Webb, 2013; Lewis and
 Silkstone, 2017) on the selected six thunderstorms (discussed in **Section 3**), these thunderstorms are categorised as supercell

(storms 1A, 1B, 1C, 2B and 2C) or single-cell (storm 2A). For example, we can select the supercell thunderstorms and combine the individual datasets to create a supercell dataset from which to sample inter-event times.

610 A comparison between the cumulative distribution functions (CDFs) for all six individual thunderstorms and the common supercell dataset is shown in **Fig. 17**. The inter-event times are sampled from these CDFs following the methodology described in **Section 4.2**.



615 **Figure 17: Cumulative distribution function (CDF) for the inter-event time $\Delta\tau$ for all six identified thunderstorms and the combined supercell thunderstorm dataset. Individual storms within the storm-system recorded on 28 June 2012 (Storms 1A, 1B and 1C) are indicated by solid lines, while those from storm-system recorded on 1 July 2015 (Storms 2A, 2B and 2C) are indicated by dashed lines. Storm 2A in indicated by a grey line due to being single-cell thunderstorm and is not added to the supercell dataset (black solid line).**

620 **Figure 17** shows the varying CDFs between supercell and single-cell (storm 2A as dashed grey line), showing two clearer distribution peaks for storm 2A. This is expected from what we observed of the inter-event time distribution in **Fig. 12** and **Fig. 13**. The difference between the CDFs of the supercells from both storm-systems is also evident. For the storm system recorded on 28 June 2012 (storms 1A, 1B and 1C), the CDFs shows similar behaviour to the storm system recorded on 1 July 2015 (storms 2B and 2C) but have a distribution peak smaller by an order of magnitude.

625 **Figure 14** also illustrates the contrast in the number of inter-event times n recorded during both storm systems. Storms 1A, 1B and 1C have a combined number of inter-event times $n = 21,500$, while the combined supercell dataset has $n = 23,357$ inter-



event times. The supercell CDF closely resembles that of storms 1A, 1B and 1C with a heavier tail due to the presence of inter-event time data from storms 2B and 2C.

The second step of the inter-event time generation is sorting and re-indexing a sampled inter-event time dataset from the first phase (detailed in Section 4.2). This phase introduces temporal structure in the sampled inter-event time dataset and completes creating an inter-event time dataset representative of real-world lightning data. The results of this two-phase generation procedure for creating synthetic inter-event time datasets representative of storms 1A and 2C are shown in Fig. 18 (all storms are shown in Appendix H).

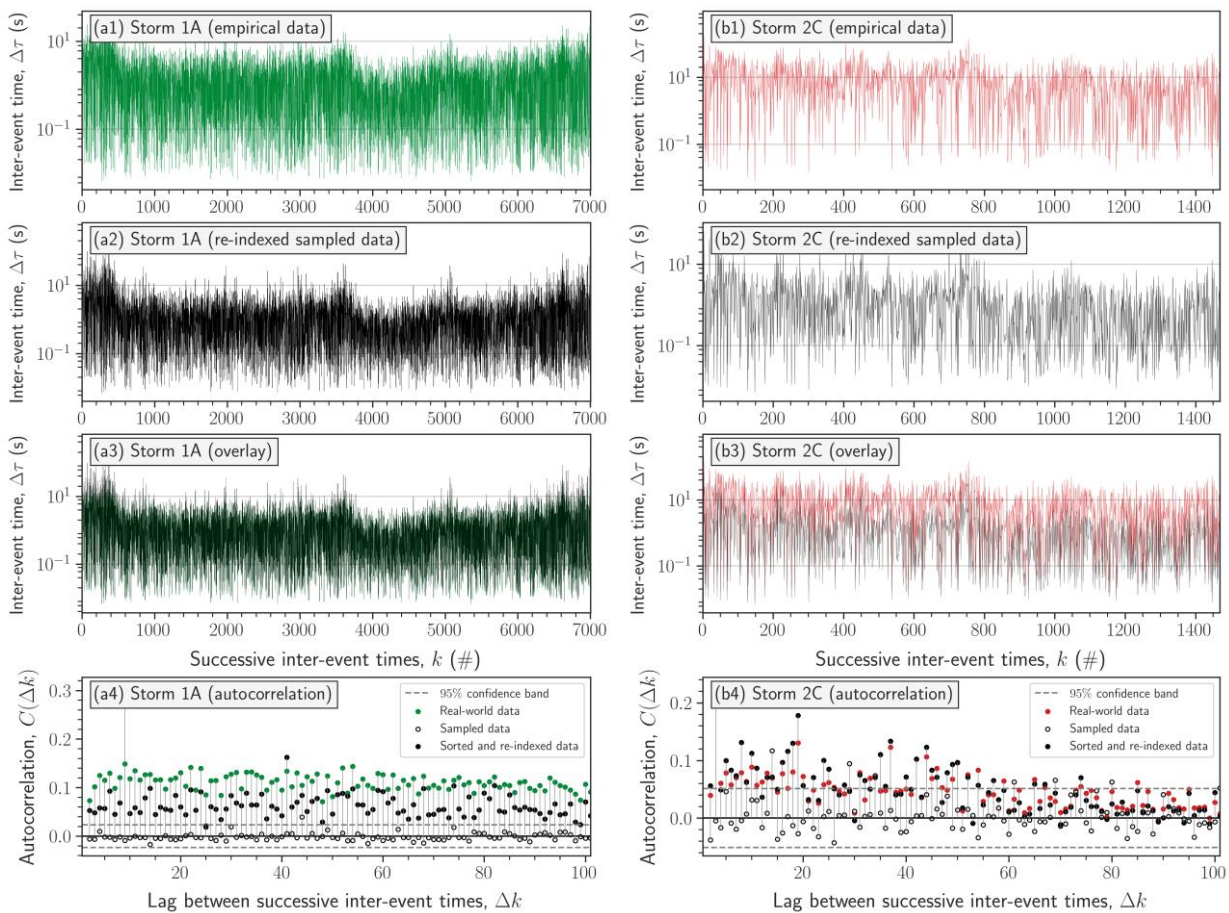


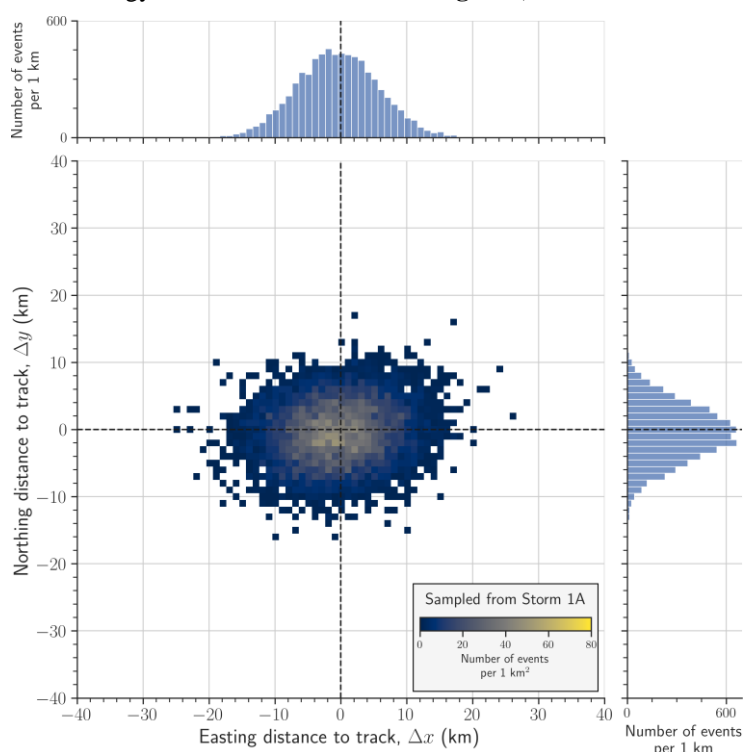
Figure 18: Sampling, sorting and re-indexing procedure based on the combined supercell inter-event time $\Delta\tau$ dataset and thunderstorm (a#) 1A, (b#) 2C. The first subfigure shows the original cut inter-event time time-series in natural time k . The second subfigure shows this sampled time-series being sorted and re-indexed based on the individual thunderstorm, where the indices of sorted time-series coincide between the two time-series. The third subfigure shows the overlay between the original time-series and the sorted and re-indexed one in natural time k . The fourth subfigure shows the overlay between the original time-series and the

In Fig. 18, the sampling, sorting and re-indexing procedure has returned synthetic inter-event time datasets that are representative of supercell thunderstorms in value and representative of individual thunderstorms in their temporal structure.

The difference between the inter-event time values between storms 1A, 1B, 1C and storms 2B and 2C is evident in (b3). The sampled, sorted and re-indexed dataset (grey line) have lower inter-event time values than original storm 2C (red line), which is expected from the discussion of **Fig. 17**.

645 6.2 Sampling distances to the movement track

The approach to creating a dataset of distances to the movement track is detailed in **Section 4.3** and the results of this sampling methodology is shown for storm 1A in **Fig. 19** (all storms are shown in **Appendix G**).



650 **Figure 19: 2D spatial count of lightning strikes per 1 km² of easting and northing distances to the movement track in natural time k for a bivariate Gaussian distribution based on storm 1A with window size $\Delta w = 500$ events. Only bins with more than 1 lightning strike are coloured and the plot is zoomed onto $[-40, 40]$ km intervals for both easting and northing distance. The marginal bin counts per 1 km are given for both dimensions and the parameters of the bivariate Gaussian distribution are ($\mu_x = -0.46$ km, $\mu_y = -0.61$ km, $\sigma_{xx} = 37.25$ km², $\sigma_{yy} = 17.83$ km², $\sigma_{xy} = 2.33$ km²).**

655 In **Fig. 19**, the 2D and marginal counts of lightning strikes show clear contrast to **Fig. 15**. This sampling approach, by using a bivariate Gaussian distribution, has not captured the minor peaks in northing and easting distance to track values. For marginal counts, both easting and northing dimensions reach similar values to the real-world data, but the 2D counts reach values of only 50–60 events per 1 km².



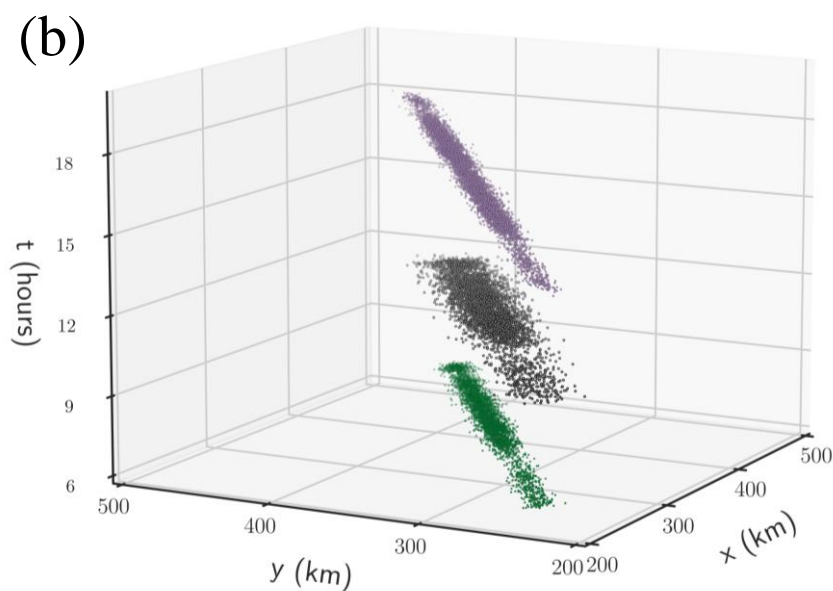
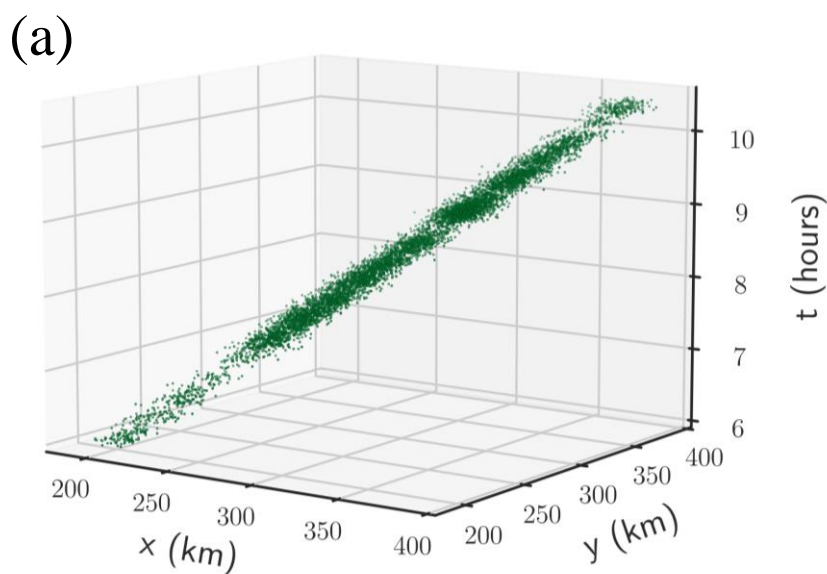
6.3 Creating a representative spatio-temporal model

660 A spatio-temporal model of point events produced by a moving point source is defined to generate synthetic lightning strike datasets. This model would incorporate lightning strike variables as constants or sampled datasets. For the sampled variables, the procedures for generating inter-event times and distances to the movement track were detailed in **Section 6.1** and **Section 6.2**, respectively.

665 This spatio-temporal model generates a point event dataset representative of lightning strikes (point events) produced by a single thunderstorm (moving point source). When combining multiple runs of this model, the point event dataset would be representative of a storm-system. A single run of this model can be described as the following procedure:

- Set constant variables:
 - Initiation point (x_0, y_0, t_0) .
 - Movement speed v .
 - Movement direction α .
 - 670 • Set sampled variables:
 - Generate inter-event time dataset.
 - Generate distance to the movement track dataset.
1. Place a point event – around the initiation point, place a point event according to the first generated easting Δx_1 and northing Δy_1 distance to the movement track values.
 - 675 2. Move along the track – starting from the initiation point, move in the movement direction with the set movement speed for a time period equal to the first inter-event time value $\Delta \tau_1$.
 3. Repeat steps 1 and 2 until exhausting the sampled variables.

680 From this procedure and discussion from **Section 6.1** and **Section 6.2**, it is necessary to select a particular thunderstorm when creating a synthetic lightning strike dataset to set the sampled variables. A single run of the model to produce a lightning strike dataset representative of storm 1A is shown in **Fig. 20a** and this run with an additional two runs of the model to form a three-storm-system shown in **Fig. 20b**. For the two additional model runs, the bivariate Gaussian distribution for the distance to the movement track variable is set with parameters $(\mu_x = 0, \mu_y = 0, \sigma_{xx} = 10 \text{ km}, \sigma_{yy} = 10 \text{ km})$. The correlation parameter for the two additional runs is set at $\rho = 0$ and $\rho = 0.9$. No other of the constant or sampled variables are changed for these model runs.



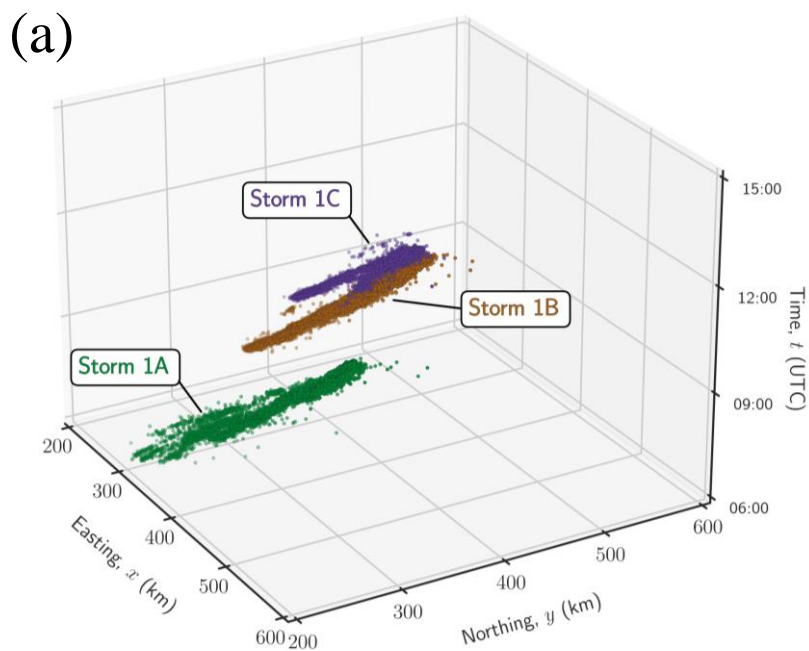
685

Figure 20: (a) A single run of the spatio-temporal model to produce a lightning strike dataset representative of storm 1A and a (b) synthetic three-storm-system with varying spatial spread parameters. In (a), the initiation point is set at $(x_0 = 200 \text{ km}, y_0 = 200 \text{ km}, t_0 = 6 \text{ h})$. The movement speed value is set at $v = 58 \text{ km h}^{-1}$ as per the characterisation of the movement speed variable (Fig. 11 and Appendix Fig. D1). Inter-event times are sampled, sorted and re-indexed as per Fig. 18 (a1-a4). Easting and northing distances are sampled from the bivariate Gaussian distribution shown in Fig. 19. The first (green) storm is identical to (a) with bivariate Gaussian distribution parameter set from parameter characterisation ($\mu_x = -0.46 \text{ km}, \mu_y = -0.61 \text{ km}, \sigma_{xx} = 37.25 \text{ km}^2, \sigma_{yy} = 17.83 \text{ km}^2, \sigma_{xy} = 2.33 \text{ km}^2$). The second (dark grey) storm is based on bivariate Gaussian distribution with parameters ($\mu_x = 0, \mu_y = 0, \sigma_{xx} = 10 \text{ km}, \sigma_{yy} = 10 \text{ km}, \rho = 0$). The third (purple) storm has parameters ($\mu_x = 0, \mu_y = 0, \sigma_{xx} = 10 \text{ km}, \sigma_{yy} = 10 \text{ km}, \rho = 0.9$). For all storms, the movement speed is kept the same at $v = 58 \text{ km h}^{-1}$ and inter-event time distribution is representative of storm 1A.

690



695 In **Fig. 20**, the flexibility of the model is demonstrated. A model run representative of a lightning strike dataset produced by a thunderstorm is compared with additional runs where only one lightning variable is changed to examine the visual effect of end-member values for the particular variable. Another example, where additional model runs are representative of storms 1B and 1C, are generated to create a synthetic storm-system representative of the first case study (**Section 3.2**), is shown in **Fig. 21**.



700

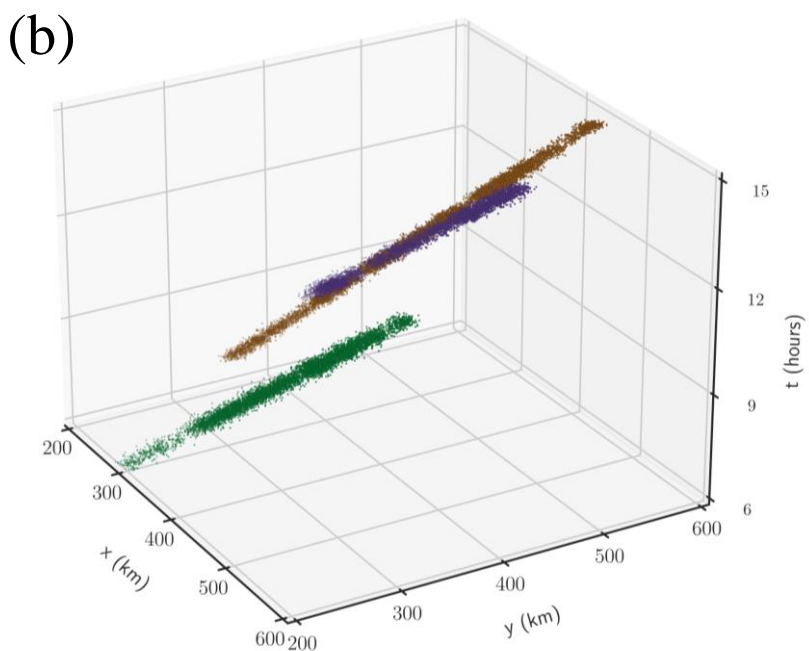


Figure 21: A synthetic three-storm-system (b) that consists of individual synthetic storms that would be representative of Storms 1A, 1B and 1C from case study 1 (a). The movement speed values, re-indexed inter-event time values and spatial spread parameter distributions are selected for each storm using Table 4.



705 In **Fig. 21**, the synthetic storm-system (b) is assigned both constant and sampled variables to represent the lightning strike
datasets from case study 1 (a). The synthetic lightning strike datasets propagate further in the spatial and temporal domains than
the real-world datasets on which they are based. As this is case study 1, the effect of the heavy tail of the supercell inter-event
time dataset has been discussed in **Fig. 17**. We also note the assumption of straight-line propagation of the moving point source
(thunderstorm) producing the individual point events, which is a simplification as discussed in the modelling approach to the
710 spatial spread of the lightning strikes (**Section 4.4**).

7. Discussion

The characterisation (**Section 5**) and modelling (**Section 6**) aspects in this study of lightning strikes as point events generated
by a moving source were based on two selected case studies of increased lightning activity (**Section 3**). This section discusses
the following five aspects related to our modelling approach for lightning strikes: (i) relevance to different categories of
715 thunderstorms, (ii) lightning inter-event time characterisation, (iii) estimating lightning cluster movement speeds, (iv)
estimating lightning cluster spatial spread, and (v) overall motivation and limitations.

Relevance of our modelling approach for lightning strikes associated with different categories of thunderstorms. Each case
study described a storm system consisting of three thunderstorms over a single day of the observed increase in storm activity.
To characterise and model these thunderstorms, the lightning strike data for both days was gathered by the ATDnet LLS over
720 the United Kingdom. The two case studies categorised five of the six identified thunderstorms as supercells. In other
characterisation of lightning strikes as point events studies (e.g. [Enno et al., 2020; Mezuman et al., 2014; Anderson and
Klugmann, 2014]), the characterisation added to lightning climatology research without emphasis on particular thunderstorm
types, indicating the novelty of this approach and the potential of further research. In Anderson and Klugmann (2014) the
diurnal flash density characterisation included case study 1 (**Section 3.2**), but without separation of characterisation results for
725 individual thunderstorms. Although five out of the six thunderstorms in these case studies were supercells, there were clear
differences in their characterisation results (e.g. empirical distribution differences in **Fig. 17**), indicating a further research
direction into identifying and characterising further case studies of more varied thunderstorm categories

Generality of our approach for lightning inter-event time characterisation. While applicable to these case studies, it is
acknowledged that the characterisation results of lightning associated with given thunderstorms cannot be generalised to
730 describe all thunderstorms due to the variations in the characterisation results between the studies. To address this lack of
generality for lightning associated with thunderstorm characterisation, the creation of a supercell inter-event time $\Delta\tau$ dataset
(**Fig. 14**) was done for modelling the inter-event time variable $\Delta\tau$. The limitation for modelling this particular physical variable
is the dataset size discrepancy between the case studies (i.e., the first case study has $n = 21,600$, while the combined supercell
dataset has $n = 23,457$ lightning strikes). The values sampled from this supercell dataset are more representative of the first
735 case study. In contrast, the larger inter-event time $\Delta\tau$ values of the second case study created a heavier tail for the combined
distribution. The characterisation results return value intervals similar to those of other studies focusing on physical variable



740 characterisation. Inter-event time values range from below 0.01 s to over 100 s for individual storms from both case studies. For storms 1A, 1B and 1C, the empirical distributions cover a range of 0.01 s to 20–30 s. In Ballarotti et al. (2012), a study conducted over Vale do Paraíba, Brazil using high-speed cameras, returned an arithmetic mean for the inter-stroke time interval of 92 ms (millisecond). In Saba et al. (2006) over southern Brazil, a dataset of 608 inter-stroke time intervals had an arithmetic mean of 83 ms. Over different study areas, such as the eastern Mediterranean and Israel (Yair et al., 2014) and Arizona, the United States (Stall et al., 2009), the mean inter-stroke interval was found to be 93 ms and 98 or 84 ms respectively (depending on whether strikes that used a pre-existing lightning channel or created new ground contacts). These results are in good agreement with the range for the distribution of inter-event times found in this paper for storms 1A, 1B, 1C.

745 *Estimating lightning cluster movement speed.* Speed values for storms 1A–1C, were similar, ranging between 47–60 km h⁻¹ from the best plane fit and the linear fit in lag space of lightning associated with each storm. For storms 2A and 2C, the two methodologies returned higher movement speed values of 101–111 km h⁻¹. Storm 2B had a value range of 66–67 km h⁻¹, similar to the first case study. Currently, we are not aware of other peer-review publications that have estimated the movement speed of a thunderstorm from lightning as a point event dataset. Such estimates are usually based on two-dimensional radar reflectivity data (e.g. the automated cell detection algorithm KONRAD (Lang, 2001) used in Wapler and James (2015) to
750 calculate the movement speed of thunderstorms over Central Europe spanning from 2007–2012.

Estimating lightning cluster spatial spread. For the distance to the lightning cluster movement track variable to estimate the spatial spread of the lightning strikes as a cluster of point events (Section 4.4), the bivariate Gaussian distribution fit to model the data was selected for simplicity, similar to Finke (1999). We are not aware of other peer-review publications estimating the distance to the lightning cluster movement track. The movement track estimates are usually done by temporal windows. In
755 Strauss et al. (2013), additional precipitation data were used to estimate storm cells and their centroid locations over 10-minute intervals were used as points along the movement tracks. In Kunz et al. (2020), 26,000 severe convective storm tracks between 2005–2014 were estimated from two-dimensional radar reflectivity data. They estimated the storm tracks by using a modified version of the cell-tracking algorithm TRACE3D (Handwerker, 2002). Such approaches were deemed as too complex as the
760 objective of the characterisation process is to provide an estimate for the spatial spread parameter for the models. The characterisation of the spatial spread variable (**Fig. 16**) showed a non-trivial empirical distribution. Still, no other potential distributions was evaluated on the data and this is a potential future research direction. Another potential research direction is the modelling of the movement track with a curve rather than a straight line. We followed this approach when characterising the spatial spread (**Section 4.4**), but it would be useful to be able to incorporate this in the modelling (**Section 6**).

765 *Motivation for the implemented modelling approach and its limitations.* The motivation for modelling lightning strikes was to create synthetic point event datasets generated by a moving point source representative of ‘real-world’ lightning strike data. Modelling and sampling approaches were proposed for the inter-event time and distance to the movement track variables (**Section 6**). No direct sampling of characterised variables was implemented in the spatio-temporal model of lightning strikes as point events in Finke (1999). The approach to designing the spatio-temporal model was selected to have complete control
770 over the constant and sampled variables. The model can generate any point event datasets produced by a moving source,

depending on the sets of input parameters. The model also has clear procedures for propagating the moving point source (i.e. thunderstorm) and the placement of point events along this point source (i.e. lightning strikes). The simplicity of such a model is acknowledged, but such an approach establishes a direct way to produce synthetic lightning strike data representative of the particular case studies, allowing for the simulation of a specific category of thunderstorm or extending this framework to other natural hazards that can be characterised as point events produced by a moving source (e.g. tornado touchdown locations).

775

8. Conclusions

This study presents a comprehensive characterisation and modelling of thunderstorm associated lightning strikes as spatio-temporal point events, focusing on two thunderstorm systems over the United Kingdom. Through detailed analysis of these two real-world datasets, we successfully identified and characterised the movement speed, inter-event time distribution, and spatial spread of lightning strikes for six individual thunderstorms.

780

Our findings highlight distinct patterns in lightning strike behaviour, such as the following: lightning cluster movement speeds ranging from 47–59 km/h and 67–111 km/h for the two storm systems, respectively; lightning inter-event times demonstrating a wide range of times, with notable density peaks at around 0.1 s and between 1–10 s, underscoring the variability and complexity of lightning strike occurrences; spatial spread of lightning strike clusters with typical distances up to 80 km from the storm track, with one outlier reaching 226 km.

785

The synthetic lightning strike model developed in this study provides a robust tool for generating realistic point event datasets. This model, which incorporates empirically derived parameters from real-world data, offers valuable insights for simulating lightning strike events and can aid in improving forecasting models for lightning-related hazards.

Our research contributes to a deeper understanding of lightning strike dynamics and offers a methodological framework that can be applied to other spatio-temporal natural hazard events. Future work could expand on this foundation by incorporating additional variables and exploring different storm types and regions to further refine and confront the model.

790

In conclusion, this study enhances our ability to characterise and model lightning strikes, offering implications for hazard assessment and risk management in meteorological studies.



Appendix A. List of publications on modelling natural hazards as point events.

795

Table A1. Summary Table of publications on using spatio-temporal point process models to model natural hazard processes.

No.	Title	Authors	Natural hazard	Mathematical model (extended description with how attributes are incorporated into the model)
1	Spatio-temporal log-Gaussian Cox processes for modelling wildfire occurrence: the case of Catalonia, 1994–2008	Serra et al. (2014)	Wildfire	A log-Gaussian Cox process with its log-intensity function estimated from a linear predictor consisting of terms for the expected number of events, covariates and their parameters and interaction between events.
2	Spatial–temporal clustering of tornadoes	Malamud et al. (2016)	Tornado	The number of lines and the spatial and temporal spacings between consecutive events are estimated from real-world data.
3	Structured Spatio-Temporal Shot-Noise Cox Point Process Models, with a View to Modelling Forest Fires	Møller and Díaz-Avalos (2010)	Wildfire	A shot-noise Cox process with its intensity function inferred.
4	Spatio-temporal models for large-scale indicators of extreme weather	Heatona et al. (2011)	Extreme weather event	A non-homogeneous Poisson process with the intensity function having parameters of a generalised extreme value distribution.
5	Is Timber Insurable? A Study of Wildfire Risks in the U.S. Forest Sector Using Spatio-temporal Models	Chen et al. (2014)	Wildfire	Various.
6	A Review of Self-Exciting Spatio-Temporal Point Processes and Their Applications	Reinhart (2018)	Earthquake	Various modification of the self-exciting point process models are discussed.
7	Spatio-temporal point process statistics: A review	González et al. (2016)	Tornado	For real-world data summary statistics were provided for various point processes.



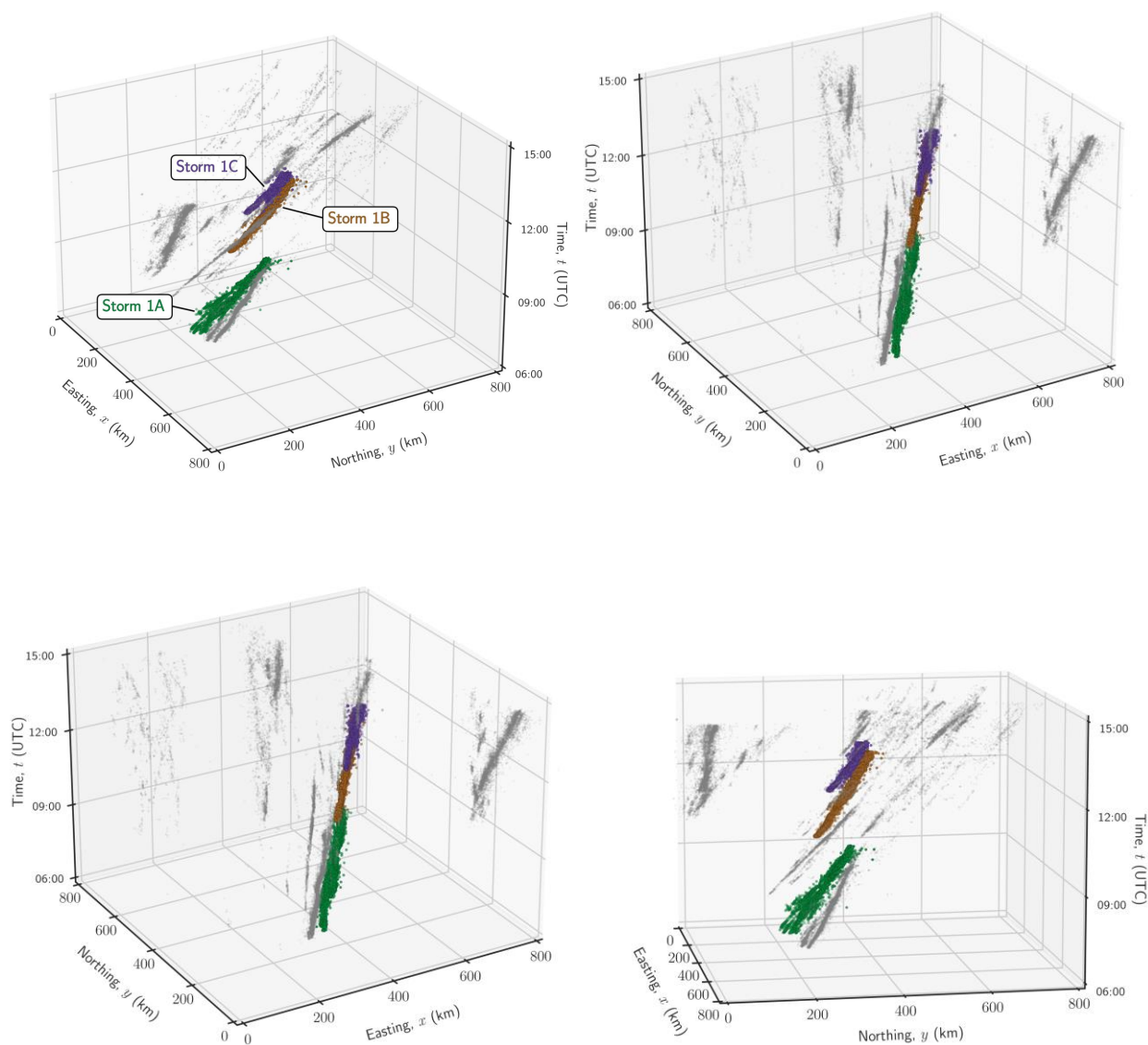
No.	Title	Authors	Natural hazard	Mathematical model (extended description with how attributes are incorporated into the model)
8	Assessing spatio-temporal eruption forecasts in a monogenetic volcanic field	Bebbington (2013)	Volcano eruption	Intensity at a given point is determined from the nearest neighbours with further discussion on methods for determining their number.
9	Spatio-temporal avalanche forecasting with Support Vector Machines	Pozdnoukhov et al. (2011)	Avalanche release point	Avalanche forecast is made based on binary classification results from support vector machines.
10	Point process modeling of wildfire hazard in Los Angeles County, California	Xu and Schoenberg (2011)	Wildfire	Spatio-temporal point process models with their intensity functions consisting of varying sets of parameters.
11	A hierarchical Bayesian spatio-temporal model for extreme precipitation events	Ghosha and Mallick (2011)	Extreme weather event	A non-homogeneous Poisson process with the intensity function having parameters of a generalised extreme value distribution.
12	Probabilistic estimation of long-term volcanic hazard with assimilation of geophysics and tectonic data	Jaquet et al. (2012)	Volcano eruption	Cox processes are used as models for further implementation in a forecasting framework.
13	A spatio-temporal Poisson hurdle point process to model wildfires	Serra et al. (2014)	Wildfire	Poisson hurdle process consists of two stages and specified in a way to gather together the two processes theoretically involved in the presence of wildfires: the occurrence of being a big wildfire and the frequency of big wildfires per spatial unit.



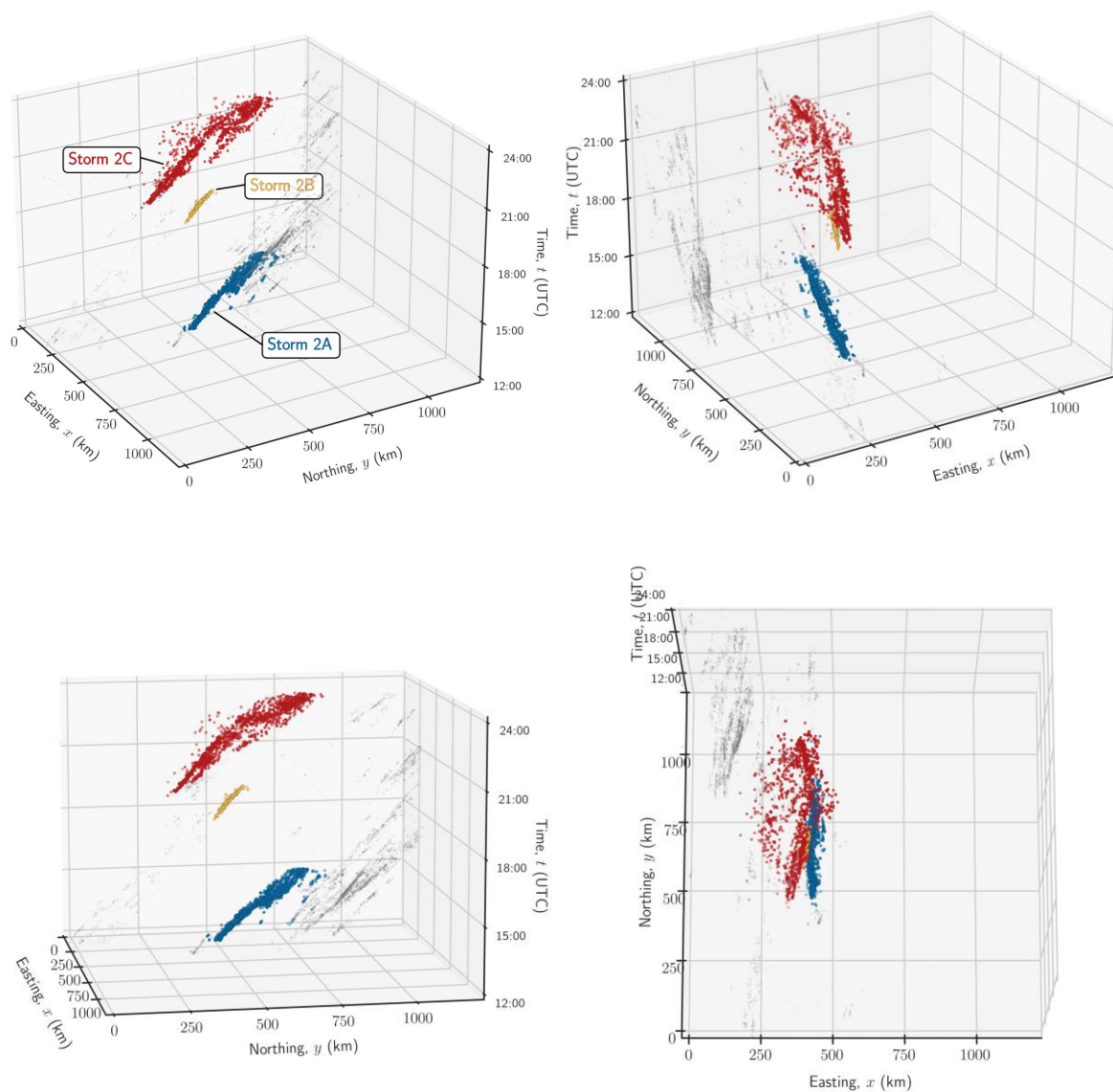
No.	Title	Authors	Natural hazard	Mathematical model (extended description with how attributes are incorporated into the model)
14	A spatio-temporal modelling framework for assessing the fluctuations of avalanche occurrence resulting from climate change: application to 60 years of data in the northern French Alps	Eckert et al. (2010)	Avalanche release point	A non-homogeneous Poisson process with the intensity function consisting of terms for the expected number of events and a relative risk term.
15	Spatial and Spatio-Temporal Log-Gaussian Cox Processes: Extending the Geostatistical Paradigm	Diggle et al. (2013)	-	For real-world data analyses were provided for various point processes.
16	Detecting and modeling multi-scale space-time structures: the case of wildfire occurrences	Gabriel et al. (2017)	Wildfire	A log-Gaussian Cox process with its log-intensity function estimated from a linear predictor consisting of terms for inhibition between events, covariates and their parameters and interaction between events.
17	Analysis of tornado reports through replicated spatiotemporal point patterns	Gonzalez et al. (2020)	Tornado	A non-homogeneous Poisson point process with its intensity function estimated from an edge-corrected nonseparable estimator of Gaussian kernels.
18	Earthquake Modelling at the Country Level Using Aggregated Spatio-Temporal Point Processes	van Lieshout and Stein (2012)	Earthquake	A marked spatio-temporal clustered point process with incorporation of parents and offspring generation.
19	Second-order analysis of inhomogeneous spatio-temporal point process data	Gabriel and Diggle (2009)	-	For real-world data analyses were provided for various point processes.
20	Spatio-temporal modelling of extreme storms	Economou et al. (2014)	Hurricane	A non-homogeneous Poisson process models the high intensity points events along cyclone tracks.



Appendix B. Spatial extent and propagation of the lightning strike occurrences for both storm systems.



800 **Figure B1: Additional angles of the 3D spatial extent and propagation of the lightning strike occurrences plots in Figure 3. Lightning strikes are projected onto the OSGB 1936 / British National Grid northing/easting coordinates, assigned to the identified thunderstorms corresponding to the relevant synoptical analysis.**



805 **Figure B2:** Additional angles of the 3D spatial extent and propagation of the lightning strike occurrences plots in Fig. 8. Lightning strikes are projected onto the OSGB 1936 / British National Grid northing/easting coordinates, assigned to the identified thunderstorms corresponding to the relevant synoptical analysis.



Appendix C. 2D spatial count of lightning strikes in easting and northing.

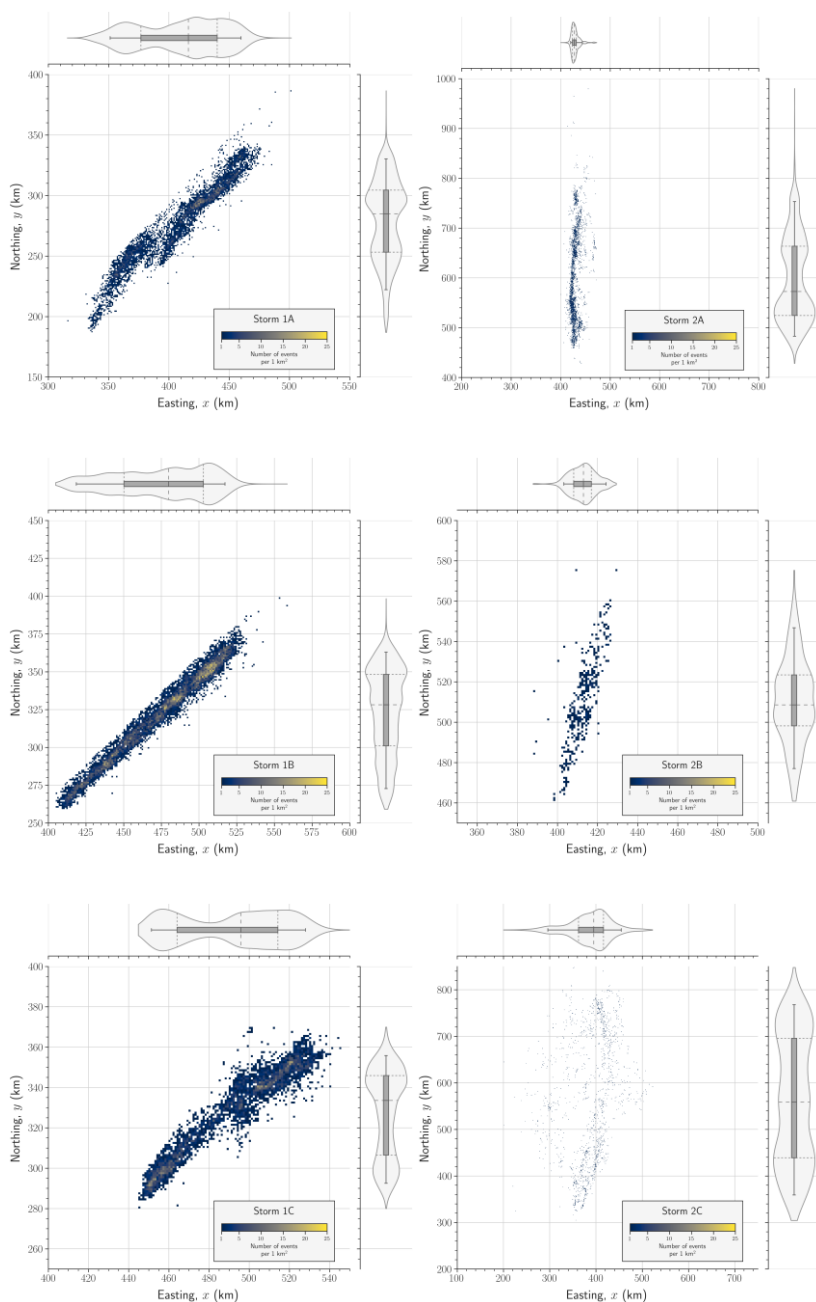


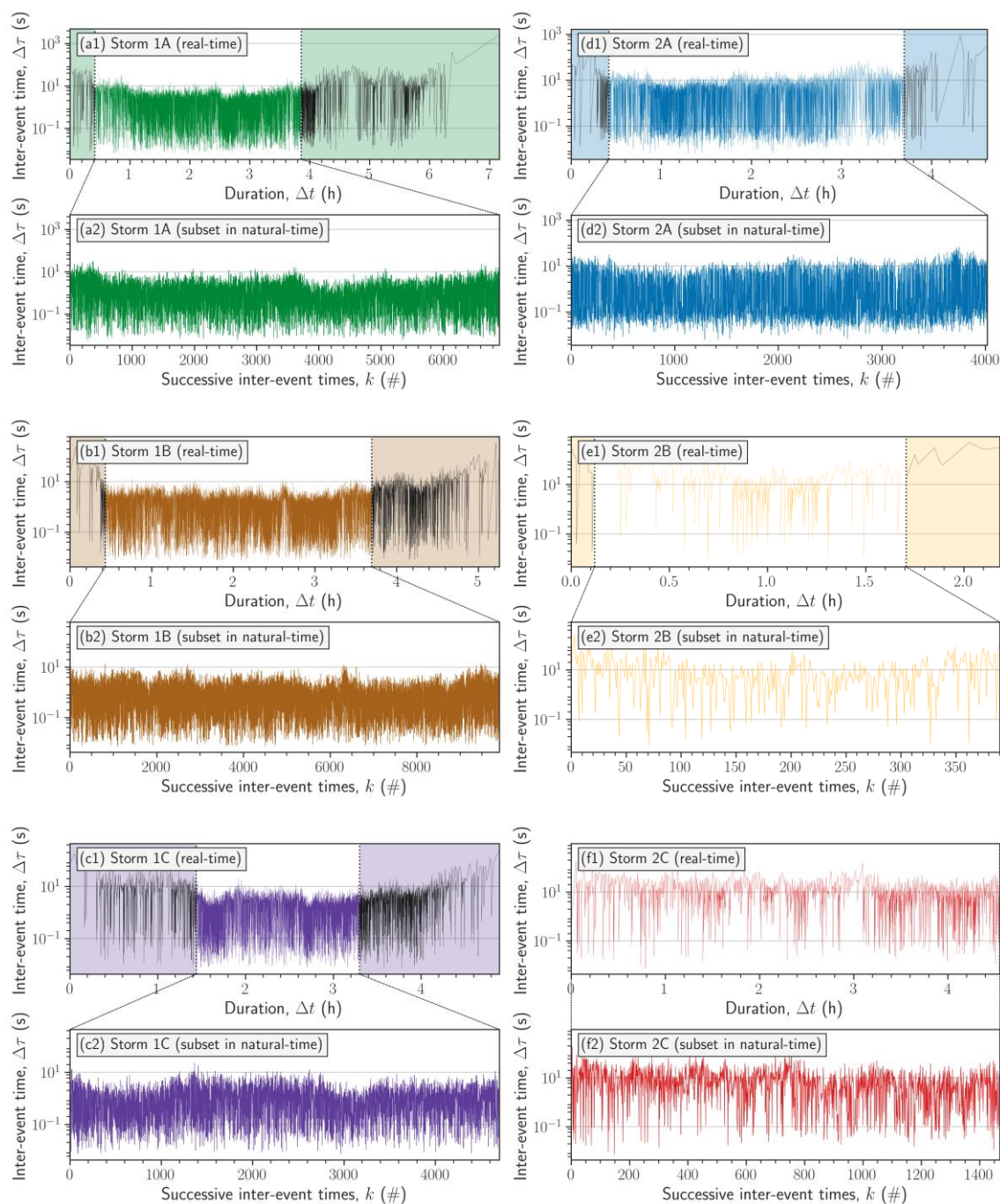
Figure C1: 2D spatial count of lightning strikes per 1 km^2 of the OSGB 1936 / British National Grid northing/easting coordinates for thunderstorms 1A, 1B, 1C, 2A, 2B and 2C as per the legend in each subplot. Only bins with more than 1 lightning strike are coloured. Note that the northing and easting extents are the same, but the axes limits differ. For both the easting and northing values, the marginal distribution is indicated by overlapping boxplots and violinplots. Boxplots indicate the quartiles, have whiskers for the 5th and 95th percentiles, while the violinplots are cut at the last value.

810

815



Appendix D. Cutting time series of inter-event times.

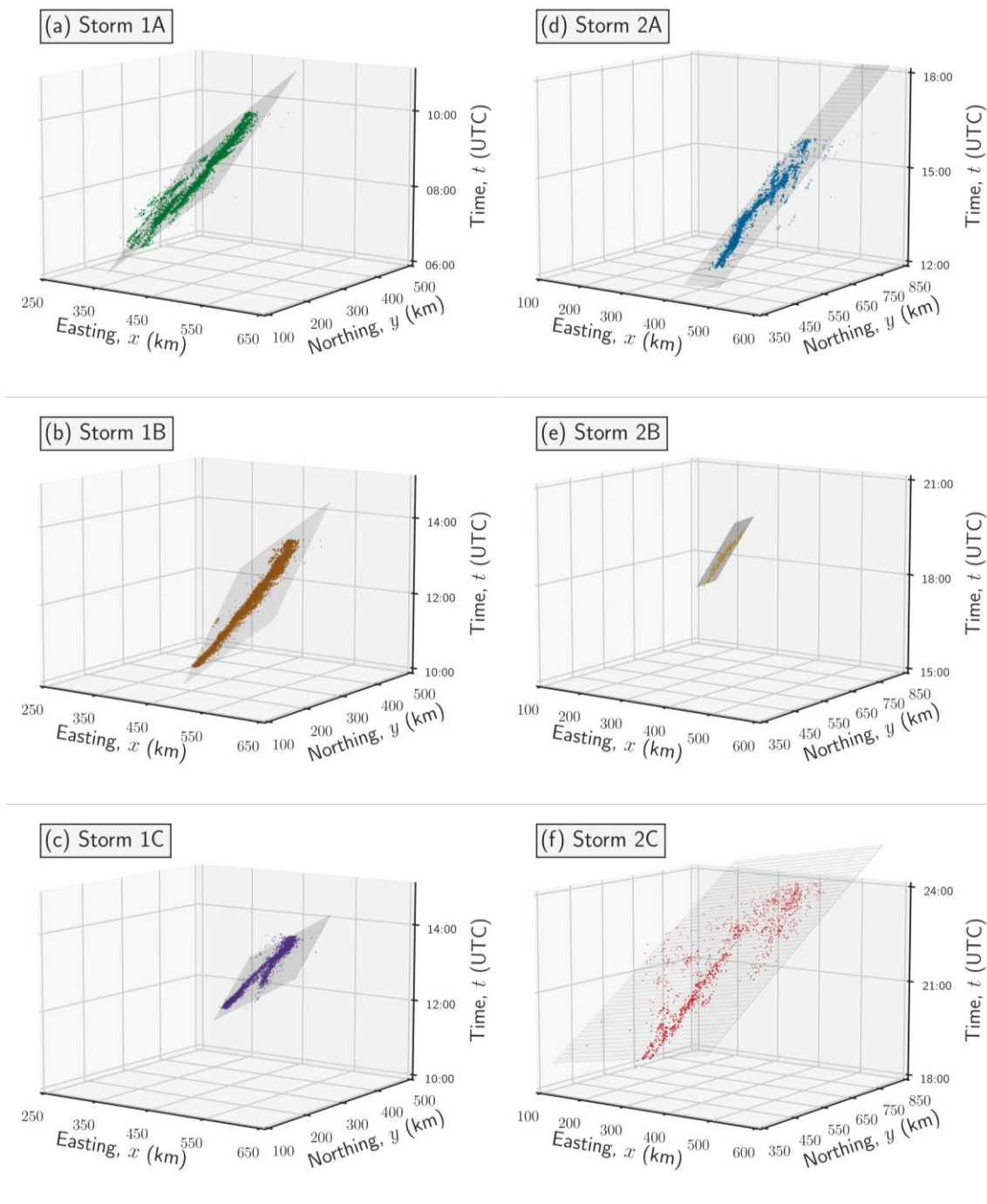


820

Figure D1: Subplots showing the cutting of inter-event time $\Delta\tau$ time-series in real-time t (removal of black line in upper subfigure) and the subsequent inter-event time time-series in natural time k (lower subfigure) for thunderstorms (a1, a2) 1A, (b1, b2) 1B, (c1, c2) 1C, (d1, d2) 2A, (e1, e2) 2B and (f1, f2) 2C.



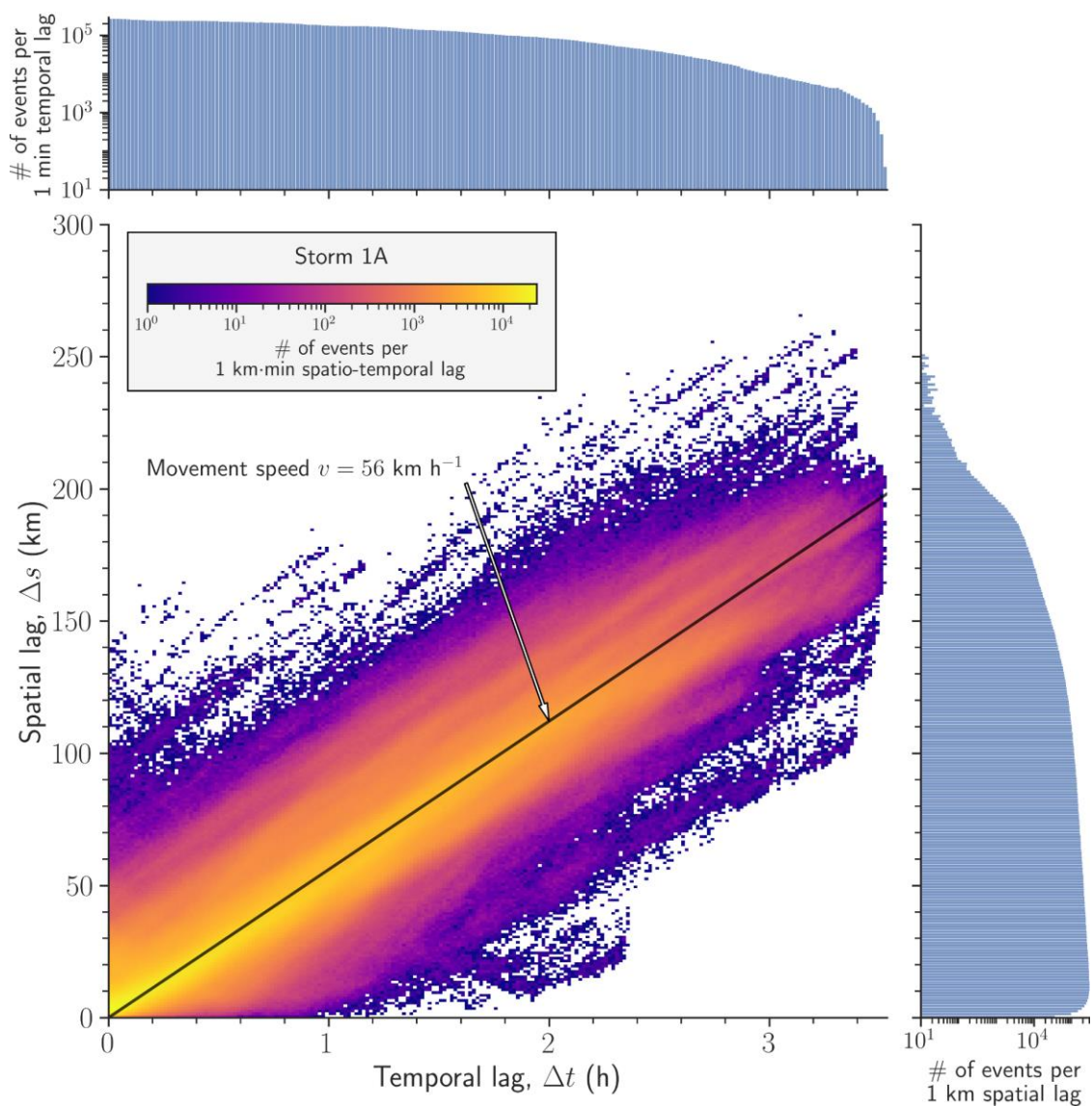
825 **Appendix E. Least-squares plane-fit solution to the lightning strike datasets.**



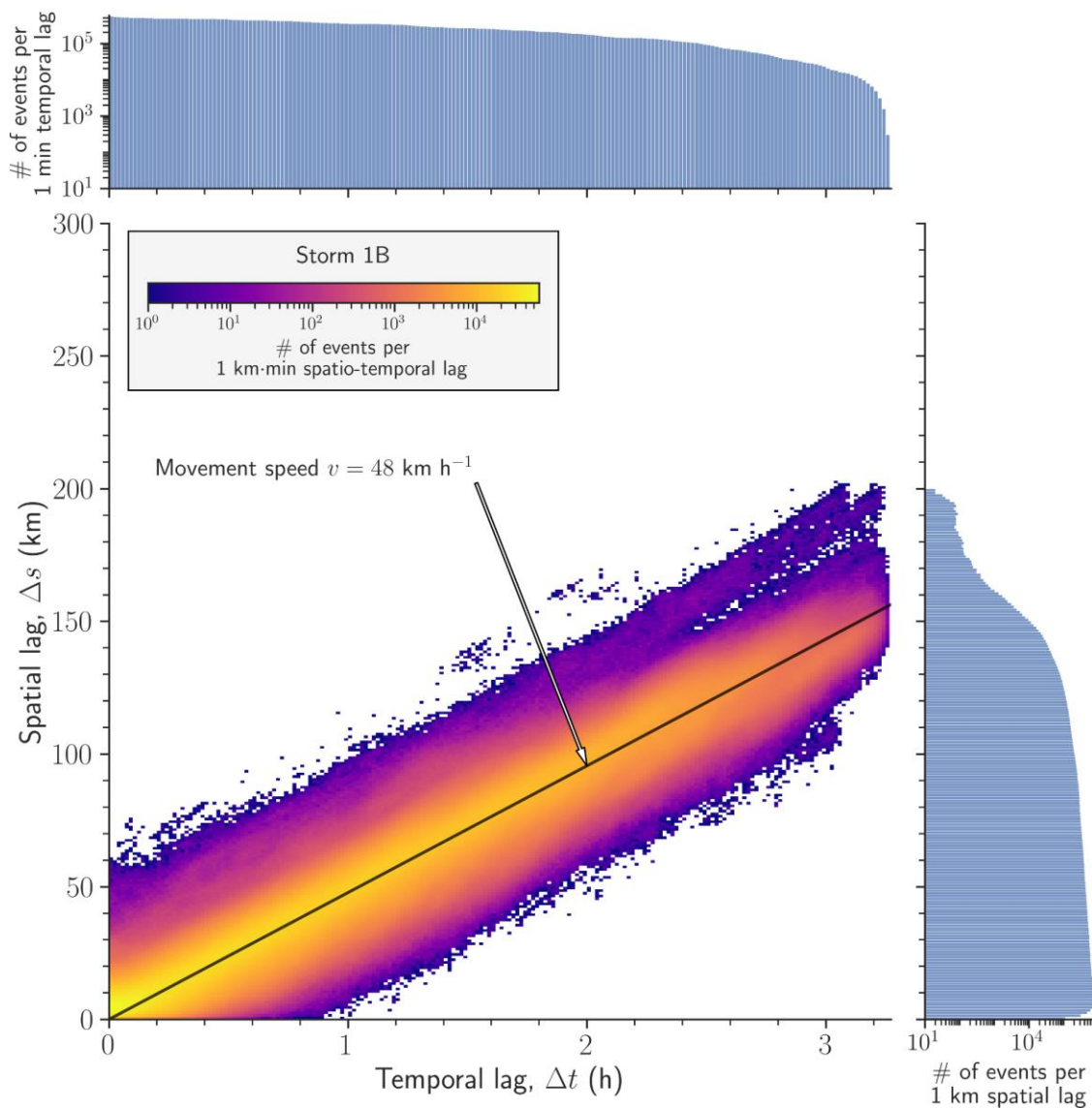
830 **Figure E1:** Least-squares plane-fit solution to the lightning strike datasets for thunderstorms (a) 1A, (b) 1C, (c) 2B and (d) 2C. The colour scheme for lightning strikes of each storm is consistent with Figures 2 to 5 in the main text, and the best-fit plane is drawn as grey wireframe. Note that all three axes have different extents for each storm, while the ratio between the axes is constant.



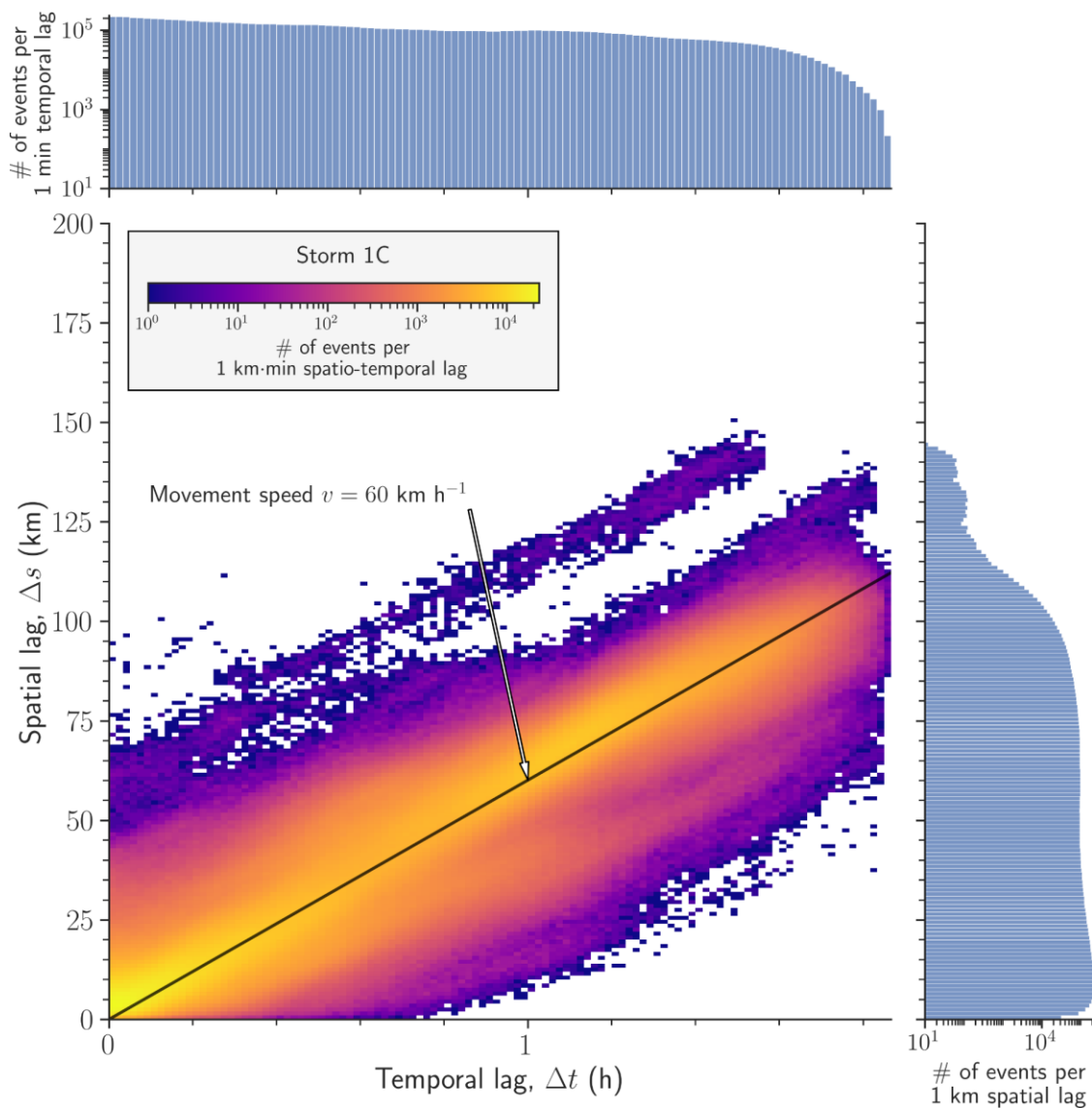
Appendix F. Linear least-squares fit to estimate storm movement speed in the spatio-temporal lag space.



835 **Figure F1:** Storm 1A (28 June 2012, $n = 7,001$ events, $v = 56 \text{ km h}^{-1}$) least-squares linear-fit solution and 2D count of lightning strikes per 1 km-min in the spatio-temporal lag space. Bins are coloured according to the given logarithmic colour scale. The marginal bin counts per 1 km spatial lag and 1 min temporal lag are given above and to the right of the main plot. The abrupt vertical end of lightning strike data at $\Delta t = 3.45 \text{ h}$ occurs due to the removal of inter-event time values (see Fig. 11). The solid black line indicates the best-fit linear line passing through the point of origin.



840 **Figure F2: Storm 1B (28 June 2012, $n = 9,901$ events, $v = 48 \text{ km h}^{-1}$) least-squares linear-fit solution and 2D count of lightning strikes per 1 km-min in the spatio-temporal lag space. Bins are coloured according to the given logarithmic colour scale. The marginal bin counts per 1 km spatial lag and 1 min temporal lag are given above and to the right of the main plot. The abrupt vertical end of lightning strike data at $\Delta t = 3.25 \text{ h}$ occurs due to the removal of inter-event time values (see Fig. 11). The solid black line indicates the best-fit linear line passing through the point of origin.**



845

Figure F3: Storm 1C (28 June 2012, $n = 4,701$ events, $v = 60 \text{ km h}^{-1}$) least-squares linear-fit solution and 2D count of lightning strikes per 1 km-min in the spatio-temporal lag space. Bins are coloured according to the given logarithmic colour scale. The marginal bin counts per 1 km spatial lag and 1 min temporal lag are given above and to the right of the main plot. The abrupt vertical end of lightning strike data at $\Delta t = 1.9 \text{ h}$ occurs due to the removal of inter-event time values (see Fig. 11). The solid black line indicates the best-fit linear line passing through the point of origin.

850

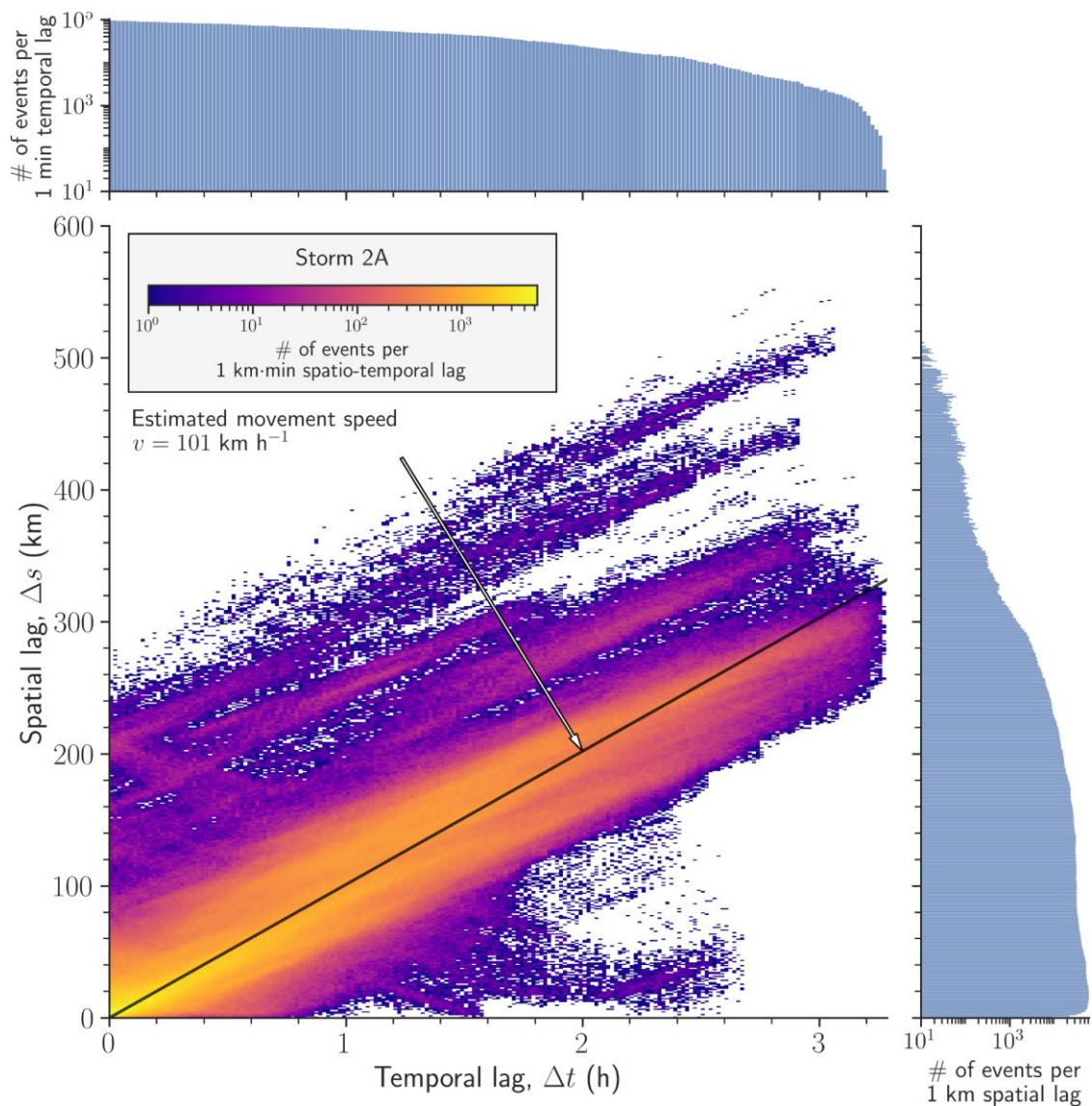


Figure F4: Storm 2A (1 July 2015, $n = 4,019$ events, $v = 101 \text{ km h}^{-1}$) least-squares linear-fit solution and 2D count of lightning strikes per 1 km-min in the spatio-temporal lag space. Bins are coloured according to the given logarithmic colour scale. The marginal bin counts per 1 km spatial lag and 1 min temporal lag are given above and to the right of the main plot. The abrupt vertical end of lightning strike data at $\Delta t = 3.25 \text{ h}$ occurs due to the removal of inter-event time values (see Fig. 11). The solid black line indicates the best-fit linear line passing through the point of origin.

855

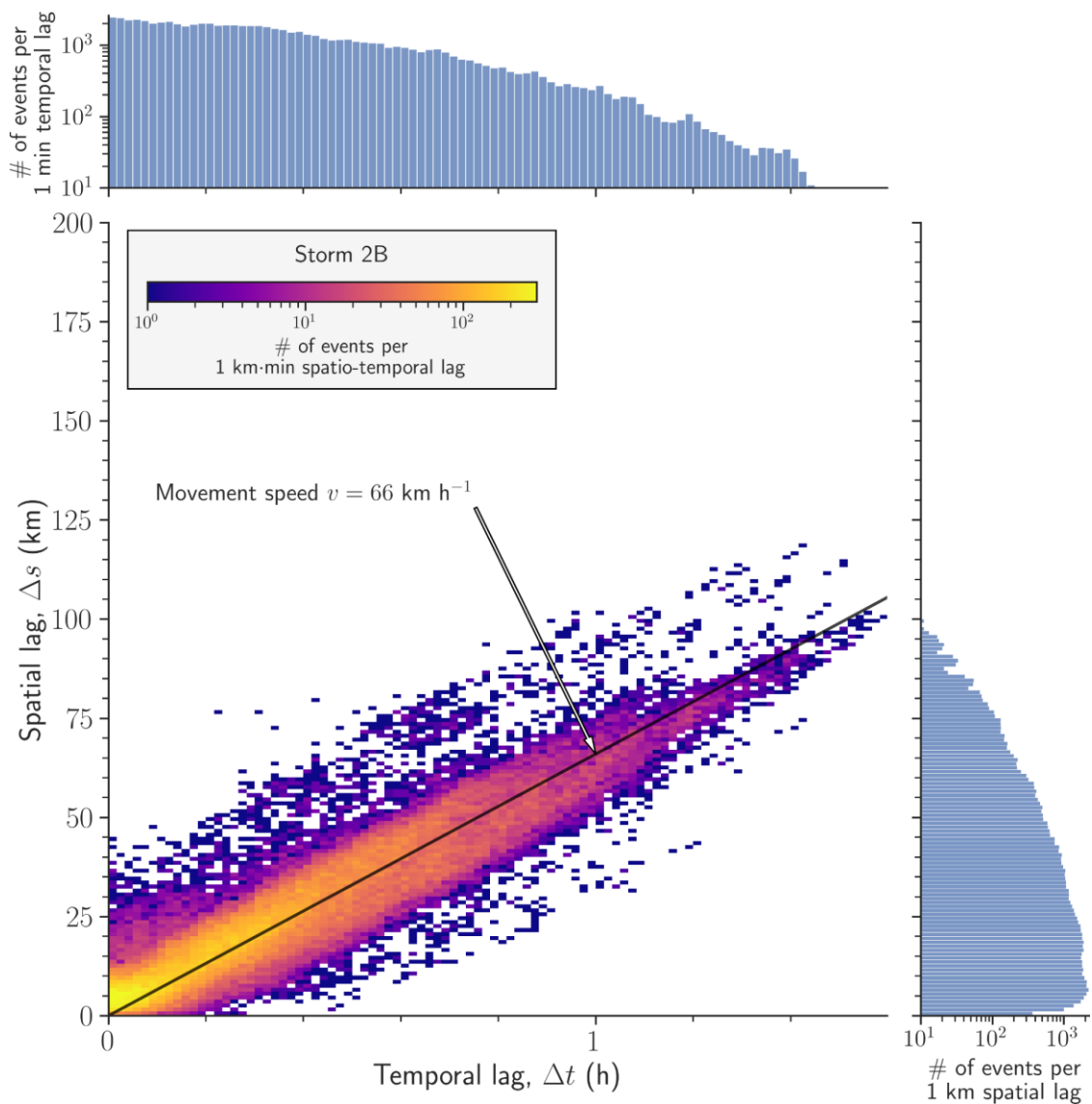


Figure F5: Storm 2B (1 July 2015, $n = 390$ events, $v = 66 \text{ km h}^{-1}$) least-squares linear-fit solution and 2D count of lightning strikes per 1 km-min in the spatio-temporal lag space. Bins are coloured according to the given logarithmic colour scale. The marginal bin counts per 1 km spatial lag and 1 min temporal lag are shown above and to the right of the main plot. The solid black line indicates the best-fit linear line passing through the point of origin.

860

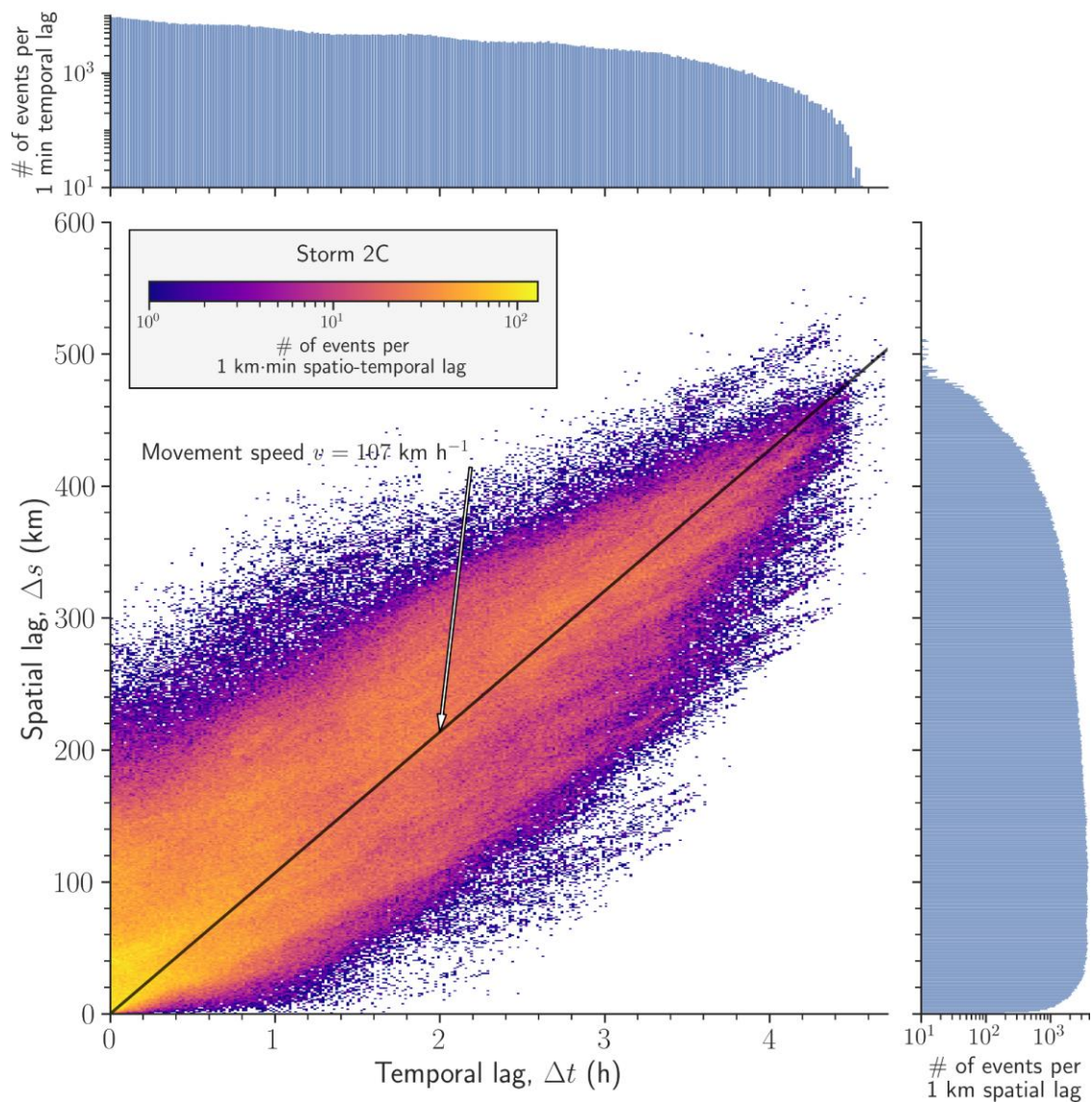
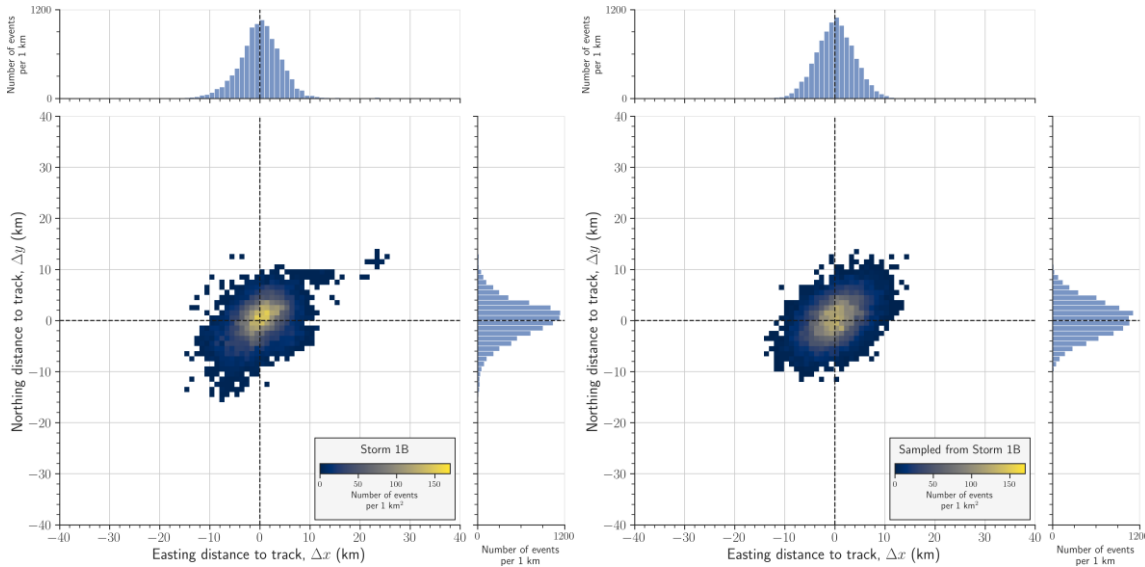


Figure F6: Storm 2C (1 July 2015, $n = 1,469$ events, $v = 107 \text{ km h}^{-1}$) least-squares linear-fit solution and 2D count of lightning strikes per 1 km-min in the spatio-temporal lag space. Bins are coloured according to the given logarithmic colour scale. The marginal bin counts per 1 km spatial lag and 1 min temporal lag are shown above and to the right of the main plot. The solid black line indicates the best-fit linear line passing through the point of origin.

865

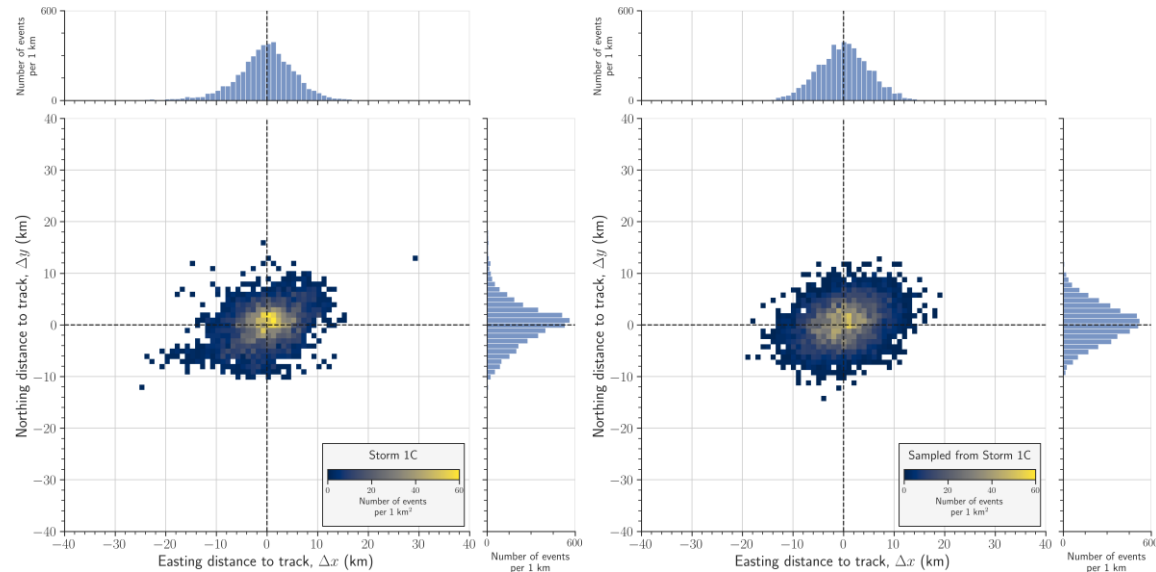


Appendix G. Bivariate Gaussian fit to spatial spread variable to sample easting and northing distances.



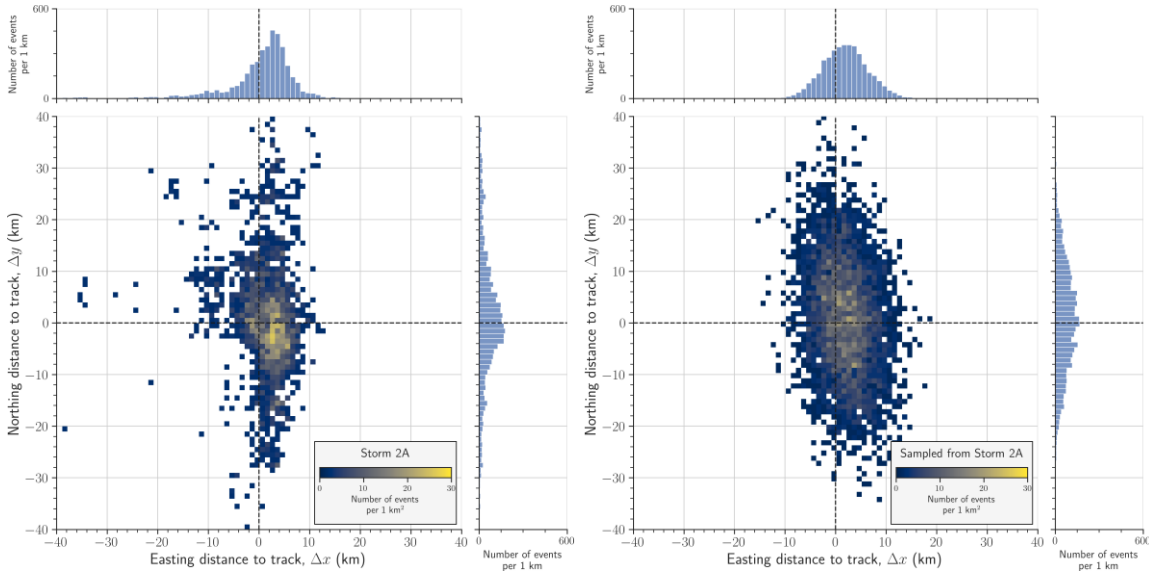
870

Figure G1: 2D spatial count of lightning strikes per 1 km² of easting and northing distances to the movement track in natural time k for thunderstorm 1B (left subfigure) and for a bivariate Gaussian distribution based on thunderstorm 1B (right subfigure) for window sizes $\Delta w = 500$. Only bins with more than 1 lightning strike are coloured and the plot is zoomed onto $[-40, 40]$ km intervals for both easting and northing distance. The marginal bin counts per 1 km are given for both dimensions.

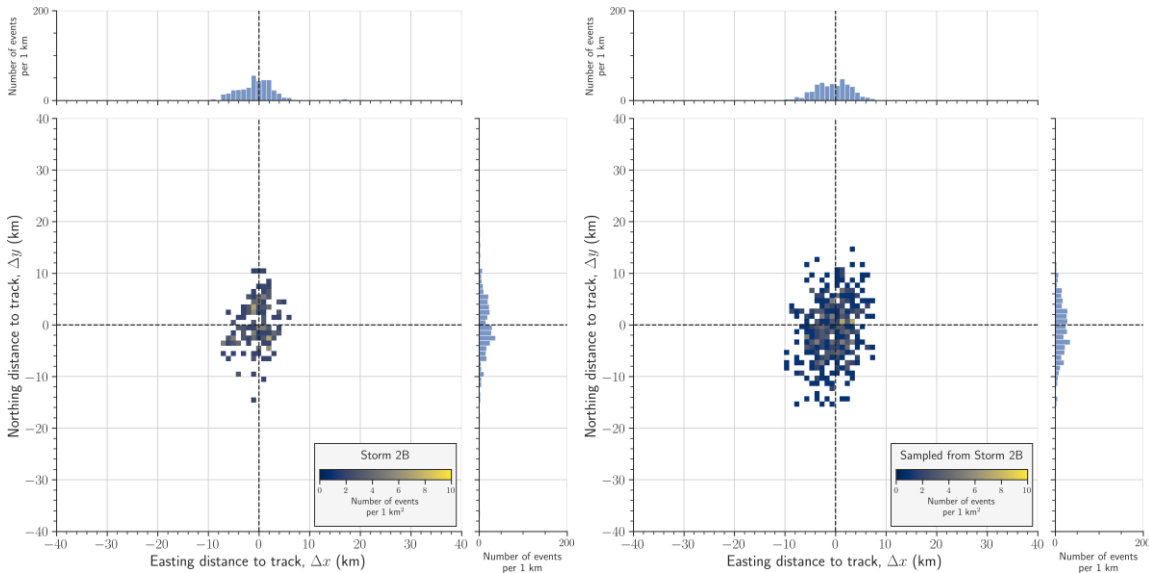


875

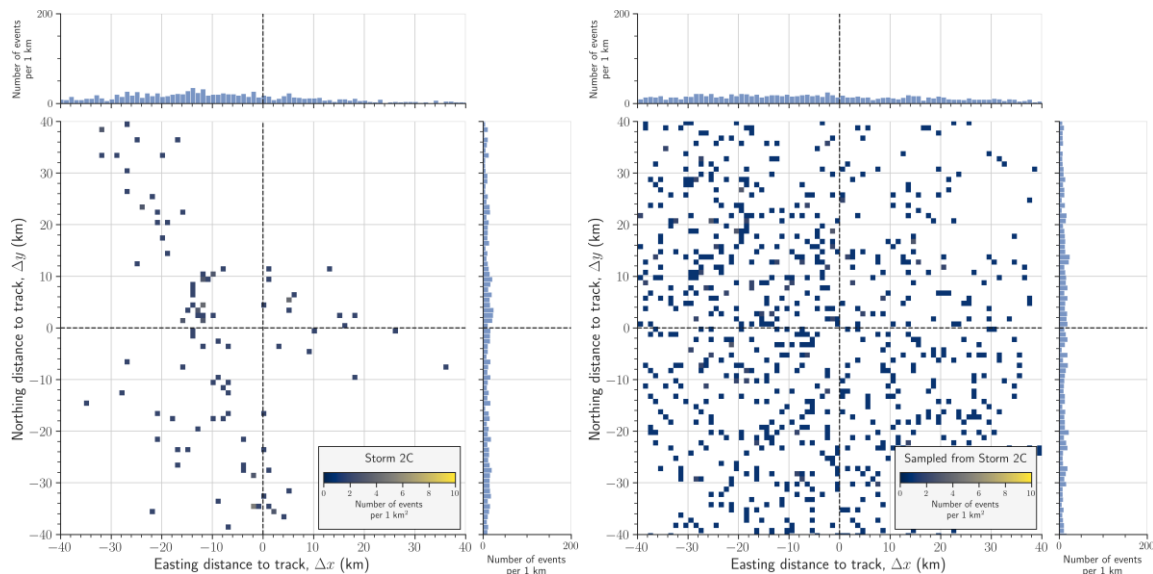
Figure G2: 2D spatial count of lightning strikes per 1 km² of easting and northing distances to the movement track in natural time k for thunderstorm 1C (left subfigure) and for a bivariate Gaussian distribution based on thunderstorm 1C (right subfigure) for window sizes $\Delta w = 500$. Only bins with more than 1 lightning strike are coloured and the plot is zoomed onto $[-40, 40]$ km intervals for both easting and northing distance. The marginal bin counts per 1 km are given for both dimensions.



880 **Figure G3: 2D spatial count of lightning strikes per 1 km² of easting and northing distances to the movement track in natural time k for thunderstorm 2A (left subfigure) and for a bivariate Gaussian distribution based on thunderstorm 2A (right subfigure) for window sizes $\Delta w = 500$. Only bins with more than 1 lightning strike are coloured and the plot is zoomed onto $[-40, 40]$ km intervals for both easting and northing distance. The marginal bin counts per 1 km are given for both dimensions.**



885 **Figure G4: 2D spatial count of lightning strikes per 1 km² of easting and northing distances to the movement track in natural time k for thunderstorm 2B (left subfigure) and for a bivariate Gaussian distribution based on thunderstorm 2B (right subfigure) for window sizes $\Delta w = 500$. Only bins with more than 1 lightning strike are coloured and the plot is zoomed onto $[-40, 40]$ km intervals for both easting and northing distance. The marginal bin counts per 1 km are given for both dimensions.**



890 **Figure G5: 2D spatial count of lightning strikes per 1 km² of easting and northing distances to the movement track in natural time k for thunderstorm 1C (left subfigure) and for a bivariate Gaussian distribution based on thunderstorm 1C (right subfigure) for window sizes $\Delta w = 500$. Only bins with more than 1 lightning strike are coloured and the plot is zoomed onto $[-40, 40]$ km intervals for both easting and northing distance. The marginal bin counts per 1 km are given for both dimensions.**



895 **Appendix H. Sampling, sorting and re-indexing procedure for inter-event time variable.**

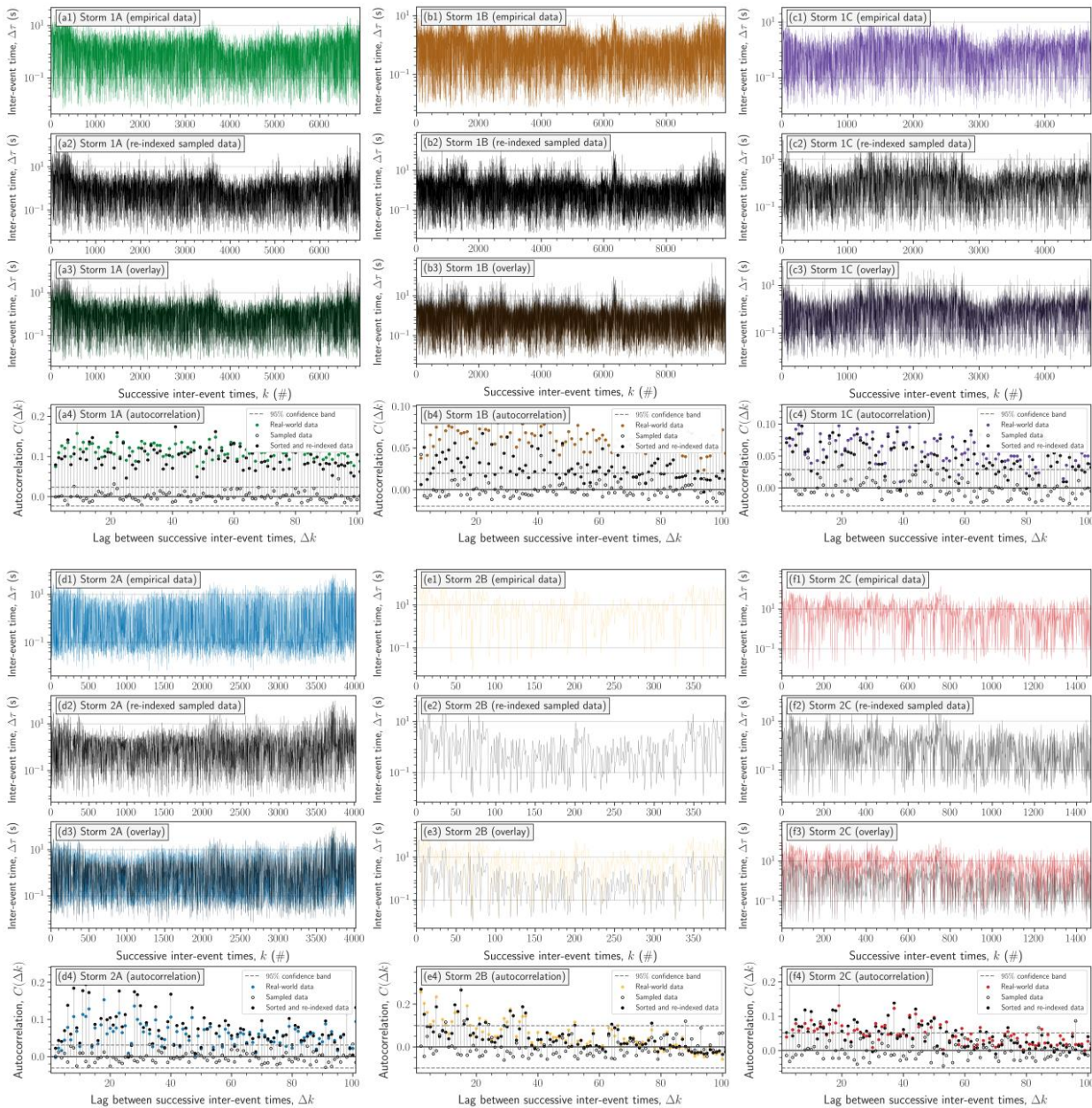


Figure H1: Sampling, sorting and re-indexing procedure based on the combined supercell inter-event time $\Delta\tau$ dataset and thunderstorm (a#) 1B, (b#) 1C, (c#) 2A and (d#) 2B. The first subfigure shows the original cut inter-event time series in natural time k . The second subfigure shows this sampled time series being sorted and re-indexed based on the particular thunderstorm, where the indices of the sorted time series coincide between the two time series. The third subfigure shows the overlay between the original time-series and the sorted and re-indexed one in natural time k . The fourth subfigure shows the overlay between the original time series and the sorted and re-indexed one in natural time k .

900



905 *Data availability.* The lightning strike point event data were obtained from the UK Met Office.

Author contributions. All authors discussed the whole plan of this article. UZ designed and implemented all the experiments, prepared all the data, and finished the draft, including all figures in the article. BDM and DP supervised the research and revised the article.

Competing interests. Bruce D. Malamud is on the editorial board of this journal.

910 *Acknowledgements.* Uldis Zandovskis was supported by the Engineering and Physical Sciences Research Council (EPSRC) PhD studentship as part of EPSRC Centre for Doctoral Training in Cross-Disciplinary Approaches to Non-Equilibrium Systems (Award ref. 1950247).

915 *Financial support.* Uldis Zandovskis was supported by the Engineering and Physical Sciences Research Council (EPSRC) PhD studentship as part of EPSRC Centre for Doctoral Training in Cross-Disciplinary Approaches to Non-Equilibrium Systems (Award ref. 1950247).

References

- Anderson, G. and Klugmann, D.: A European lightning density analysis using 5 years of ATDnet data, *Nat. Hazards Earth Syst. Sci.*, 14, 815–829, doi:10.5194/nhess-14-815-2014, 2014.
- Artigas, S. E. S.: Stochastic modeling of lightning occurrence by Nonhomogeneous Poisson Process, *International Conference on Lightning Protection (ICLP)*, Vienna, Austria, 1–7, doi:10.1109/ICLP.2012.6344400, 2012.
- 920 Atluri, G., Karpatne, A., and Kumar, V.: Spatio-temporal data mining: A survey of problems and methods, *ACM Computing Surveys (CSUR)*, 51(4), 1–41, doi:10.1145/3161602, 2018.
- Ballarotti, M. G., Medeiros, C., Saba, M. M., Schulz, W., and Pinto Jr, O.: Frequency distributions of some parameters of negative downward lightning flashes based on accurate-stroke-count studies, *J. Geophys. Res.*, 117, D06112, doi:10.1029/2011JD017135, 2012.
- 925 Beirle, S., Koshak, W., Blakeslee, R., and Wagner, T.: Global patterns of lightning properties derived by OTD and LIS, *Nat. Hazards Earth Syst. Sci.*, 14, 2715–2726, doi:10.5194/nhess-14-2715-2014, 2014.
- Chowdhuri, P., Anderson, J. G., Chisholm, W. A., Field, T. E., Ishii, M., Martinez, J. A., ... and Short, T. A.: Parameters of lightning strokes: a review, *IEEE Trans. Power Del.*, 20(1), 346–358, doi:10.1109/TPWRD.2004.835039, 2005.
- 930 Clark, M. R., and Webb, J. D.: A severe hailstorm across the English Midlands on 28 June 2012, *Weather*, 68(11), 284–291, doi:10.1002/wea.2162, 2013.
- Diggle, P. J., Chetwynd, A. G., Häggkvist, R., and Morris, S. E.: Second-order analysis of space-time clustering, *Statistical Methods in Medical Research*, 4(2), 124–136, doi:10.1177/096228029500400203, 1995.



- 935 Dwyer, J. R., and Uman, M. A.: The physics of lightning, *Physics Reports*, 534(4), 147–241,
doi:10.1016/j.physrep.2013.09.004, 2014.
- Eckert, N., Parent, E., Kies, R., and Baya, H.: A spatio-temporal modelling framework for assessing the fluctuations of
avalanche occurrence resulting from climate change: application to 60 years of data in the northern French Alps, *Climatic
Change*, 101(3), 515–553, doi:10.1007/s10584-009-9718-8, 2010.
- 940 Economou, T., Stephenson, D. B., and Ferro, C. A.: Spatio-temporal modelling of extreme storms, *The Annals of Applied
Statistics*, 8(4), 2223–2246, doi:10.1214/14-AOAS766, 2014.
- Enno, S. E., Anderson, G., & Sugier, J.: ATDnet detection efficiency and cloud lightning detection characteristics from
comparison with the HyLMA during HyMeX SOP1, *Journal of Atmospheric and Oceanic Technology*, 33(9), 1899–1911,
doi:10.1175/JTECH-D-15-0256.1, 2016.
- 945 Enno, S. E., Sugier, J., Alber, R., and Seltzer, M.: Lightning flash density in Europe based on 10 years of ATDnet data,
Atmospheric Research, 235, 104769, doi:10.1016/j.atmosres.2019.104769, 2020.
- Finke, U.: Space–time correlations of lightning distributions, *Monthly Weather Review*, 127(8), 1850–1861,
doi:10.1175/1520-0493(1999)127<1850:STCOLD>2.0.CO;2, 1999.
- 950 Gaffard, C., Nash, J., Atkinson, N., Bennett, A., Callaghan, G., Hibbett, E., Taylor, P., Turp, M., and Schulz, W.: Observing
lightning around the globe from the surface, 20th International Lightning Detection Conference, Tucson, Arizona, 21–23,
2008.
- Galanaki, E., Kotroni, V., Lagouvardos, K., and Argiriou, A.: A ten-year analysis of cloud-to-ground lightning activity over
the Eastern Mediterranean region, *Atmospheric Research*, 166, 213–222, doi:10.1016/j.atmosres.2015.07.008, 2015.
- González, J. A., Rodríguez-Cortés, F. J., Cronie, O., and Mateu, J.: Spatio-temporal point process statistics: a review, *Spatial
Statistics*, 18, 505–544, doi:10.1016/j.spasta.2016.10.002, 2016.
- 955 González, J. A., Hahn, U., and Mateu, J.: Analysis of tornado reports through replicated spatiotemporal point patterns,
Journal of the Royal Statistical Society: Series C (Applied Statistics), 69(1), 3–23, doi:10.1111/rssc.12375, 2020.
- Handwerker, J.: Cell tracking with TRACE3D—A new algorithm, *Atmospheric Research*, 61(1), 15–34, doi:10.1016/S0169-
8095(01)00100-4, 2002.
- 960 Ivezić, Ž., Connolly, A. J., VanderPlas, J. T., and Gray, A.: Statistics, data mining, and machine learning in astronomy. In
Statistics, Data Mining, and Machine Learning in Astronomy, Princeton University Press, 134, 2014.



- Jaquet, O., Lantuéjoul, C., and Goto, J.: Probabilistic estimation of long-term volcanic hazard with assimilation of geophysics and tectonic data, *Journal of Volcanology and Geothermal Research*, 235, 29–36, doi:10.1016/j.jvolgeores.2012.05.003, 2012.
- Kisilevich, S., Mansmann, F., Nanni, M., and Rinzivillo, S.: *Spatio-temporal clustering*, Springer US, 855–874, 2009.
- 965 Kotroni, V., and Lagouvardos, K.: Lightning in the Mediterranean and its relation with sea-surface temperature, *Environ. Res. Lett.*, 11(3), 034006, doi:10.1088/1748-9326/11/3/034006, 2016.
- Kunz, M., Wandel, J., Fluck, E., Baumstark, S., Mohr, S., and Schemm, S.: Ambient conditions prevailing during hail events in central Europe, *Nat. Hazards Earth Syst. Sci.*, 20, 1867–1887, doi:10.5194/nhess-20-1867-2020, 2020.
- Lang, P.: Cell tracking and warning indicators derived from operational radar products, In *Proceedings of the 30th International Conference on Radar Meteorology*, Munich, Germany, 245–247, 2001.
- 970 Lee, A. C.: An operational system for the remote location of lightning flashes using a VLF arrival time difference technique, *Journal of Atmospheric and Oceanic Technology*, 3(4), 630–642, doi:10.1175/1520-0426(1986)003<0630:AOSFTR>2.0.CO;2, 1986.
- Lewis, M. W. and Silkstone, N.: Improvements in nowcasting capability: analysis of three structurally distinct severe thunderstorms across northern England on 1 July 2015, *Weather*, 72(4), 91–98, doi:10.1002/wea.2837, 2017.
- 975 Malamud, B. D., Turcotte, D. L., and Brooks, H. E.: Spatial–temporal clustering of tornadoes, *Nat. Hazards Earth Syst. Sci.*, 16, 2823–2834, doi:10.5194/nhess-16-2823-2016, 2016.
- Mezuman, K., Price, C., and Galanti, E.: On the spatial and temporal distribution of global thunderstorm cells, *Environ. Res. Lett.*, 9(12), 124023, doi:10.1088/1748-9326/9/12/124023, 2014.
- 980 Mohee, F. M., and Miller, C.: Climatology of thunderstorms for North Dakota, 2002–06, *Journal of Applied Meteorology and Climatology*, 49(9), 1881–1890, doi:10.1175/2010JAMC2400.1, 2010.
- Møller, J., and Díaz-Avalos, C.: Structured spatio-temporal shot-noise Cox point process models, with a view to modelling forest fires, *Scandinavian Journal of Statistics*, 37(1), 2–25, doi:10.1111/j.1467-9469.2009.00670.x, 2010.
- 985 Nash, J., Atkinson, N. C., Hibbett, E., Callaghan, G., Taylor, P. L., Odams, P., Jenkins, D., Keogh, S., Gaffard, C. and Walker, E.: The new Met Office ATDNET lightning detection system, In *Proceedings of the WMO Technical Conference on Instruments and Observing Methods*, 94, 2006.
- Priestley, M. B.: *Spectral analysis and time series: Univariate series*, London: Academic Press, 890, 1981.
- Rakov, V. A., and Uman, M. A.: *Lightning: physics and effects*, Cambridge University Press, 2003.



Rakov, V. A.: The physics of lightning, *Surveys in Geophysics*, 34(6), 701–729, doi:10.1007/s10712-013-9230-6, 2013.

990 Richard, P., Delannoy, A., Labaune, G., and Laroche, P.: Results of spatial and temporal characterisation of the VHF-UHF radiation of lightning, *Journal of Geophysical Research: Atmospheres*, 91(D1), 1248–1260, doi:10.1029/JD091iD01p01248, 1986.

Saba, M. M. F., Ballarotti, M. G., and Pinto Jr, O.: Negative cloud-to-ground lightning properties from high-speed video observations, *Journal of Geophysical Research: Atmospheres*, 111(D3), doi:10.1029/2005JD006415, 2006.

995 Schulz, W., Cummins, K., Diendorfer, G., and Dorninger, M.: Cloud-to-ground lightning in Austria: A 10-year study using data from a lightning location system, *Journal of Geophysical Research: Atmospheres*, 110(D9), doi:10.1029/2004JD005332, 2005.

Serra, L., Saez, M., Mateu, J., Varga, D., Juan, P., Díaz-Ávalos, C., and Rue, H.: Spatio-temporal log-Gaussian Cox processes for modelling wildfire occurrence: the case of Catalonia, 1994–2008, *Environ. Ecol. Stat.*, 21(3), 531–563, doi:10.1007/s10651-013-0267-y, 2014.

Shao, X. M., and Krehbiel, P. R.: The spatial and temporal development of intracloud lightning, *Journal of Geophysical Research: Atmospheres*, 101(D21), 26641–26668, doi:10.1029/96JD01803, 1996,

Soriano, L. R., De Pablo, F., and Tomas, C.: Ten-year study of cloud-to-ground lightning activity in the Iberian Peninsula, *Journal of Atmospheric and Solar-Terrestrial Physics*, 67(16), 1632–1639, doi:10.1016/j.jastp.2005.08.019, 2005.

1005 Stall, C. A., Cummins, K. L., Krider, E. P., and Cramer, J. A.: Detecting multiple ground contacts in cloud-to-ground lightning flashes, *Journal of Atmospheric and Oceanic Technology*, 26(11), 2392–2402, doi:10.1175/2009JTECHA1278.1, 2009.

Steiger, S. M., Orville, R. E., and Huffines, G.: Cloud-to-ground lightning characteristics over Houston, Texas: 1989–2000, *Journal of Geophysical Research: Atmospheres*, 107(D11), ACL-2, doi:10.1029/2001JD001142, 2002.

1010 Strauss, C., Rosa, M. B., and Stephany, S.: Spatio-temporal clustering and density estimation of lightning data for the tracking of convective events, *Atmospheric Research*, 134, 87–99, doi:10.1016/j.atmosres.2013.07.008, 2013.

Taszarek, M., Czernecki, B., and Koziół, A.: A cloud-to-ground lightning climatology for Poland, *Monthly Weather Review*, 143(11), 4285–4304, doi:10.1175/MWR-D-15-0206.1, 2015.

1015 Telesca, L., Bernardi, M., and Rovelli, C.: Time-scaling analysis of lightning in Italy, *Communications in Nonlinear Science and Numerical Simulation*, 13(7), 1384–1396, doi:10.1016/j.cnsns.2007.02.001, 2008.



van Lieshout, M. N. M., and Stein, A.: Earthquake modelling at the country level using aggregated spatio-temporal point processes, *Math. Geosci.*, 44(3), 309–326, doi:10.1007/s11004-011-9380-3, 2012.

Wapler, K., and James, P.: Thunderstorm occurrence and characteristics in Central Europe under different synoptic conditions, *Atmospheric Research*, 158, 231–244, doi:10.1016/j.atmosres.2014.07.011, 2015.

1020 Xu, H., and Schoenberg, F. P.: Point process modeling of wildfire hazard in Los Angeles County, California, *The Annals of Applied Statistics*, 5(2A), 684–704, doi:10.1214/10-AOAS401, 2011.

Yair, Y. Y., Aviv, R., and Ravid, G.: Clustering and synchronisation of lightning flashes in adjacent thunderstorm cells from lightning location networks data, *Journal of Geophysical Research: Atmospheres*, 114(D9), doi:10.1029/2008JD010738, 2009.

1025 Yair, Y., Shalev, S., Erlich, Z., Agrachov, A., Katz, E., Saaroni, H., ... and Ziv, B.: Lightning flash multiplicity in eastern Mediterranean thunderstorms, *Nat. Hazards Earth Syst. Sci.*, 14, 165–173, doi:10.5194/nhess-14-165-2014, 2014.

Zaliapin, I., Gabrielov, A., Keilis-Borok, V., and Wong, H.: Clustering analysis of seismicity and aftershock identification, *Physical Review Letters*, 101(1), 018501, doi:10.1103/PhysRevLett.101.018501, 2008.

1030 Zaliapin, I., and Ben-Zion, Y.: Earthquake clusters in southern California I: Identification and stability, *Journal of Geophysical Research: Solid Earth*, 118(6), 2847–2864, doi:10.1002/jgrb.50179, 2013.